The suitability and consequence of renal tubule specific adipose triglyceride lipase ablation for the study of targeted lipid accumulation in the kidney

by

Phillip Marvyn

A thesis
presented to the University of Waterloo
in fulfillment of the
thesis requirement for the degree of
Master of Science
in
Kinesiology

Waterloo, Ontario, Canada, 2015

AUTHOR'S DECLARATION

This thesis consists of material all of which I authored or co-authored: see Statement of Contributions included in the thesis. This is a true copy of the thesis, including any required final revisions, as accepted by my examiners.

I understand that my thesis may be made electronically available to the public.

STATEMENT OF CONTRIBUTIONS

Chapter 3 of this thesis contains materials from a published paper (1). I would like to acknowledge the co-authors who contributed to the research described in this thesis:

- Ryan Bradley
- Emily Button
- Emily Mardian
- Dr. Robin Duncan

Published Paper: Marvyn, P. M., Bradley, R. M., Button, E. B., Mardian, E. B., and Duncan, R. E. (2015) Fasting upregulates adipose triglyceride lipase and hormone-sensitive lipase levels and phosphorylation in mouse kidney. *Biochemistry and Cell Biology, in press*

ABSTRACT

The mechanism of disease onset for chronic kidney disease (CKD) is not fully understood. A rise in CKD rates has occurred concomitant with the rise in prevalence of obesity. We hypothesized that renal lipid accumulation, which occurs in obesity, is an early mediator of kidney dysfunction, and that it may drive pathological changes associated with CKD, including increased incidence of diabetes and CVD. To elucidate a possible role for lipid accumulation in kidney dysfunction and associated co-morbidities, a renal-tubule-specific model is required that is not confounded by the plethora of systemic metabolic changes that can occur in obesity. To develop this, I first characterized renal lipolysis to identify promising target proteins. I found that total [^{3}H] triolein hydrolase activity of kidney lysates was significantly increased by 15% in the fasted state, and that adipose triglyceride lipase (*Atgl*) and hormone-sensitive lipase (*Hsl*) mRNA expression were time-dependently increased by fasting, along with other fatty acid metabolism genes (*Ppar*α, *Cd36*, and *Aox*). ATGL and HSL protein levels were also significantly induced (by 239$\pm$7% and 322$\pm$8%, respectively) 16 h after food withdrawal. Concomitant with changes in total protein levels, there was an increase in ATGL phosphorylation at the AMPK-regulated serine 406 site in the 14-3-3 binding motif, and an increase in HSL phosphorylation at serine 565 and 660 that are regulated by AMPK and PKA, respectively. Using immunofluorescence, I further demonstrated nearly ubiquitous expression of ATGL in the renal cortex, with a concentration on the apical/lumenal surface of some cortical tubules.

My findings suggested that ATGL-mediated lipolysis may be a suitable process to target to generate a model for elucidation of the role of lipid accumulation in kidney dysfunction. In this regard, I used transgenic mice expressing Cre recombinase under control of a renal-tubule-

specific promoter, and mated them with mice that harbour LoxP sites in the regions flanking the first exon of ATGL, in order to make renal-tubule-specific ATGL knockout mice (KSAKO). All studies reported utilized male mice only. Male KSAKO mice gained weight faster than wildtype mice. However, at 20 weeks, body weights were not significantly different. We found an increase in kidney and liver weights in KSAKO mice, and decreases in adipose tissue depot masses at 20 weeks of age. ATGL mRNA and protein were reduced in whole kidneys of KSAKO mice by 25% and 33%, respectively. There was a compensatory 74% increase in *Hsl* mRNA at 20 weeks of age in male KSAKO mice. Specificity of ATGL knockout was confirmed by immunoblotting for ATGL in heart and adipose tissue of KSAKO mice, where ATGL was not reduced compared to wildtype. In fact, ATGL was induced in peri-renal WAT by 248%, which may help to explain the significantly reduced tissue mass. Glucose tolerance and insulin sensitivity were tested. KSAKO mice were initially found to be more insulin sensitive at 9 weeks of age, but then more insulin resistant at 16 weeks of age. Impaired insulin sensitivity and glucose tolerance in adult mice occurred concomitant with increased renal mRNA expression of markers of inflammation and fibrosis, including *Il-6* (312% increase) and *fibronectin* (38% increase). The ablation of renal *Atgl* also resulted in an increase in plasma triacylglycerol (TAG) levels, although this did not reach significance with the number tested. Taken together, my findings indicate an important role for renal lipolysis in the mediation of whole body glucose and TAG metabolism. Further study will be required to elucidate the mechanism(s) underlying the disruption to glucose handling in KSAKO mice. These findings will be important for understanding the pathobiology of kidney disease, and the role of kidney lipid metabolism in the risk of diabetes and cardiovascular disease.

ACKNOWLEDGEMENTS

I would like to thank my supervisor Dr. Robin Duncan for taking the chance on me as a researcher. I would also like to thank her for her guidance and patience over the last two years. She is an inspiration and I hope to have the knowledge and passion she continues to express when I find my career. Finally I would like to express my gratitude for taking the huge amount of time to teach, show, edit, re-edit, and review my written work, I am thankful you took the time to help me in this journey, I know it will be a vital skill in the years to come.

I would like to thank my lab members Ryan Bradley, Marcia Dominigos, Emily Button, Ash Hashemi, Emily Mardian for assisting, and teaching me in the lab. I would also like to thank them for putting up with my shenanigans and keeping the lab supportive even on the worst of days.

Thank you to my friends who have supported me and pushed me to be better. I couldn't have done it without the Cardill Crew.

I would like to sincerely thank my parents, Ed and Kelly, for continuing to support me in my pursuit towards finding my ultimate passion. They have always light-heartedly said that I am going to be a professional student however; I am glad that they still support me in whatever path I choose to take.

to my family.

ESRR.

Table of Contents

LIST OF FIGURES

LIST OF TABLES

INTRODUCTION

1 in 10 North Americans has chronic kidney disease (CKD) and millions more are at risk (2,3). This life threatening disease causes kidney function to deteriorate, creating a condition where kidneys can no longer sufficiently filter the blood. CKD leaves the patient with a severely reduced quality of life and when left untreated will succumb to the disease. CKD is characterized by a reduction in kidney function over several months and is diagnosed by a glomerular filtration rate (GFR) less than 60 ml/min/1.73m^2 for at least 3 months (4). With a continued loss of GFR, patients are dependent on routine dialysis to artificially filter their blood, costing $49 billion annually in the US alone (5). Even with life supporting dialysis, the probability of surviving the first five years with kidney failure is only 35 percent (3). Despite the enormity of the problem, there are currently no therapeutic strategies to directly prevent or treat CKD, and mechanisms mediating the onset of CKD are poorly understood.

The progressive rise in CKD rates in Canada over the last 50 years can be linked in part to an aging population, since incidence of CKD is dramatically higher in individuals over 65 yrs (3). However, the rate of increase in incidence of CKD has stabilized in recent years, even though the demographic continues to age, suggesting that other factors are also involved. In this regard, obesity is another major risk factor for CKD, and the rise in obesity in recent decades has been closely paralleled by increases in CKD incidence (Figure 1).

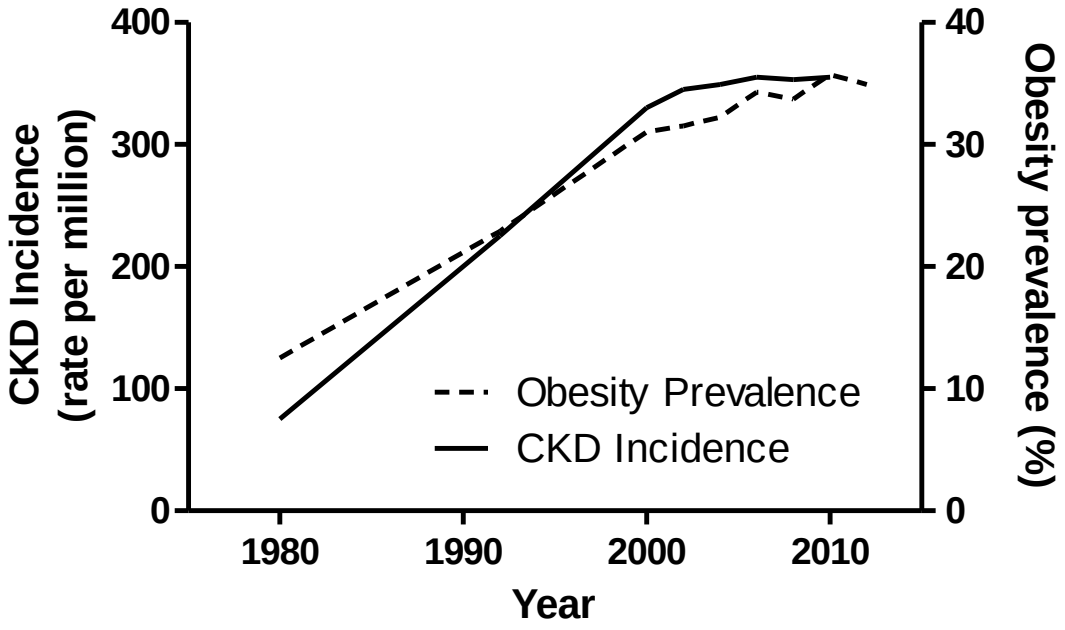

Figure 1: The relationship between obesity prevalence and CKD incidence.
Data adapted from (3,6)

Much of this link has been causally attributed to the accompanying rise in obesity-related conditions such as hypertension and hyperglycemia, since about 50% of dialysis patients have three or more comorbid conditions (7,8) that can damage glomeruli. However, obesity remains a risk factor for End-Stage Renal Disease (ESRD), or renal failure, even after adjustment for confounding co-morbidities such as diabetes and hypertension (9), indicating that other obesity-related factors must play a role in damaging the kidneys. In addition, while it is well established that renal disease can be caused by pre-existing metabolic conditions, the reverse also appears to be true. Renal disease increases the risk of developing new-onset metabolic syndrome (10), diabetes mellitus (11) and cardiovascular disease (12). Awareness of this appears to be growing. For example, the term “renocardiac syndrome” was recently coined (13) to describe the initiation of cardiovascular disease following kidney damage, although the term

"cardiorenal syndrome", denoting the development of kidney disease in patients with heart disease, has been used for over 60 years. Despite this, relatively little mechanistic insight is available into the pathological factor(s) linking kidney disease to the initiation of other metabolic conditions.

The mediators of renal injury in obesity are not fully identified, characterized, or understood. Although numerous metabolic changes occur in obesity (14), TAG overstorage both in adipose tissue, and ectopically in non-adipose tissues, is a hallmark of the dysregulated obese state (15). Most cells of the body are capable of storing intracellular TAG, at least to some extent (16). With rising levels of adiposity, lipid droplets of cellular TAG accumulate in non-adipose tissues (17), and accumulation of renal TAG has been found to be associated with increasing BMI in humans (18). Lipid-mediated toxicity, or "lipotoxicity" is the term used to identify cellular damage and cell death caused by lipids. However, whether ectopic kidney lipid accumulation is merely a benign consequence of obesity, or whether it can initiate lipotoxicity, is currently unknown.

In several forms of kidney injury, lipid droplets are reported to appear prior to infiltration by white blood cells, suggesting that they may actually cause damage (19). Mechanistically, it is highly likely that accumulation of lipids in the kidney leads to pathological changes. Lipid droplet accumulation and over storage in the kidney is associated with CKD and diabetes (20). Studies have demonstrated an association between obesity-induced and diabetes-induced lipid droplet accumulation in renal cells and renal pathology (21,22). Additionally, pathological changes have been found in kidneys of mice transgenic for sterol regulatory element-binding protein 1 (SREBP1) that causes renal lipid accumulation as a result of increased fat synthesis in

the kidney (23). However, results in all of these models are confounded by the lack of a kidney-specific or renal tubule-specific approach. In obesity-induced or diabetes-induced models of renal lipid accumulation, metabolic, energetic, or hormonal changes in the blood and other tissues could influence events in the kidney, including the development of inflammation and the relative partitioning of fuel substrates. Likewise, in the SREBP1 transgenic model, overexpression of the transgene in liver and adipose tissue, in addition to kidney, may influence renal effects (23). Thus, whether accumulation of lipid in the kidney causes renal injury has not yet been investigated in a targeted and specific manner.

Investigating the effects of isolated renal lipid accumulation on kidney health is important for understanding the pathology of obesity in CKD, and development of a targeted model would greatly facilitate this work. Additionally, development of a targeted model of renal TAG overstorage could shed new light on the relationship between kidney damage and the onset of CKD-associated co-morbidities. The cause of greater rates of development of new-onset diabetes mellitus in patients on renal dialysis is currently unknown (11). Additionally, while it is known that specific blood lipid abnormalities, particularly increases in plasma levels of TAGs and TAG-rich lipoproteins such as very low-density lipoproteins (VLDL), are often seen in CKD, the origins of these changes are not well understood (24). Thus, development of a model of renal tubule-specific TAG overstorage would allow for investigation not only of pathological changes occurring in the kidney, but also of potential mechanisms underlying whole-body metabolic disturbances in kidney disease.

Achieving renal lipid accumulation (i.e. renal steatosis), in the absence of lipid accretion in other organs, requires a highly targeted approach that is not possible with diet or

pharmaceutical agents. Gene deletion or gene overexpression, targeted to renal tubules, could achieve a specific model of fat accumulation. There are many possible targets. The amount of TAG stored in a tissue is dependent on the balance between fat uptake, synthesis, and utilization, with different protein regulators acting at each step. Evidence suggests that targeting proteins involved in fat breakdown and utilization may be particularly effective. Lipolysis is the enzymatic process by which fatty acids are sequentially cleaved from the glycerol backbone of TAG. In white adipose tissue, the major storage site of TAG in mammals, the hydrolysis of TAG by lipolytic enzymes has been well characterized (16). Renal lipolysis has not yet been described, but evidence from gene knockout mice suggests that some of the principle protein regulators of adipocyte lipolysis may be functionally significant in kidney. In particular, mice that are totally deficient in adipose triglyceride lipase (ATGL), the enzyme that catalyzes the initial step in TAG hydrolysis, have a substantial accumulation of TAG in all tissues of the body, including kidney (25). Although broad changes in whole body lipid metabolism were evident in this non-targeted model, it does support a potential critical role for ATGL in renal lipid breakdown and accumulation that deserves further investigation.

CHAPTER 2

Biochemical Foundations

Introduction

To elucidate a role for renal lipolysis in the pathogenesis of kidney disease we must first understand the fundamentals of lipid breakdown in the body. The ability to switch between the fed and fasted state is a critical metabolic process, which enables a constant supply of energy substrates to meet the demands of all tissues. Instrumental to this switch is the ability to activate lipolysis. In this section we review the purpose of lipid mobilization during fasting and the key enzymes involved in initiating this process. We also review what is currently known about lipid handling in the kidney to form a foundation upon which to discuss the development and pathology of renal lipid accumulation. And, finally, we review the fundamentals of probing glycemia control, in order to help understand the role of renal lipid accumulation in the development of secondary co-morbidities such as insulin resistance.

Lipid mobilization in fasting

Higher eukaryotes have developed the ability to maintain the provisional release of nutrients, despite fluctuations in the external environment. Endogenous glycogen and lipid stores allow the body to maintain a constant supply of energy substrates irrespective of exogenous availability. The liver is the main provisional supplier of glucose for the body, storing it in response to elevated postprandial glucose levels and circulating insulin, and releasing it in response to a fall in blood glucose levels coupled with a rise in circulating levels of the hormones glucagon and norepinephrine (26). However, hepatic glycogen stores are limited to

~100 g (~400 kcal) in a typical adult (27), and are unable to supply adequate energy substrates alone for prolonged periods, even in individuals at rest. Additionally, it is metabolically critical that liver glycogen stores are conserved, because glucose-dependent tissues, such as the brain and red blood cells, cannot readily utilize other fuel sources. Lipid beta-oxidation is optimal for long term energy supply in part due to its caloric efficiency which yields about 9 kcal/g compared to 4 kcal/g for glucose. With fasting, a rise in glucagon and norepinephrine stimulates the hydrolysis of adipose tissue TAG resulting in a net increase in the release of free fatty acids (16). Most tissues are able to take up circulating free fatty acids (28). However, because excess free fatty acids are cytotoxic, they are typically stored upon uptake as TAG (29,30). In order to mobilize fatty acids for cellular uses including energy metabolism, free fatty acids must be hydrolyzed from TAG and released from the lipid droplet. This process is termed lipolysis.

The regulated process of lipolysis contains three main enzymes, ATGL, hormone-sensitive lipase (HSL) and monoglyceride lipase (MGL). These enzymes hydrolyze fatty acids from TAG in a step-wise manner. A summary of the characterization of these enzymes follows.

Adipose Triglyceride Lipase

Adipose triglyceride lipase, otherwise known as desnutrin or Pnpla2, belongs to the patatin domain-containing protein family that consists, in humans, of nine members. Discovery of ATGL was reported simultaneously in 2004 by three laboratories (31-33). It was selected as a candidate protein for study based on its differential expression in adipocytes compared to liver or skeletal muscle, and because it was structurally homologous to known lipases containing the GXSXG motif and alpha/beta (a/b) hydrolase folds that are characteristic of serine esterases.

The murine gene for ATGL encodes a 486 amino acid protein with a mass of 54 kDa (31). *Atgl* is found to be highly transcriptionally expressed in white and brown adipose tissues as well as cardiac muscle, skeletal muscle, testis and kidney (31), although protein expression in kidney has not yet been reported. White adipose tissue *Atgl* mRNA was also found to be under nutritional control, being induced with fasting (34). Evidence of ATGL TAG lipase activity comes from both *in vitro* and *in vivo* assays. The overexpression of ATGL in both HEK293 (31) and COS-7 (32) cells results in a decrease in TAG and an increase in free-fatty acid release to the medium, with no change to phospholipids, and ATGL also does not express any activity for cholesteryl or retinyl-ester bonds (32,35). Further evidence of the specific activity of ATGL is that TAG lipase activity is reduced by up to 60% in isolated *Atgl* knockout adipocytes (34), and TAG lipase activity is reduced by 70% when adipose tissue extract is treated with a polyclonal antibody against ATGL (32).

The substrate and stereo-selectivity of ATGL in the catalytic release of free fatty acids from TAG is preferentially for the hydrolysis of long-chain fatty acid esters at the sn-2 position of the glycerol backbone generating sn-1,3 diacylglycerol (DAG), with little activity for the sn-1 position (35). However, in the presence of its co-activator CGI-58, ATGL also generates sn-2,3 DAG, with similar preference for both sn-1 and sn-2 position (35).

CGI-58 is a lipid-droplet associated protein that is widely reported to activate ATGL under conditions where lipolysis is stimulated, by facilitating translocation of ATGL from the cytosol to the lipid droplet (36,37). ATGL is also regulated by the activity of kinases, and is known to contain two serine residues that are subject to phosphorylation (34). In the mouse, these phosphorylation sites have been shown to be phosphorylated through the action of

AMPK (34,38). AMPK is a sensor for low energy states and is activated during fasting and exercise (39). However, the role of AMPK-mediated phosphorylation of ATGL in fasting induced lipolysis is not fully understood.

The activation of ATGL initiates the rate limiting step of TAG breakdown, resulting in the release of fatty acids to match supply with demand. The diacylglycerol (DAG) product of TAG hydrolysis by ATGL continues through the lipolysis pathway.

Hormone-Sensitive Lipase

The second step in TAG catabolism involves HSL. HSL was discovered when it was found that hormonal stimulation induced lipolytic activity in adipose tissue (40,41). HSL contains a motif found in several lipases, the α/β hydrolase fold that is characterized by alternating alpha-helices and beta-sheets, and that contains a catalytic triad of serine, aspartate or glutamate, and histidine (42). The serine residue at position 423 within the catalytic domain of HSL was found to be essential for hydrolase and esterase activity (43). After ATGL cleaves a fatty acid from TAG, a DAG is formed, which HSL hydrolyzes to release another acyl chain, forming monoacylglycerol. The HSL-catalyzed reaction favours the sn-1,3 DAG substrate, however, HSL will act on other species (35). The HSL enzyme also possesses TAG lipase activity, but its specificity for DAG is 10 times higher than that for TAG (35).

The regulation of HSL involves both changes in phosphorylation state and co-enzyme activation. In the fasted state the catecholamine norepinephrine causes the activation of protein kinase A (PKA) through G-protein coupled cyclic-AMP (cAMP)-mediated signalling (44). A rise in cAMP concentrations results in increased binding of this nucleotide to the negative

regulatory subunit of PKA, resulting in release of the catalytic subunits that become active and phosphorylate HSL on multiple sites, including the activation sites Ser 653 (45), Ser659 (46) and Ser660 (46). PKA can also phosphorylate perilipins, a family of lipid droplet proteins, to increase HSL and ATGL recruitment to the lipid droplet (47). In the postprandial state, insulin exerts its anti-lipolytic effects, at least in part, through activation of phosphodiesterase 3B that degrades cAMP (16). A reduction in cAMP allows the regulatory subunits to sequester the catalytic subunits, reducing activation of PKA and stimulated lipolysis (16). This effect is enhanced by the activation of protein phosphatase-1 by insulin, which dephosphorylates HSL, causing its inactivation (48). HSL also contains a Serine 565 (S565) site (46), which has been shown to be phosphorylated by AMPK (49). The phosphorylation of S565 has been shown to inhibit HSL activity in WAT(50), however activation of lipolysis in muscle has been associated with increased S565 phosphorylation (51). Thus, whether AMPK activates or inhibits HSL is still unclear, and may be tissue specific.

Monoglyceride lipase

MGL is a 33 kDa hydrolase, first found in adipose tissue in 1971 (52), but subsequently found to be expressed relatively ubiquitously in all tissues. MGL is a specific monoacylglycerol hydrolase, acting at the last step of TAG breakdown on monoacylglycerols (MAG) at the 1-(3-) and 2- ester bonds at equal rates. MGL exhibits almost no activity for DAG, TAG, or cholesteryl ester substrates (53), and has activity with MAG that is 100 fold higher than the activity of HSL with DAG (54). This enzyme is therefore not rate limiting in the TAG hydrolysis pathway for fatty acid mobilization. Additionally, it is found in the cytoplasm rather than on the lipid droplet where

TAG is stored. For these reasons, we choose to focus on the effects of ATGL and HSL in the study of renal TAG lipolysis.

Kidney lipid metabolism

The majority of work on lipolysis has been performed in adipose tissue, while kidney lipolysis and renal lipid metabolism overall remains understudied. It is likely, however, that lipolysis is particularly important in the kidney. This organ is exposed to both circulating complex lipids and NEFA, as well as NEFA bound to albumin in the urinary filtrate, making it highly susceptible to the accumulation of TAG (55,56). Indeed, in the fasted state, circulating levels of adipose-derived NEFA rise, and the kidneys increase the uptake of NEFA from the plasma (57) and reuptake of albumin-bound fatty acids from glomerular filtrate (55,56,58). The kidney also expresses several receptors for the uptake of lipids. Megalin, Cubilin and Amnionless are membrane proteins expressed along proximal tubules that are capable of interacting with lipid transport molecules including apolipoproteins and albumin (59) (and references therein). Renal tubule cells express receptors for the major classes of lipoproteins (60-62), as well as fatty acid transporters (17,63). And, the kidney can also take up TAG NEFA generated through lipoprotein lipase-mediated hydrolysis (64,65). Increases in the uptake of NEFA in fasting make it a major fuel source for the kidney, accounting for up to half of renal oxygen consumption in this state (66).

Evidence indicates, however, that incoming FFA are not used directly, but first esterified into TAG (29,30). Lipolysis is therefore required to mobilize these stores for use (57,67). A critical role for ATGL in particular in this process is supported by studies in ATGL knockout mice

demonstrating significant TAG accumulation in the kidneys (25). Indeed, total deficiency of ATGL in mice has been shown to cause TAG accumulation in essentially all tissues analyzed, ultimately resulting in premature death due to contractile failure of TAG-suffused cardiac muscle. Although subsequent studies have examined effects of tissue-specific loss of ATGL in heart, liver, skeletal muscle, and brain, researchers have yet to investigate the role of ATGL in kidney, despite the fact that ATGL total null mice showed the second largest accumulation of TAG in this organ (an approximate 16-fold increase)(25). The finding of significantly elevated renal TAG in ATGL total-null mice provides strong evidence of an important role for ATGL in kidney. However, there are limitations to the direct interpretation of this finding. This model was a global ATGL knockout, and there were a host of significant changes including changes in adipocyte lipolysis and blood lipid and blood glucose levels that could indirectly affect kidney fat accumulation. It therefore cannot be conclusively determined from that model whether the renal lipid accumulation reported was due entirely to changes in renal lipolysis or whether other metabolic changes were the cause of TAG accumulation. In fact, very little is known about renal lipolysis, and it has not yet been reported whether ATGL protein is even found in kidney.

Blood glucose clearance

Insulin-independent effects

The concentration of blood glucose is tightly controlled, at around 5 mM. During fasting, blood glucose concentration remains constant, as a result of the balance between metabolic usage and hepatic glucose production. The liver is responsible during the post-absorptive state

for the majority of endogenous glucose production, while most glucose uptake occurs in insulin-insensitive (brain and splanchnic) tissues (68). Fasting blood glucose concentration is associated with plasma insulin level, because of the ability of this hormone to shut down hepatic glucose production. The uptake of glucose by tissues during the fasted state is largely mediated by the concentration gradient between the plasma and cytosol, which is termed glucose 'mass action'. Only 25% of glucose uptake occurs in insulin-sensitive tissues, primarily skeletal muscle, during fasting conditions (68).

Insulin-dependent effects

In the absorptive state, the increase in blood glucose concentration stimulates the pancreas to release insulin. When insulin is released into circulation, tissues sensitive to insulin, through insulin-receptors, are stimulated to recruit glucose transporters to allow glucose to enter the cell. Skeletal muscle, adipose tissue, and liver are responsible for the majority of blood glucose clearance resulting in a decrease in blood glucose concentrations. Skeletal muscle is responsible for about 2/3 of post-prandial glucose clearance (69).

Insulin also causes blood glucose concentration to decrease due to its effect on liver. Although the liver does not express insulin-regulated GLUT4 receptors for glucose uptake, the inhibition of hepatic glucose production contributes to the decrease in blood glucose concentration.

Fasting glucose concentration is an indication of insulin sensitivity. Hepatic glucose production is the prominent supplier of blood glucose and this remains constant in the fasted

state. The inability of the liver to respond to insulin and decrease glucose production results in an elevated fasted blood glucose concentration, suggesting reduced insulin sensitivity.

Physiological effects following intraperitoneal injection of glucose

Glucose tolerance testing (GTT) assesses the ability of tissues to respond to a bolus of injected glucose, in order to clear glucose from the blood. This ability is the result of combined effects of insulin secretion, insulin action and glucose 'mass action' (70). This test allows for the identification of disruptions to glucose metabolism that are associated with metabolic syndrome and diabetes. Animals are typically fasted overnight for 16 hours, baseline blood glucose concentrations are measured, and then an intraperitoneal (*i.p.*) injection of glucose is given (70). Injected glucose is absorbed into the blood stream from the peritoneal cavity, and blood glucose concentrations rise.

The expected response is for the blood glucose concentration to rise rapidly, stimulating insulin release, and triggering an increase in insulin-mediated GLUT4-dependent glucose disposal, and inhibition of hepatic glucose production. After about 90 min, glucose concentration should be returned to baseline in animals with normal insulin sensitivity.

Insulin resistance is the inability of tissues to respond appropriately to insulin. Insulin resistance would present as a greater increase in blood glucose concentration and slower return to baseline of blood glucose relative to control animals following *i.p.* glucose injection, due to blunted insulin-mediated glucose disposal and impaired suppression of hepatic glucose production. However, animals with a defect in insulin synthesis or release would have a

similarly impaired response to injected glucose. Thus, it is also necessary to directly examine the effect of insulin injection on dynamic blood glucose regulation.

Physiological effects following intraperitoneal injection of insulin

Insulin tolerance testing (ITT), also called insulin stress testing, assesses whole body insulin action (70). Animals are fasted for a short period (5-6 h), and baseline blood concentrations are measured, and then an *i.p.* injection of insulin is given (70). Insulin injection will stimulate insulin-mediated uptake of glucose as well as inhibit hepatic glucose production.

The expected response is for blood glucose to decrease from a fasted level following insulin injection and to return to baseline about 60 min after injection. Insulin resistance will present as an attenuated decrease in blood glucose concentration following insulin injection, owing to reduced insulin action. However, if the insulin injection forces a decrease in blood glucose below 4.44 mM, the anti-insulin response from the adrenal system dominants (71) and may lead to confounding interpretations. Thus, insulin injections are only given to mice after a short (5-6 h) fast, rather than after a 16 h fast as is done in glucose tolerance testing.

CHAPTER 3- Fasting upregulates lipolysis in mouse kidney

Results from this chapter have been published (1).

Rationale

Lipolysis is the enzymatic process by which fatty acids are sequentially cleaved from the glycerol backbone of TAG. In adipocytes, the major storage site of TAG in mammals, the release of NEFA by lipolytic enzymes has been well characterized (16). TAG is primarily hydrolyzed by ATGL to form DAG, which is subsequently hydrolyzed by HSL, although this enzyme has TAG hydrolase activity as well. These enzymes are expressed in other tissues including kidney (31,72), although not all reports agree (73), and the presence of ATGL protein in kidney has not yet been demonstrated. Thus, whether these enzymes are indeed present in kidney, and whether they are regulated to match changing requirements for lipolysis-derived substrates, remains to be fully characterized. This understanding has importance for renal health, given the role of fatty acids in renal energy metabolism and the detrimental consequences of renal steatosis (23).

Objectives

To characterize renal TAG lipolysis, in order to identify a suitable target enzyme for the generation of a model of renal tubule-specific lipid accumulation.

Characterization will include investigation of:

i. Renal TAG lipolysis activity in the fasted and non-fasted states
ii. Expression, regulation and phosphorylation of lipolysis enzymes in kidney in the fasted and non-fasted states
iii. Renal beta-oxidation capacity in the fasted and non-fasted states

iv. Kidney tissue localization of ATGL

Hypotheses

A 16 hour fast will:

1. Induce TAG hydrolase activity in kidneys of mice
2. Increase kidney ATGL and HSL mRNA expression and protein levels
3. Increase the activating ATGL 14-3-3 binding domain sequence phosphorylation
4. Increase the activating HSL S660 and S565 phosphorylations
5. Increase activation of cAMP-activated protein kinase A (PKA) and 5'-adenosine monophosphate-activated protein kinase (AMPK) in kidneys
6. Increase beta-oxidation in kidneys of mice
7. Shift the respiratory exchange ratio towards 0.7 in mice, indicating greater lipid beta-oxidation

Furthermore, ATGL will be expressed in most cells of the kidney.

Methods

Study design (feeding and timeline)

Protocols were approved by the Animal Care Committee at the University of Waterloo, with all procedures performed in accordance with the Canadian Council on Animal Care. C57Bl/6J mice were bred in the Central Animal Facility at the University of Waterloo from founders originally purchased from Jackson Laboratories (Bar Harbor, Maine, USA). Fourteen to twenty-four wk-old female mice were group housed in a controlled environment with constant temperature and humidity with a standard 12h light: 12h dark cycle. Animals were provided ad libitum with water and a standardized control diet for 9 d (Research Diets #D12450H, New Brunswick, New Jersey, USA) prior to experiments. Non-fasted mice were euthanized at 9 am. Fasted mice had food withdrawn at 5 pm and were randomized to fast for 4, 8, or 16 h overnight, prior to CO_2 asphyxiation and tissue collection.

Assessing *Atgl* and *Hsl* mRNA expression

Total RNA was prepared from whole kidneys using TRI Reagent® (Sigma Aldrich, Mississauga, Ontario, Canada). TRI Reagent® was added to a whole kidney and homogenized using a Polytron tissue homogenizer to isolate and preserve RNA from cells. Chloroform was added and samples were centrifuged to separate RNA from cell constituents. The aqueous phase, containing the RNA, was pipetted into a clean tube. Isopropanol was added and samples were centrifuged to precipitate the RNA. The RNA pellet was then washed with ethanol, resuspended in RNAase free water, and heated for 10 min at 55 °C, to denature RNAases.

Two μg of RNA was reverse transcribed using a high-capacity cDNA reverse transcriptase kit (Life Technologies, Burlington, Ontario, Canada) containing a reaction buffer, random primers

and dNTP mix and heated in a thermal cycler at 25°C for 10min, 37°C for 120min, 85°C for 5 min and then kept at 4°C. qPCR was performed using SsoFast EvaGreen master mix (Bio-Rad Laboratories, Mississauga, Ontario, Canada) containing SsoFast Eva Green super mix, forward and reverse primers (Table 1) and amplified with the conditions: 95°C for 2 min, followed by 40 cycles of 95°C for 10 s, 60°C for 20 s, followed by melt curve analysis to verify a single amplicon. Expression of test genes was normalized to *18s* and analyzed by the delta Ct method.

Table 1: Primer Sets used for PCR reactions

Gene	Direction	Sequence	Product Size
Atgl	forward	5'-aacgccactcacatctacgg-3'	113 bp
	reverse	5'-gcctccttggacacctcaata-3'	
Hsl	forward	5'-ggagtctatgcgcaggagtg-3'	80 bp
	reverse	5'-gcttcttcaaggtatctgtgcc-3'	
Aox	forward	5'-gctgcggagacaggttgtcatcg-3'	105 bp
	reverse	5'-gctccttgcgcagatcgggattc-3'	
Cd36	forward	5'-tcctctgacatttgcaggtccatct-3'	103 bp
	reverse	5'-aggcaaaggcgttggctggaa-3'	
Pparα	forward	5'-ccgaacattggtgttcgcagctgt-3'	91 bp
	reverse	5'-caggggacaaccagaggacccag-3'	
ATGL-LoxP	forward	5'-ctcaccgccacagcgctggtcac-3'	HM- 315 bp
	reverse	5'-gtccctctctaccgcttctac-3'	HT- 180 bp
KSP-CRE	forward	5'-aggttcgttcactcatgga-3'	277 bp
	reverse	5'-tcgaccagtttagttaccc-3'	
Fn1	forward	5'-acatggctttaggcggacaa-3'	75 bp
	reverse	5'-ttcggcaggtatggtcttgg-3'	
TNF-α	forward	5'-caacgccctcctggccaacg-3'	114 bp
	reverse	5'-tcggggcagccttgtccctt-3'	
Il-β	forward	5'-cctgctggtgtgtgacgttccc-3'	84 bp

	reverse	5'-gggtccgacagcacgaggct-3'		
Il-6	forward	5'-gctggagtcacagaaggagtggct-3'	117	bp
	reverse	5'-ggcataacgcactaggtttgccgag-3'		
18s	forward	5’-gatccattggagggcaagtct-3'	79	bp
	reverse	5’-aactgcagcaactttaatatacgctatt-3’		

Immunodetection of ATGL and HSL

Whole kidneys were homogenized on ice using a Polytron in lysis buffer (50 mM Tris, pH 7.4, 0.1 M sucrose, 1 mM EDTA, 5mM sodium fluoride, 10mM sodium orthovanadate, with protease inhibitor cocktail (1:100) (Sigma Aldrich, Mississauga, Canada), followed by centrifugation at 9,000 × g for 15 min at 4°C, and determination of protein concentrations by bicinchoninic acid assay (Sigma Aldrich, Mississauga, Canada). Heat denatured lysates in Laemmli buffer with 2-mercaptoethanol were electrophoresed through 10% SDS-PAGE gels and wet-transferred to nitrocellulose membranes at a constant 350 mA for 90 min. Membranes were blocked overnight at 4°C with 5% (w/v) blocker in TBST. Membranes incubated for 2 h at room temperature with primary antibodies (mouse-Anti-ATGL, Cell Signaling, Danvers, MA, USA) (mouse-Anti-HSL, Cell Signaling, Danvers, MA, USA) (mouse-Anti-HSL-S565, Cell Signaling, Danvers, MA, USA) (mouse-Anti-HSL-S660, Cell Signaling, Danvers, MA, USA) (mouse-Anti-14-3-3, Cell Signaling, Danvers, MA, USA) (mouse-Anti-ACC, Cell Signaling, Danvers, MA, USA) (mouse-Anti-ACC-S79, Cell Signaling, Danvers, MA, USA) (mouse-Anti-AMPK, Cell Signaling, Danvers, MA, USA) (mouse-Anti-HSL, Cell Signaling, Danvers, MA, USA) (mouse-Anti-HSL-S565, Cell Signaling, Danvers, MA, USA) (mouse-Anti-HSL-S660, Cell Signaling, Danvers, MA, USA) (mouse-Anti-14-3-3, Cell Signaling, Danvers, MA, USA) (mouse-Anti-ACC, Cell Signaling, Danvers,

MA, USA) (mouse-Anti-ACC-S79, Cell Signaling, Danvers, MA, USA) (mouse-Anti-Beta-Actin, Cell Signaling, Danvers, MA, USA) (1:1000 in TBST with 2% blocker), then washed 3 times in TBST, then incubated for 1 h with horseradish peroxidase-conjugated secondary antibodies (Santa Cruz Biotechnology, Dallas, TX, USA) (1:5000 in TBST with 2% blocker), then washed 3 times in TBST. Immunoblots were visualized by enhanced chemiluminescence on a ChemiGenius 2 Bio-Imaging System (Syngene Technologies, Palos Heights, IL). Bovine serum albumin (BSA) was used as a blocker for phospho-specific antibodies, and skim milk powder was used for all others.

For detection of phosphorylated 14-3-3 binding motif in ATGL, lysates (1000 μg) were first immunoprecipitated by tumbling overnight at 4 °C with rabbit anti-ATGL (1:200), then captured by tumbling for 1 h with protein A/G agarose beads. Samples were centrifuged and washed with lysis buffer 3 times. Laemmli buffer with beta-mercaptoethanol was then added to immunoprecipitated ATGL samples and heated at 95 °C to separate protein from agarose beads, and treated as above for SDS-PAGE separation.

In-vitro TAG hydrolase assay

Reactions were initiated by addition of lysates containing 100 μg of protein in 100 μl of lysis buffer to 100 μl of reaction mixture containing 300 μM triolein with [9,10-^{3}H(N)]triolein (0.15 μCi per reaction) (Perkin Elmer Radiochemicals, Massachusetts, USA), 25 μM egg yolk lecithin, 100 μM sodium taurocholate, 2% BSA (w/v), 1 mM DTT, and 50 mM potassium phosphate (pH 7.2) and allowed to react for 1 hr (32,74). Reactions were terminated after 1 h at 37°C by addition of 0.25 ml of methanol: chloroform (1:2). Extraction of lipids, by Bligh and Dyer

method (75), was performed by vortexing sample after addition of methanol:chloroform, then addition and mixing of 0.25 mL of ddH_2O, then centrifugation at 1000x g for 5 minutes to separate aqueous and organic phases. The organic phase was collected and dried under a N_2. Samples were reconstituted in 50 µL of chloroform and applied to a silica gel G plate. Sseparation of total lipids was performed by thin layer chromatography using hexane: diethyl ether: glacial acetic acid (80:20:2). The band corresponding to NEFA was identified by comparison with known standards under iodine vapours, scraped, and quantified by liquid scintillation counting.

Beta-Oxidation

Fresh kidneys were excised, cut sagittally and weighed. Kidney sections were added to a 14 ml Falcon tube containing 1 ml of Kreb's buffer (126 mM NaCl, 2.5 mM KCl, 25 mM NaHCO3, 1.2 mM NaH2PO4, 1.2 mM MgCl2, 2.5 mM CaCl2, pH 7.2) supplemented with 3mM glucose and 1% BSA plus 0.1 µCi [^{14}C]palmitic acid. A 500 µl Eppendorf tube was attached to the inside of the falcon tube containing a 1x1 cm filter paper soaked in 20% KOH to capture released CO_2. Falcon tubes were enclosed with parafilm. The reaction was incubated for 1 h at 37 °C with gentle shaking. The reactions were stopped at 1 h by adding 0.25ml of H2SO4 (5N) by injection through parafilm. Reactions were left covered at 37C for an additional 30 min. The 1x1 cm filter papers were scintillation counted for radio-labelled [^{14}C]-CO_2.

Immunohistochemistry

Kidneys were frozen in Cryo O.C.T. compound (Tissue Tek, Fisher Scientific, Mississauga, Canada), sliced to 8 µm, adhered to glass microscope slides, then fixed with 4%

paraformaldehyde for 10 min, washed with PBS, and permeabilized with 0.5% Triton X-100 for 5 min. Sections were then washed with PBS, blocked with 5% goat IgG serum in PBS for 1 h, incubated at room temperature for an additional hour with rabbit anti-ATGL antibody (1:100) in PBS, washed again with PBS, and incubated for 1 h with Alexa Fluor® 488-conjugated anti-mouse IgG (Cell Signaling, Danvers MA). Sections were stained with DAPI (1 µg/mL) for 15 min, and mounted with coverslips using Prolong Antifade (Life Technologies, Burlington, Canada). Slides were imaged on an Axio Observer Z1 structured-illumination fluorescent microscope equipped with an AxioCam HRm camera and analyzed with AxioVision software (CarlZeiss).

cAMP Assay

Kidneys snap frozen in liquid nitrogen were homogenized using a handheld Polytron in 10 volumes (ml/g tissue) of trichloroacetic acid (5% in water) on ice and then centrifuged at 1,500 x g, after which the supernatant was transferred to a new glass tube. Samples were then extracted using 5-volumes of water-saturated ether per volume of supernatant by vigorous vortexing for 10 s, after which the aqueous and organic layers were allowed to separate. The upper organic phase was carefully removed and discarded, and the lower aqueous phase was extracted twice more. Samples were then heated to 70°C for 5 min to evaporate any remaining ether, and then cAMP concentrations were determined using a commercially available competitive ELISA assay (Cayman Chemical, Ann Arbor, MI, USA). Diluted samples (1:10) were added to 96-well plate precoated with anti-rabbit IgG. Samples were then incubated with acetylcholinesterase-linked cAMP (tracer) and cAMP antiserum for 18 hours at 4°C. Wells were emptied by inverting and tapping plates gently on a hard surface and washed with wash buffer five times. Plates were quantified by the addition of Ellman's Reagent and incubation for 1 h,

which reacts with acetylcholinesterase, allowing quantification of its product 5-thio-2-nitrobenzoic acid, which has strong absorbance at 412 nm. The amount of tracer bound, and thus intensity of absorbance, is inversely proportional to the concentration of cAMP in the sample because of binding competition between tracer- and sample-cAMP.

Comprehensive Laboratory Animal Monitoring System Measurement

On the last day of feeding, mice were placed into the Oxymax Comprehensive Laboratory Animal Monitoring System (CLAMS, Columbus Instruments) for 24 h. The Oxymax system is an open-circuit indirect calorimeter for lab animal research allowing the measurement of oxygen consumption (VO_2) and respiratory exchange ratio (RER) of mice over 24 h of feeding/fasting protocol. Oxygen consumption (VO_2) is a measure of the volume of oxygen used to convert energy substrate into ATP. Respiratory exchange ratio (RER) is the ratio of carbon dioxide production (VCO_2) divided by VO_2 and is an estimate of the fuel source for energy production based on the difference of oxygen molecules required for the oxidation of glucose and fatty acid. An RER of 0.7 indicates fat as the primary substrate while an RER of 1.0 indicates carbohydrate as the primary energy substrate. Animals were housed individually. For fasted animals, food was removed after the mice had acclimatized to the cages for 8 h, and the mice were maintained in the cage for an additional 16 h after food withdrawl.

Statistical Analysis

Statistically significant differences between two groups (i.e. fasted versus non-fasted) were assessed by Student's *t* test. Time-dependent effects of fasting on gene expression were analyzed by one-way ANOVA with Tukey's multiple comparison post-hoc test. The results are

expressed as means +/- S.E.M. Unless otherwise indicated, different groups contain at least n=4. Significance is reported as: *P<0.05; **P<0.01; ***P<0.001. Different letters represent statistically significant differences between groups.

Results

Renal lipolysis

To determine whether TAG hydrolase activity is present in the kidney, and whether changes in that activity are evident with fasting, we investigated the release of radiolabelled [^{3}H]oleate from radiolabelled [^{3}H]triolein by kidney homogenates. We found that the hydrolysis of TAG by kidney homogenates was significantly induced by 15% with fasting, as compared to non-fasted (Figure 2).

Expression of lipid enzymes in the kidney

mRNA expression of *Atgl* and *Hsl* in the kidney was analyzed by qPCR analysis and as expected, was found to be expressed in whole kidney. We measured relative levels of *Atgl* and *Hsl* mRNA by qPCR in fasted kidneys after 16 h of food withdrawal, and found a 2.2-, 2.6- fold increase, respectively (Figure 3**Error! Reference source not found.**). *Atgl* was increased early in fasting, but expression plateaued from 4 to 8 h before increasing further at 16 h, whereas *Hsl* mRNA showed a progressive induction at each time-point measured (P<0.05).

The expression of other genes in fatty acid metabolism was analyzed for fasting-mediated regulation. *Ppar-alpha*, *Cd36* and *Aox* were upregulated 2.4-, 8.2- and 35.7- fold following a 16 h fast (P<0.05), with a progressive induction at 4 and 8 h of fasting (Figure 4**Error! Reference source not found.**).

Immunodetection of lipid enzymes

Total immunodetecable levels of ATGL and HSL were measured and found, in agreement with data from mRNA measures, to both be expressed and induced in whole kidney. Following

a 16 h fast, there was an approximate 2.4- and 3- fold induction of total ATGL and HSL immunodetectable levels, respectively (Figure 5).

Immunodetection of phosphorylated lipid enzymes

To investigate whether the activation state of the enzymes involved in lipolysis is associated with the fasting-mediated change in lipolysis, we measured levels of phospho-specific forms of ATGL and HSL.

We found that fasting mediated an approximate 3-fold increase in levels of immunodetectable phospho-ATGL phosphorylated at the 14-3-3 binding domain site in immunoprecipitated ATGL. Using phospho- and site-specific antibodies we probed HSl at S565 and S660. We found a significant 4.5-fold higher content of phosphorylated S565 HSL at this position. We also found a 2.5-fold higher content of HSL phosphorylated at serine 660 (S660) (Figure 5).

Immunohistochemical detection of ATGL in kidney cortex and medulla

To investigate the localization of ATGL in kidney, we performed immunohistochemistry on frozen renal tissue sections. ATGL was found be nearly ubiquitously expressed throughout the cortex and medulla. ATGL immunopositive cells were evident within glomeruli, cortical tubules and medullary rays. Intense fluorescence was marked at the apical/lumenal surface of cortical tubule cells (Figure 6).

Assessment of markers of kinase activity

The changes in HSL and ATGL phosphorylation that we observed are predicted to be mediated by the kinases PKA and AMPK. PKA is activated by rising cAMP concentrations that

can be generated in response to circulating beta-adrenergic receptor agonists that increase during fasting (76). We measured cAMP in kidneys from non-fasted and fasted mice, but found that concentrations were not significantly different after 16 h of fasting (Figure 7).

We next investigated the possible involvement of AMPK in the phosphorylation of ATGL and HSL by immunoblotting for total AMPK, phospho-AMPK, and total and phosphospecific levels of acetyl-CoA carboxylase (ACC) that is a classical substrate for this kinase (77). Total AMPK protein levels were increased by 2.2-fold following a 16 h fast (P<0.05)(Figure 8). We found a small increase in total kidney ACC levels with fasting, but a greater increase in phospho-ACC that was phosphorylated at the AMPK-specific site Serine 79 (S79) (Figure 9). As a result, the ratio of phosphorylated ACC to total ACC increased by almost a third in the fasted state relative to the non-fasted state (1.4$\pm$0.1 vs. 1.1$\pm$0.1, P<0.05).

Respiratory exchange ratio

The ratio of carbon dioxide to oxygen consumption was used to calculate the respiratory exchange ratio (RER), to provide an estimate of metabolic substrate usage. As expected, after 16 h of fasting there was a significant reduction in the whole body respiratory exchange ratio (RER) from 0.97 in the non-fasted state to 0.74, indicating a shift toward fat as the main substrate of energy metabolism (Figure 10).

Kidney Beta-Oxidation

Kidney fatty acid beta-oxidation was measured by reaction of [^{14}C]palmitate with whole kidney homogenates, and we found a significant 1.6-fold increase in the amount of membrane

captured ^{14}C-labelled CO_2 produced from the mitochondrial respiration of radiolabelled substrate (Figure 11**Error! Reference source not found.**).

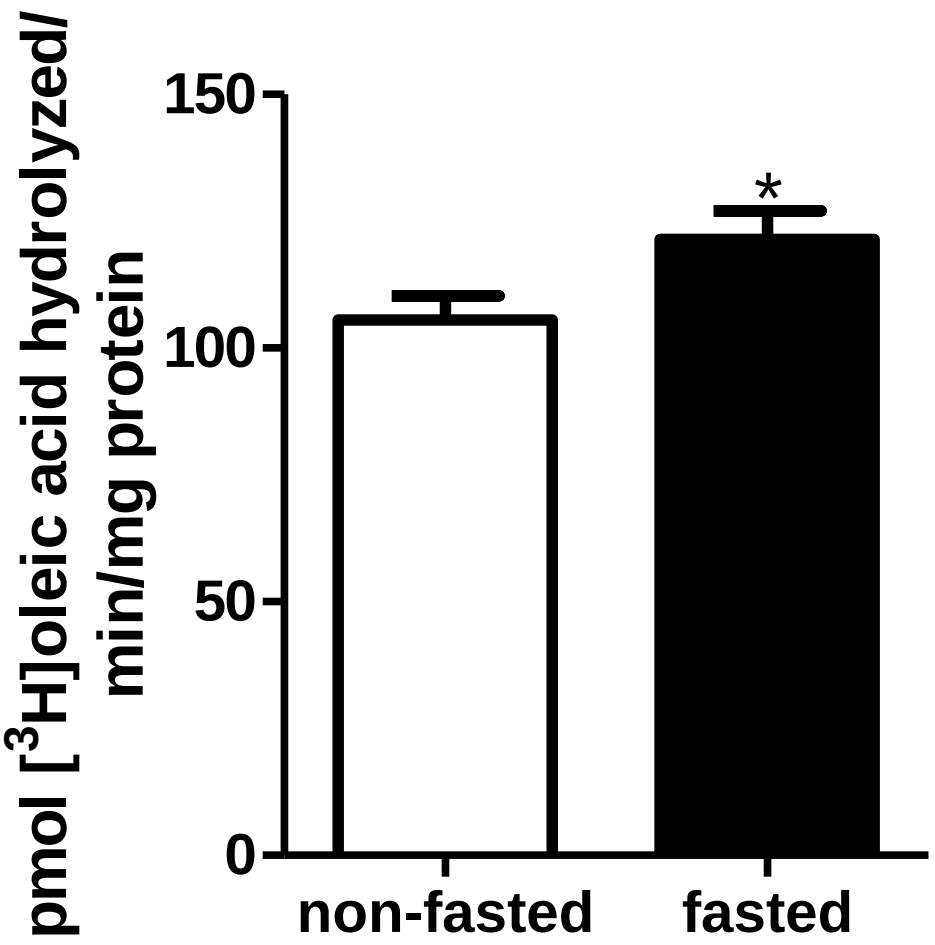

Figure 2: Lipolysis activity is increased in kidney following fasting.
Fasting induces lipolysis in whole kidney homogenates as measured by the generation of free [^{3}H]oleate from uniformly labelled [^{3}H]triolein. (n=4-6); data are means ± SEM; *P <0.05.

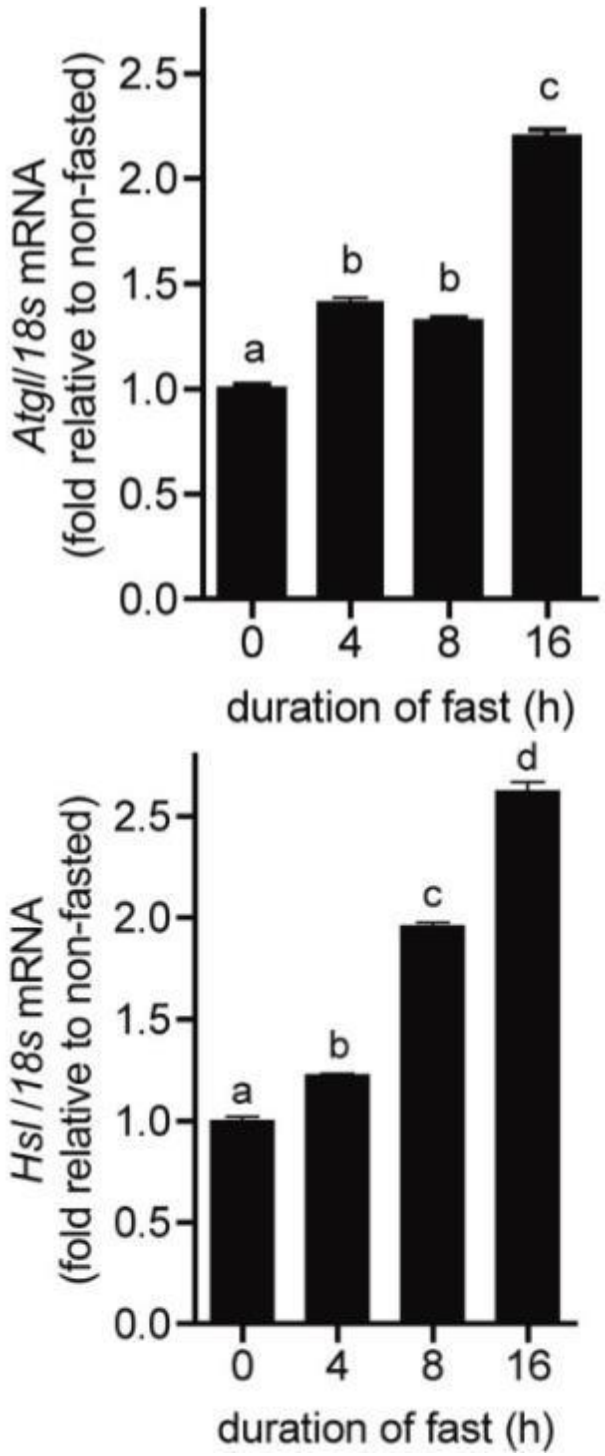

Figure 3: Fasting induces renal *Atgl* and *Hsl* mRNA.
Fasting induces mRNA expression of *Atgl* and *Hsl* in in a time-dependant manner in female mice as determined by qPCR and normalized to *18s*. Expression is shown in fed mice (time point 0) and after 4, 8, and 16 h of fasting (n=3-6); data are means ± SEM; different letters indicate significant differences between groups as determined by ANOVA with Tukey's post-hoc test for significance; $^{abcd}P<0.05$.

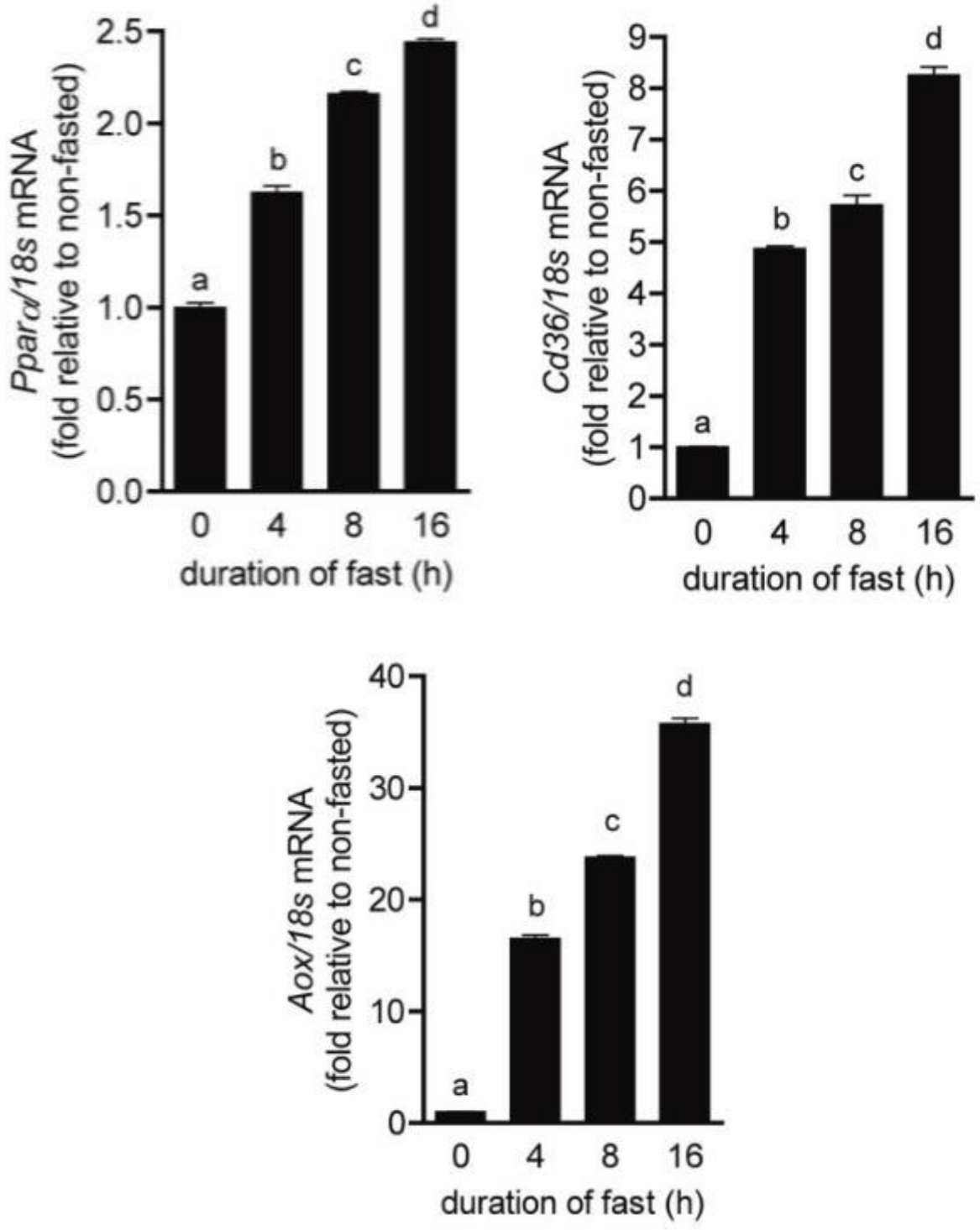

Figure 4: Fasting induces renal mRNA expression of lipid uptake and oxidative genes.
Fasting induces *Ppar-α, Cd36,* and *Aox* mRNA as determined by qPCR and normalized to 18s. Expression is shown in fed mice (time point 0) or after 4, 8, and 16 hours (h) of fasting. (n=3-6); data are means ± SEM; different letters indicate significant differences between groups as determined by ANOVA with Tukey's post-hoc test for significance; ^{abcd}P <0.05.

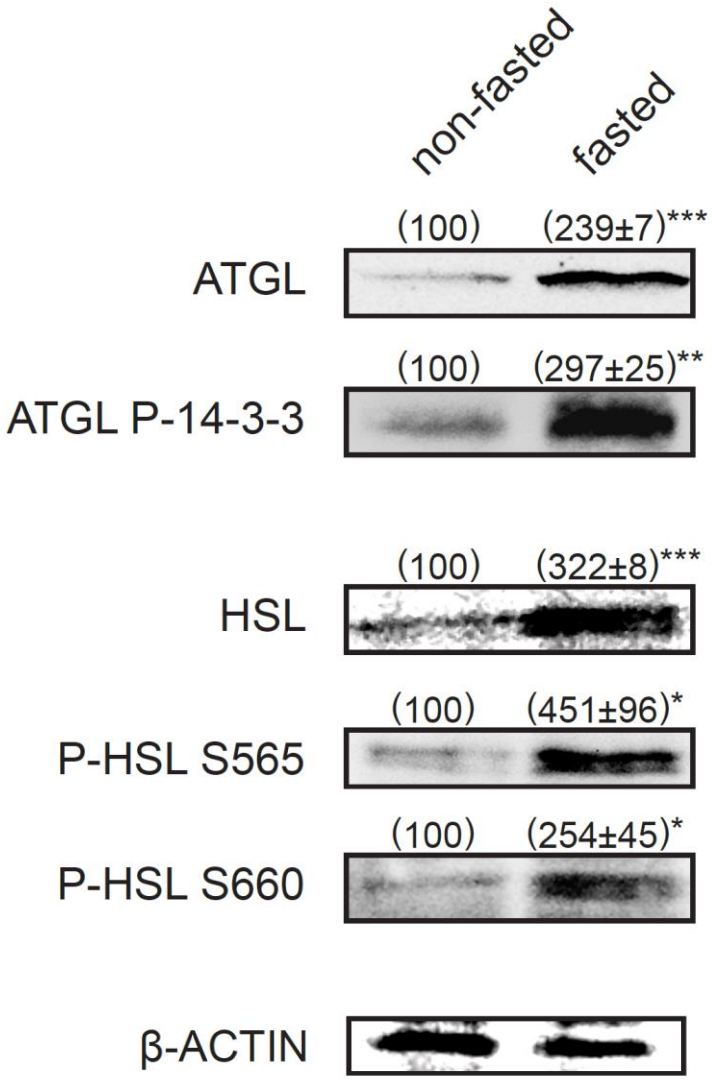

Figure 5: TAG lipolysis enzymes in kidney are regulated by fasting.
Immunoblots of ATGL, phospho-ATGL phosphorylated at the 14-3-3 binding domain, HSL, phospho-HSL phosphorylated at S565, phospho-HSL phosphorylated at S660, and control beta-ACTIN protein levels of non-fasted and fasted female mice. Fasting increases total and site-specific phosphorylation of ATGL and HSL in whole kidney homogenates (n=3-6); *P<0.05, ** P <0.01, *** P <0.001.

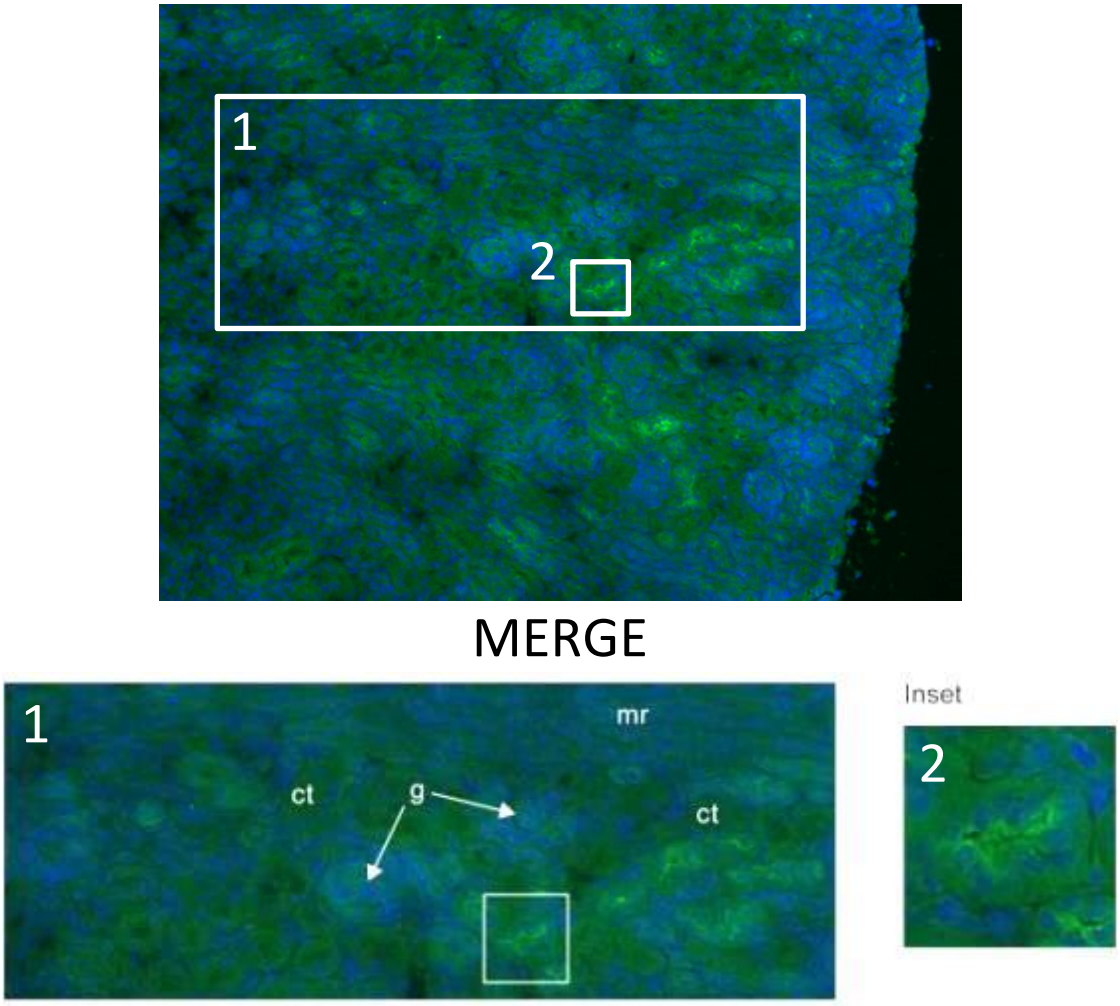

Figure 6: ATGL is immunodetected in kidney sections.
ATGL was visible by immunodetection in essentially all cell types in kidney sections. Green: Anti-ATGL, Blue: DAPI (nuclei). Top, left to right: Anti-ATGL alone, DAPI alone, merged image of ATGL and DAPI. Middle: Merged image of ATGL and DAPI staining for an axial cross-section of kidney. Insets 1 and 2 are magnifications of the merged image. Insets show increased ATGL staining intensity on the apical/ lumenal surface of renal tubule. g= glomerular cells; ct= convoluted tubules, mr= medullary rays

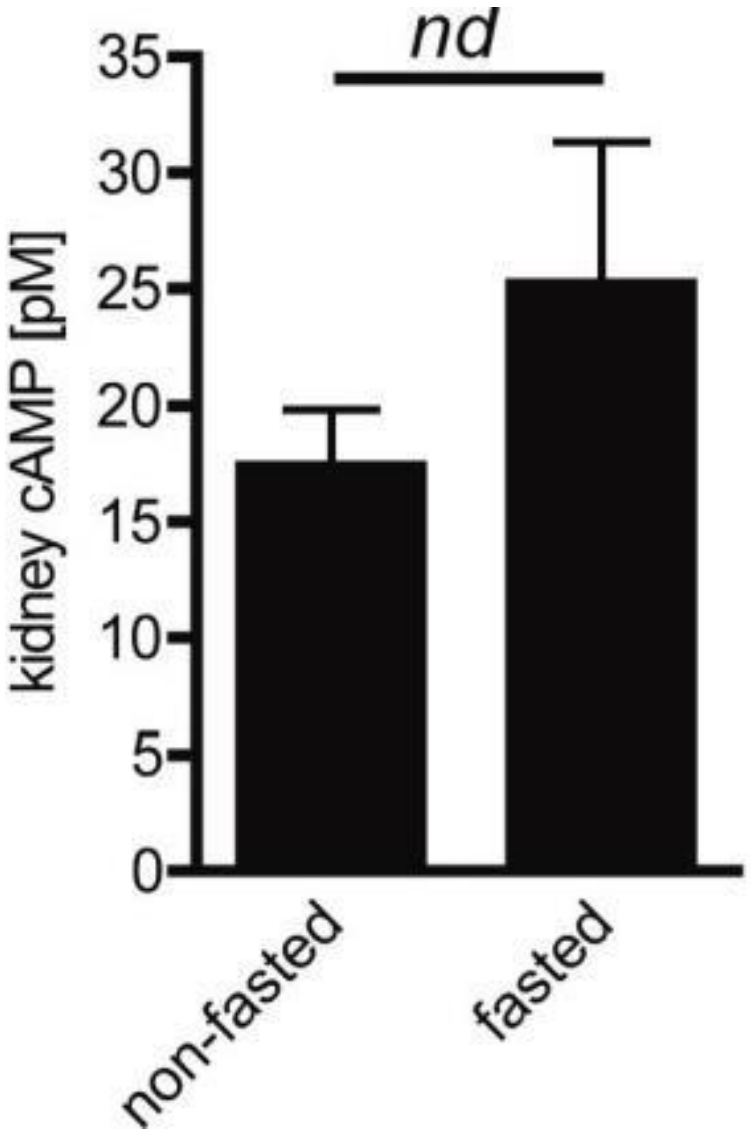

Figure 7: Kidney cAMP concentrations.
cAMP was isolated from kidneys of non-fasted and fasted mice (16 h) using water-saturated ether, and quantified by competitive ELISA. (n=4-6)

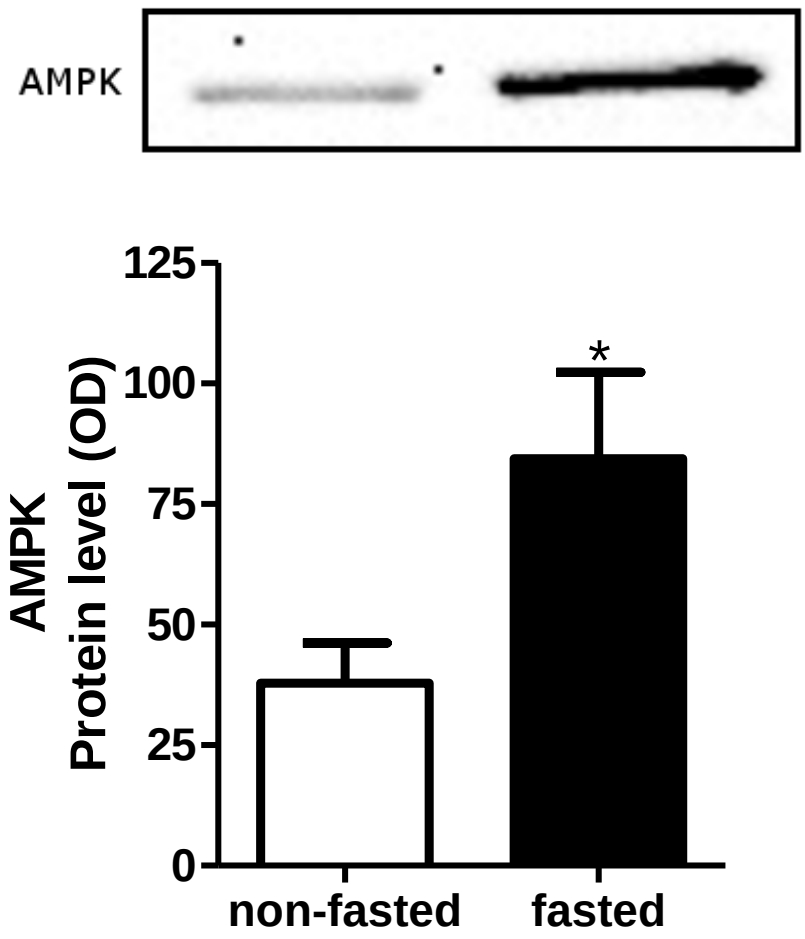

Figure 8: Fasting induces AMPK total protein in kidney.
Representative immunoblot and quantification of AMPK protein level in non-fasted and fasted female mice. AMPK protein level is induced following a 16 h fast. (n=4); *P<0.05

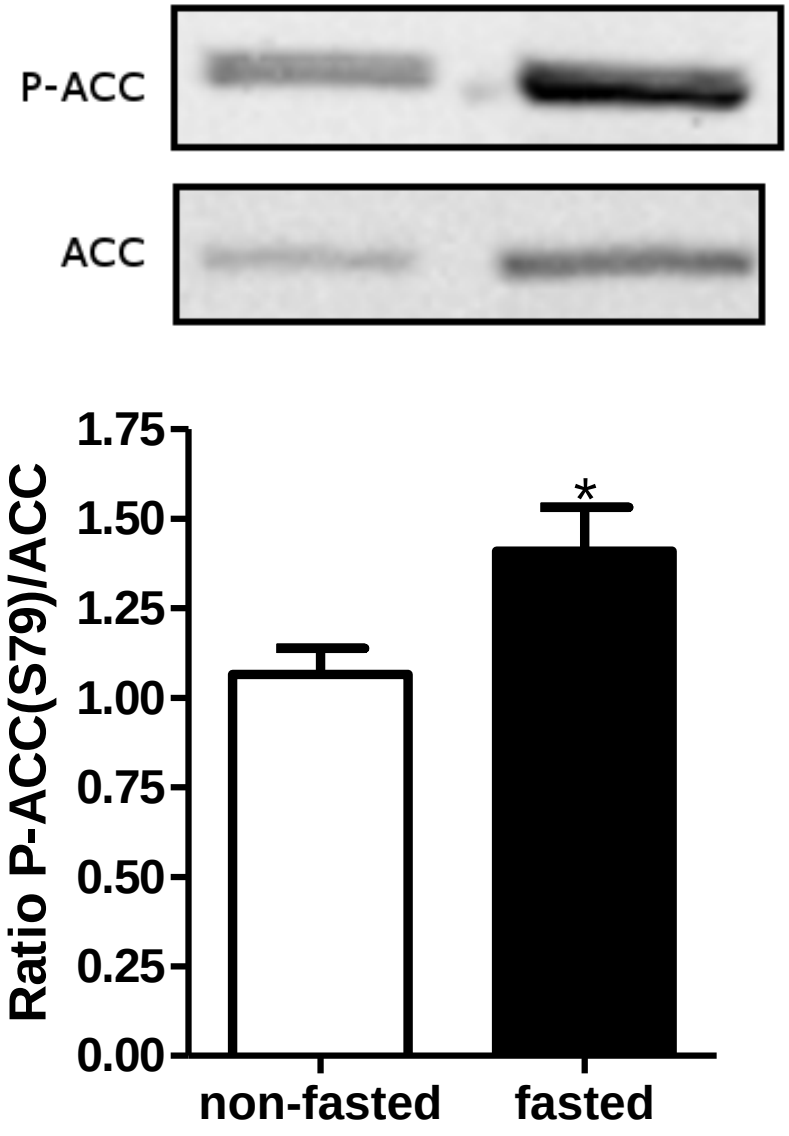

Figure 9: Fasting induces phosphorylation in the kidney of the AMPK target ACC at S79.
Top bands: Representative immunoblots of ACC and phospho-ACC phosphorylated at serine 79 in non-fasted and fasted mice. Bottom graph: The ratio of phospho-ACC to ACC protein level is higher following a 16 h fast. (n=4); *P<0.05

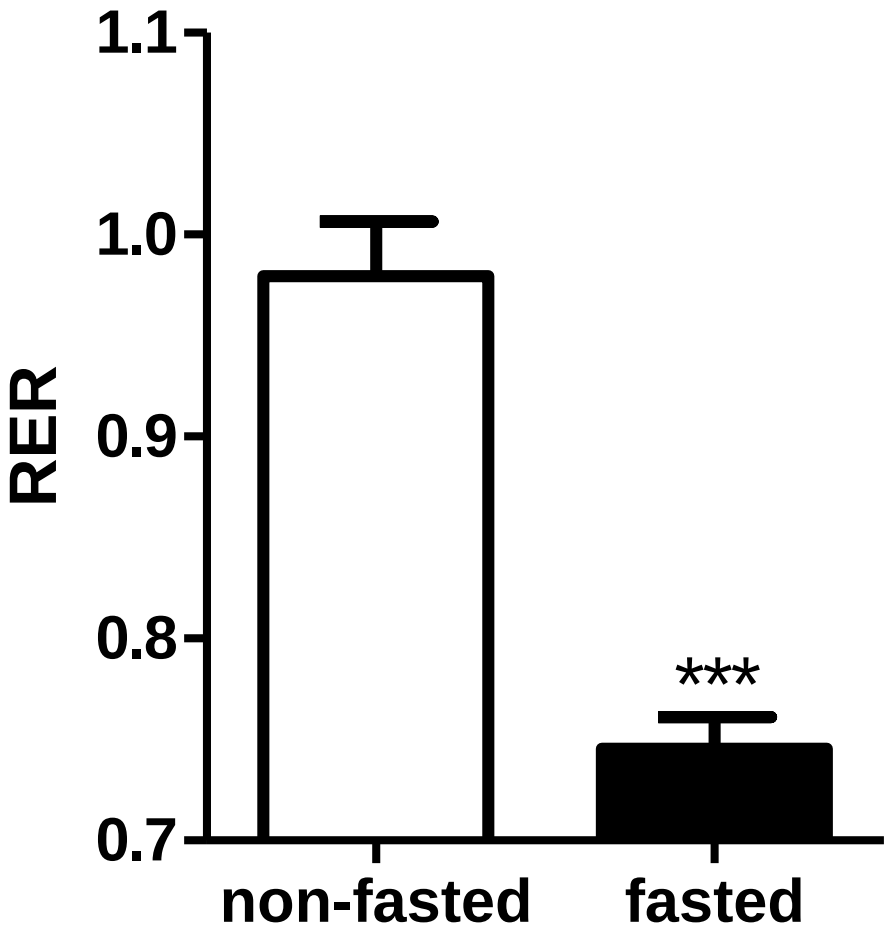

Figure 10: Respiratory exchange ratio (RER) in non-fasted and fasted mice.
The RER ratio of carbon dioxide production to oxygen consumption was measured to assess metabolic fuel usage in response to fasting. Fasted mice had lower RERs in response to fasting, indicating a shift in fuel usage from predominantly glucose metabolism to fatty acid beta-oxidation. (n=4-6); ****P*<0.001

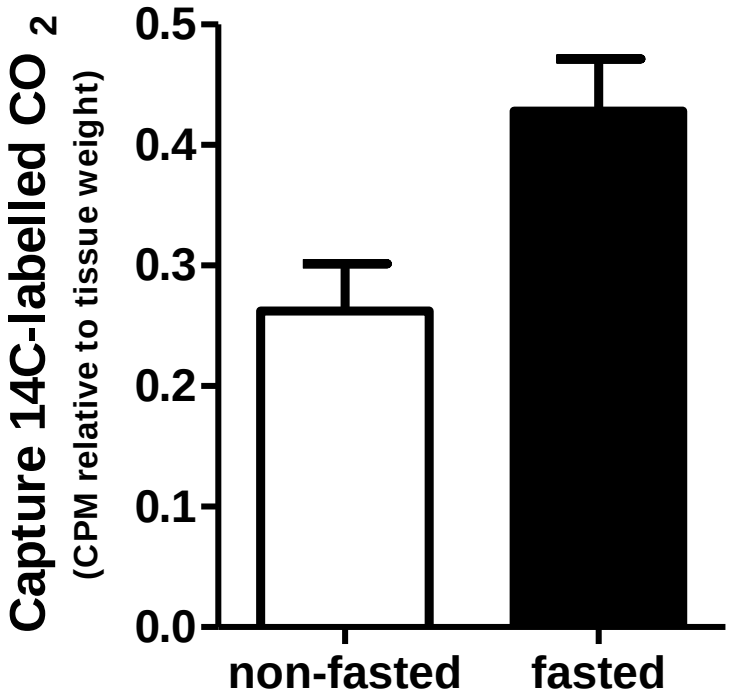

Figure 11: Whole kidney beta-oxidation.
Measure of $^{14}CO_2$ released from ^{14}C[palmitate] after reaction with kidney homogenates produced from non-fasted and 16 h fasted female mice. (n=4-6)

Discussion

To evaluate the suitability of targeting renal ATGL for the development of a lipid droplet accumulation model, I first characterized murine renal lipolysis. Here, I report the expression, regulation, and post-translational modification of ATGL and HSL, two TAG hydrolase enzymes, in murine kidney.

In agreement with others, I found that mRNA for *Atgl* and *Hsl* are expressed in murine whole kidney (31,72). I extended these findings by determining that ATGL protein is also present in the kidney, and investigated the localization of ATGL within murine kidney cryosections, finding ubiquitous expression across all cell types, with ATGL highly expressed in glomerular and tubule cells. Of interest, I found that ATGL was particularly concentrated near the apical surface of renal tubule cells, so that the action of ATGL in tubules would be concentrated around the lumen, where albumin-bound fatty acid reuptake occurs (55,56). To determine whether these lipid enzymes were nutritionally regulated in the kidney I performed immunoblots of whole kidney homogenates prepared from fasted mice and found that the expression of both ATGL and HSL was induced. I also found that transcriptional activation progressively increased after food withdrawal.

The finding of ATGL and HSL expression and nutritional regulation in the kidney suggested functional expression to support renal lipolysis. It is known that the kidney relies on fatty acid beta-oxidation (78) to meet the high metabolic demand created from regulating osmotic balance of the blood (79). I hypothesized that induction of lipolysis would occur to match substrate availability with demand since intracellular TAG is an important source of fatty acids for oxidative metabolism, particularly in the fasted state. I found total lipase activity was

significantly increased following fasting. Lipolysis is induced in states of elevated metabolic demand in order to mobilize fatty acids stored as TAG (16). Stored TAG is an important reservoir for fatty acids that can act as substrates for beta-oxidation, phospholipid synthesis, gluconeogenesis and signalling molecules. Corroborating my hypothesis of increased lipolysis to supply fatty acids as energy substrates, I found that fasting significantly increased renal fatty acid beta-oxidation, agreeing with reports that kidney extensively utilizes beta-oxidation for energy metabolism in the fasted state (66).

I also analyzed the expression of other genes involved in fatty acid metabolism for fasting-mediated regulation. Peroxisome proliferator-activated receptor alpha (*Pparα*), a master regulator of adaptive catabolic changes in lipid metabolism (80), was progressively elevated following food withdrawal, as was the Pparα-regulated fatty acid transporter *Cd36*, and Pparα-regulated acyl-CoA oxidase (*Aox*). These genes aid in the uptake and increased metabolism of fatty acids (17,63,81), and their expression, like that of *Atgl* and *Hsl*, is regulated at least in part in response to extracellular signals that change during fasting. However, PPARα-mediated gene regulation is also influenced by intracellular signals. In this regard, ATGL has been shown to be required for the generation of lipid ligands for PPAR activation (82,83), and ATGL deficiency resulted in a decrease in expression of PPARα and gamma target genes in cardiac myocytes (84). The induction of ATGL and HSL during fasting may contribute to the increased release of lipid ligands in renal cells, and this was likely a factor in the induction of PPARα target genes we observed during fasting.

I investigated kinases that may be involved in the fasting-mediated increase in renal lipolysis. We found no significant difference in levels of cAMP, which suggests that cAMP may

not be a large contributor to fasting-mediated effects. I did find an increase in total AMPK as well as an increase in the ratio of its phosphorylated target protein ACC(S79), implying that the fasting-mediated increase in renal lipolysis may be regulated by an induction of AMPK. AMPK acts as a cellular energy sensor and may be signalling to increase activity of ATGL through phosphorylation at the S406 site, to increase the supply of fatty acids for beta oxidation.

To support the notion that lipolysis is induced to match substrate supply with metabolic demand, we measured whole body oxygen consumption and carbon dioxide production and found, as expected, a reduction in RER, representing a shift towards the use of fatty acids as the main substrate for energy metabolism. The shift in whole body metabolism towards lipid oxidation serves to decrease the demand on glucose metabolism in most tissues, including kidney, in order to conserve glucose for brain energy metabolism.

The classical pathway of ATGL/HSL-mediated lipolysis is thus present and regulated by changing nutritional state within the kidney, indicating a role for lipolysis in kidney function. Given the importance of fatty acids to renal energy metabolism as well as the toxicity of excess stored lipid, these findings suggest that further investigation of the role of ATGL and HSL in renal lipid metabolism is merited.

CHAPTER 4 – Kidney renal tubule-specific ATGL ablation alters glycemic control in male mice.

Rationale

Renal accumulation of fatty acids during fasting occurs in excess of levels used for oxidation, leading to increased intracellular TAG (TAG) stores that must subsequently be hydrolyzed for use (57,67). Impaired hydrolysis, therefore, would be predicted to lead to TAG accumulation. I found ATGL mRNA and protein to be expressed in whole kidney homogenates, and I observed ATGL to be present in essentially all regions of the kidney cortex and medulla, including renal tubules. Therefore, I identified ATGL as a potentially important mediator of renal TAG hydrolysis. To determine whether ATGL is critical for renal tubule lipolysis, and to further determine whether disruption of renal tubule lipolysis causes evidence of the early pathology of CKD and the CKD-associated co-morbidities diabetes and CVD, I created a model of renal lipid accumulation by renal tubule-specific ablation of ATGL. Here, I describe the work completed to create **k**idney renal tubule-**s**pecific **A**TGL **k**nock**o**ut (KSAKO) mice, and my initial characterization of the consequences of altered renal lipolysis.

Objectives

To create and complete initial characterization of KSAKO mice as a model of lipid droplet accumulation.

Characterization will include investigating:

i. Body and tissue weights
ii. Renal expression of enzymes in lipolysis
iii. Renal expression of markers of fibrosis
iv. Renal expression of markers of inflammation

v. Kidney total TAG content

vi. Glucose tolerance and insulin sensitivity at ages 9 and 16 weeks

vii. Blood TAG concentrations

Hypotheses

Renal tubule-specific ATGL ablation will result in:

1. An increase in kidney mass, and a decrease in white adipose tissue mass, resulting in a lower body mass compared to wildtype (WT) mice.
2. A 30-50% decrease in total kidney ATGL protein level, but a compensatory induction of HSL by 20 weeks of age.
3. An increase in the mRNA expression of markers of fibrosis in the kidney by 20 weeks of age.
4. An increase in the mRNA expression of markers of inflammation in the kidney by 20 weeks of age.
5. An increase in kidney TAG concentration by 20 weeks of age.
6. Improved glucose tolerance and insulin sensitivity at 9 weeks of age, but impaired glucose tolerance and insulin sensitivity at 16 weeks of age.
7. Increased blood TAG concentrations at 20 weeks of age.

Methods

Study Design

All animal use protocols were approved by the Animal Care Committee at the University of Waterloo, with all procedures performed in accordance with the Canadian Council on Animal Care. Mice were bred in the Central Animal Facility at the University of Waterloo and were group housed in a controlled environment with constant temperature and humidity with a standard 12h light: 12h dark cycle. Male animals between 9-23 weeks of age were used for this study. Animals were provided *ad libitum* with water and a standardized chow diet prior to experiments. Fasted mice had food withdrawn at 5 pm and were fasted for 16 h overnight, prior to CO_2 asphyxiation and tissue collection.

ATGL Knockout Design

The generation of KSAKO utilized the Cre-LoxP-recombination system to excise the catalytic region of ATGL. ATGL flox/flox mice that were generously donated by Dr. Hei Sook Sul have loxP sites flanking the entire first exon that contains the serine/aspartate catalytic dyad (Figure **12**). These mice have been backcrossed for greater than 6 generations onto a C57Bl/6J background strain. In the absence of cellular cre-recombinase expression, the ATGL floxed gene is functional in all tissues of the body. We bred ATGL flox/flox mice at the University of Waterloo Central Animal Facility with commercially available transgenic mice that express cre-recombinase under control of the kidney-specific (Ksp) cadherin/cadherin 16 promoter (B6.Cg-Tg(Cdh16-cre)91Igr/J from Jackson Laboratories). These mice are also fully backcrossed (>9 generations) onto a C57Bl/6J background. Transgenic Cdh16-cre mice primarily express cre-recombinase in renal

tubule cells and glomeruli, and have been used previously to produce renal tubule-specific knockout mouse models (85,86). The expression of CRE recombinase in the presence of repeat LoxP sites results in the joining of LoxP sites and the deletion of the LoxP flanked region (Figure **12**).

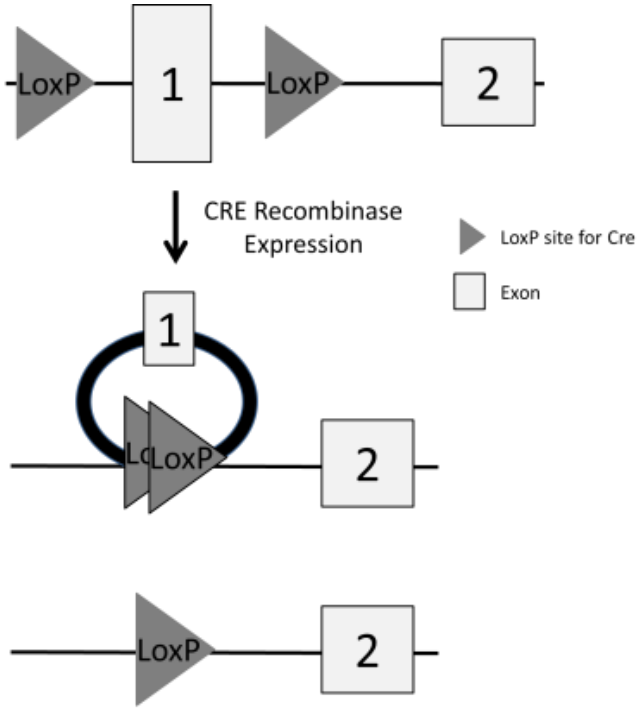

Figure 12**: CRE Recombination of LoxP sites over exon 1 of *Atgl*.**

To produce our KSAKO mice we first bred mice heterozygous for *Cre* recombinase with mice homozygous for the *Atgl* floxed allele. The progeny mice were genotyped for the presence of CRE recombinase and for heterozygosity of the *Atgl* floxed allele, and were backcrossed with mice heterozygous for the *Atgl* floxed allele, but lacking *Cre*, in order to generate mice homozygous for the *Atgl* floxed allele, with and without *Cre*. These mice were selected to become the parent generation of our study animals. Two principal breeding strategies were employed for our study generations. Breeding strategy 1: Mice homozygous for the *Atgl* floxed

allele and transgenic for *Cre recombinase* were mated with mice heterozygous for the *Atgl* floxed allele but lacking the *Cre recombinase* transgene to produce 25% KSAKO, 25% Htz, and 50% WT mice (Figure 13). KSAKO mice are progeny that are homozygous for the *Atgl* floxed allele, and transgenic for *Cre recombinase*. Mice heterozygous deficient in ATGL (Htz) mice are heterozygous for the ATGL floxed allele, and transgenic for *Cre recombinase*. Wildtype (WT) mice are not transgenic for *Cre recombinase*. WT mice may be either homozygous or heterozygous for the *Atgl* floxed allele, but in the absence of CRE Recombinase, the LoxP sites do not recombine and do not affect the structure or function of the gene, making these mice indistinguishable from unaltered C57Bl/6J mice. Breeding strategy 2: Mice homozygous for the *Atgl* floxed allele and transgenic for *Cre recombinase* were mated with mice homozygous for the *Atgl* floxed allele but lacking the transgene for *Cre recombinase* to produce 50% KSAKO and 50% WT mice (Figure 14).

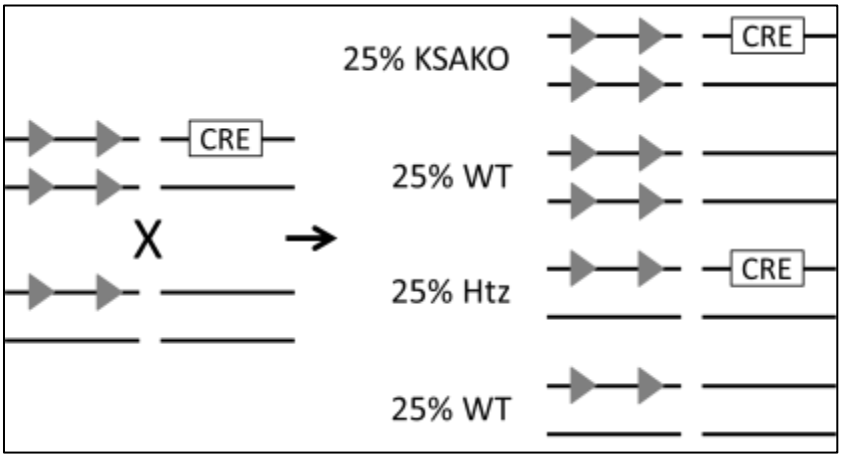

Figure 13: Breeding Strategy 1.
Left side: Mice homozygous for floxed *Atgl* and transgenic for Cre were mated with mice heterozygous for floxed *Atgl* and lacking the Cre transgene. The predicted progeny are illustrated on the Right side. Solid arrow heads illustrate LoxP sites flanking exon 1 of *Atgl*. "CRE" indicates presence of the *Cre recombinase* transgene.

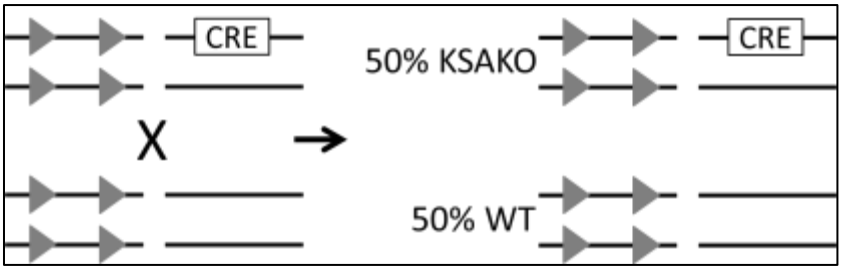

Figure 14: Breeding Strategy 2.
Left side: Mice homozygous for floxed *Atgl* and transgenic for ***Cre recombinase*** were mated with mice homozygous for floxed *Atgl* and lacking the ***Cre recombinase*** transgene. The predicted progeny are illustrated on the **Right side**. Solid arrow heads illustrate LoxP sites flanking exon 1 of *Atgl*. "CRE" indicates presence of the *Cre recombinase* transgene.

Genotyping PCR

Ear notches were taken from 4 week old mice and frozen in a -80C freezer until processing. DNA was extracted from the ear notches using a NaOH extraction procedure (87). NaOH was added to the ear notches and they were heated at 95°C for 1 h, then Tris–EDTA was added to neutralize the samples. Samples were stored at -20°C or used immediately. DNA samples were added to a mixture of Taq Polymerase (Sigma-Aldridge), containing $MgCl_2$, dNTPs, H_2O, and the appropriate forward and reverse primers (Table 1). Samples were placed in a thermal cycler (BIO-RAD) and denatured for 5 min at 95°C, then cycled for 30 cycles of denaturing for 30 s at 95°C, annealing for 30 s at 60°C, and extension for 45 s at 72°C. Following amplification, samples were loaded and separated in a 2% agarose gel containing 0.01% ethidium bromide (Sigma), and then imaged using the ChemiGenius 2 Bio-Imaging System (Syngene).

It should be noted that genotyping for knockout animals was challenging because the gene is excised only in certain cell types of the kidneys of mice expressing CRE Recombinase. Thus,

ear notches of mice contain the full *Atgl* gene that is flanked by *LoxP* sites, but that has not had exon 1 removed. The *LoxP* sequence is only 34 bp in length, which constitutes a relatively small genetic modification (Figure 15). Therefore, I devised a PCR-based genotyping protocol based on size differences produced by the presence of the LoxP site and associated vector DNA in the 3' region of exon 1. PCR for the mutant allele results in the amplification of a 315 bp amplicon containing a region of exon 1 along with the *LoxP* site in the centre. PCR for the wildtype allele goes over a region that does not contain the *LoxP* site resulting in a smaller amplicon of length 180 bp. Mice homozygous for the *Atgl* floxed allele contained a band that was 315 bp in size, while heterozygous mice contained a band at both 315 bp and 180 bp. Mice lacking the *LoxP* sites were not expected or observed in our genotyping.

We genotyped mice for the *Cre recombinase* gene using PCR. PCR for *Cre recombinase* resulted in the generation of a 270 bp amplicon in mice carrying the transgene. When combined with genotyping results for the floxed allele, this allowed us to identify KSAKO, Htz mice, and wild type control mice.

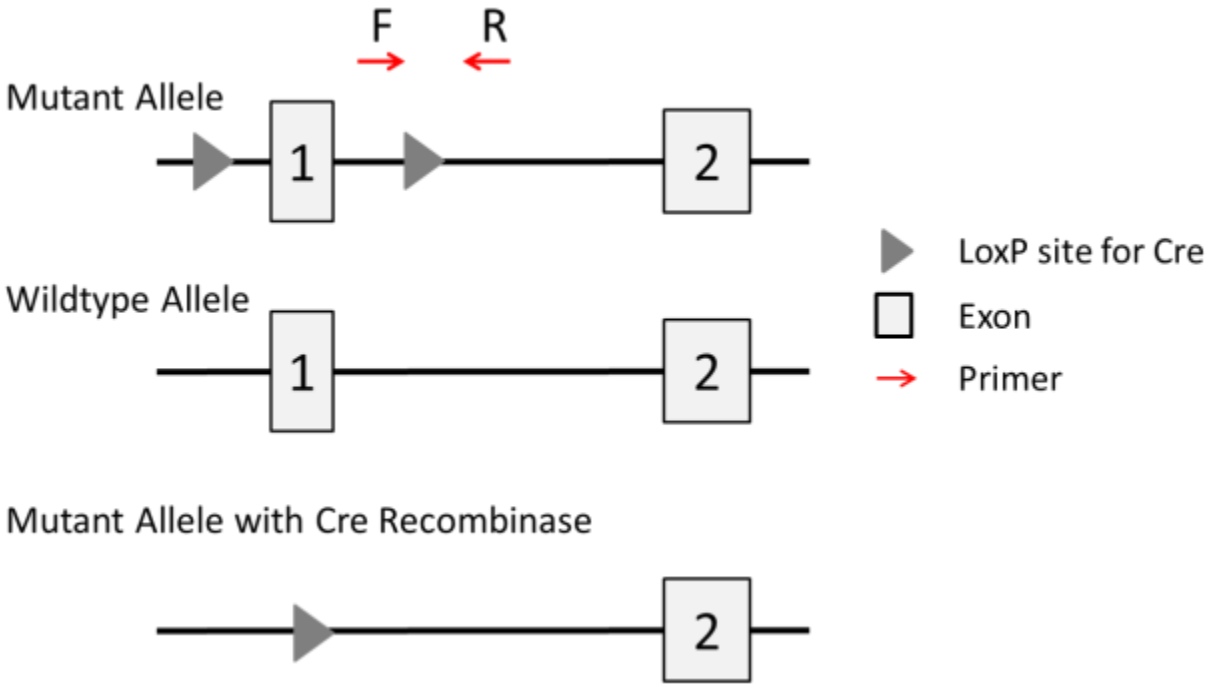

Figure 15: Primer Design for genotyping.
PCR across a region of DNA containing the *LoxP* site and associated vector DNA in floxed mice identified a 315 bp band. A 180 bp band is generated when the *LoxP* site is absent.

Adipose Tissue Depot Collection

Mice were euthanized and blood was taken by cardiac puncture. Mice were then laid in a dorsal recumbent position on the dissection table. A sagittal incision was made from the sternum to the lower pelvis region. The adipose tissue surrounding the intestinal walls, termed visceral adipose tissue, was removed by carefully peeling the adipose away from the intestines using fine tweezers. After removing the visceral adipose tissue the kidneys were exposed. The kidneys were removed with adipose tissue attached, and then the adipose surrounding the kidney, termed peri-renal adipose tissue, was excised with fine tweezers. The adipose tissue dorsal to the kidneys and lying next to the spine, termed retroperitoneal adipose tissue, was then removed. The gonadal adipose, posterior to the kidneys and surrounding the pelvic region

was excised and carefully dissected from reproductive organs. For collection of subcutaneous adipose, while holding the rib cage, the outer layer of skin was peeled away to expose the subcutaneous adipose tissue. The two subcutaneous adipose tissue depots collected lay next to the ribcage and posterior to this in the hind region. The mouse was then laid in ventral recumbency on the dissection table and a sagittal incision was made along the spine and the outer layer of skin was held open. The adipose tissue depot between the shoulder blades, termed brown adipose tissue, was excised with careful attention to remove the adipose depot from the back muscles and to avoid white adipose tissue that may surround the brown adipose (Figure 16).

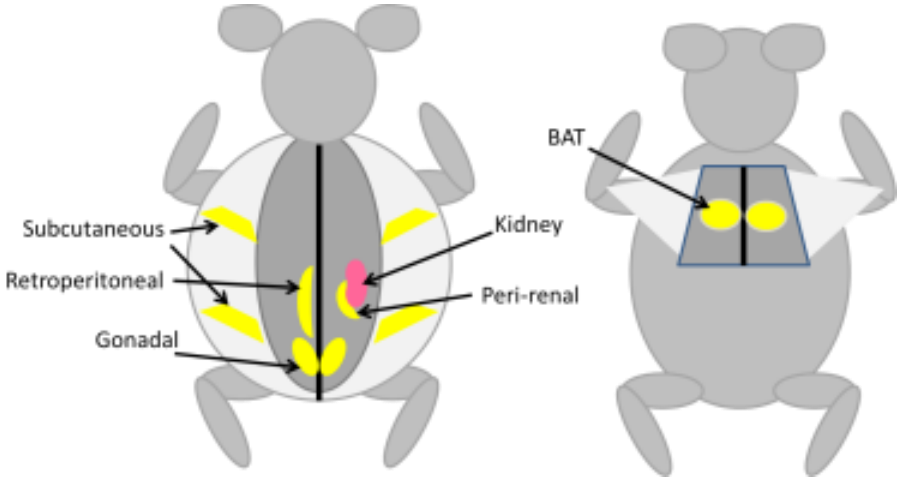

Figure 16: Locations of adipose tissue depots excised.

Immunoblotting

Whole kidneys were homogenized on ice using a Polytron tissue homogenizer in lysis buffer (150 mM NaCl, 0.5% sodium deoxycholate, 0.1% SDS, 50mM Tris, 1% Triton X100, pH 8.0) with protease inhibitor cocktail (1:100) (Sigma Aldrich, Mississauga, Canada), followed by centrifugation at 9,000 × g for 15 min at 4°C. Sample protein concentrations were determined by bicinchoninic acid assay (Sigma Aldrich, Mississauga, Canada). Laemmli buffer with 2-mercaptoethanol was added to samples followed by heat denaturing at 95 °C for 5 min. Samples were electrophoresed through 10% SDS-PAGE gels and wet-transferred to nitrocellulose membranes at a constant 350 mA for 90 min. Membranes were blocked overnight at 4°C with 5% (w/v) skim milk blocker in TBST. Membranes were then incubated, shaking for 2 h at room temperature with primary antibodies (mouse-Anti-ATGL, Cell Signaling, Danvers, MA, USA) (1:1000 in TBST with 2% blocker). Membranes were washed 3 times in TBST, then incubated for 1 h with horseradish peroxidase-conjugated secondary antibodies (Santa Cruz Biotechnology, Dallas, TX, USA) (1:5000 in TBST with 2% skim milk blocker). Membranes were washed 3 times with TBST. Immunoblots were visualized by enhanced chemiluminescence on a ChemiGenius 2 Bio-Imaging System (Syngene).

RT-qPCR

Total RNA was extracted from whole kidneys using TRI Reagent® (Sigma Aldrich, Mississauga, Ontario, Canada). Whole kidney was homogenized using a Polytron tissue homogenizer to isolate RNA from cells. Chloroform was added to samples to separate RNA from cell constituents. The aqueous phase, containing the RNA, was collected. Isopropanol was added to precipitate the RNA. The RNA pellet was washed with ethanol, resuspended in

RNAase free water, and heated for 10 min at 55°C, to denature RNAases. Two micrograms of RNA was reverse transcribed using a high-capacity cDNA reverse transcriptase kit (Life Technologies, Burlington, Ontario, Canada) containing a reaction buffer, random primers and dNTP mix and heated in a thermal cycler at 25°C for 10 min, 37°C for 120 min, 85°C for 5 min and then kept at 4°C. qPCR was performed using SsoFast EvaGreen master mix (Bio-Rad Laboratories, Mississauga, Ontario, Canada) containing SsoFast Eva Green super mix, forward and revers primers (TABLE) and amplified with the conditions: 95°C for 2 min, followed by 40 cycles of 95°C for 10 s, 60°C for 20 s, followed by melt curve analysis to verify a single amplicon. Expression of test genes were normalized to *18s* and analyzed by the delta Ct method.

Whole Kidney TAG quantification

Total lipid extraction was performed on whole kidneys according to the method of Folch (88). Whole kidneys were homogenized in 2:1 chloroform: methanol. After homogenization, sodium phosphate was added and the aqueous and organic layers were allowed to separate. A second extraction was performed to remove contaminants. The organic layer was aliquotted and dried down. The lipid was then resuspended in chloroform and spotted onto a silica gel G plate along with standards and resolved by thin layer chromatography in a hexane: diethyl ether:acetic acid (80:20:2) solvent front. Bands corresponding to TAG were identified with the standards and scraped for quantification by gas-phase chromatography.

Glucose Tolerance Testing

To perform glucose tolerance testing, mice were fasted overnight with food removal at 6pm on the evening prior to testing. Blood glucose values were measured using an ACCU-CHEK®

Aviva Nano glucose monitor (Roche Technologies, Basel, Switzerland) with blood drop samples obtained by tail prick (~3 µl). Fasting glucose measures were recorded at 12 pm. Following fasting glucose measurement *i.p.* injections of sterile 20% D-glucose solutions, prepared fresh, were given using 25 gauge (2/3 inch) injection needles. Dosages were based on weight of the animal at 2 mg glucose per gram body weight. Injections were spaced 5 min apart to allow for measurement time. Blood glucose readings were taken at 15, 30, 45, 60, 90, and 120 min after glucose *i.p.* injection.

Insulin Tolerance Testing

To perform insulin tolerance testing, mice were fasted for 5 hr on the morning of testing, with food removal at 8 am. Blood glucose values were measured using an ACCU-CHEK® Aviva Nano glucose monitor (Roche Technologies, Basel, Switzerland) with blood drop samples obtained by tail prick (~3µl). Baseline fasting glucose measures were recorded at 1 pm. Following the fasting glucose measure mice were given *i.p.* injections of a sterile 50 mU stock insulin solution with 25 gauge (2/3 inch) injection needle. Insulin solutions were prepared fresh in 1X sterile PBS. Dosages were based on weight of the animal at 0.5 mU insulin per gram of body weight. Injections were initiated 5 min apart to allow for measurement time. Blood glucose readings were taken at 15, 30, 45, 60, 90, 120 min after insulin *i.p.* injection.

Plasma Lipid Determination

Blood from animals was collected via cardiac puncture and spun at 1,500 rpm to separate plasma. Plasma was frozen at -80 degrees for further processing. A triglyceride quantification assay kit was used to assess plasma TAG (Cayman Chemical, Ann Arbor, MI, USA). 10 µl of plasma sample was added 150 µl of enzyme buffer solution. The enzyme buffer solution

contains lipase which hydrolyzes TAG to glycerol and free fatty acids. The glycerol is measured by a coupled enzymatic reaction that forms hydrogen peroxide. A peroxidase then catalyzes the redox-coupled reaction of hydrogen peroxide with a dye, producing a bright purple color. The assay was incubated at room temperature for 15 min protected from light. The reactions were quantified by measurement in a microplate reader at 550 nm. Sample readings were converted to TAG concentrations using a standard curve generated using standards supplied with the assay kit.

Statistical Analysis

Mice were divided into two groups based on expression of ATGL (WT vs KSAKO). Statistically significant differences between two groups were assessed by Student's *t* test. The results are expressed as means +/- S.E.M. Unless indicated, different groups contain at least three animals per group, although up to 22 animals per group were used for some experiments. Significance is reported as: *, $P<0.05$; **, $P<0.01$; ***, $P<0.001$.

Results

ATGL reduction in KSAKO mouse kidney

The relative expression of ATGL was determined in KSAKO mouse kidneys by qRT-PCR and western blot analysis. *Atgl* mRNA was found to be 25% lower in KSAKO mouse whole kidney homogenates than in WT kidney homogenates ($P<0.05$) (Figure 19). The total protein level of ATGL in KSAKO mouse kidneys was found to be decreased by 33% ($P<0.01$) (Figure 20, 21).

ATGL expression in other tissues

To determine whether our model of *Atgl* knockout was indeed renal tubule-specific, we assessed the expression of ATGL in additional tissues. We found no decrease in immunodetectable levels of ATGL protein in heart (Figure 22). However, there was a significant increase in peri-renal ATGL protein, by 248% ($P<0.01$) (Figure 23, Figure 24).

HSL expression in KSAKO mouse kidney

Induction of other TAG lipases could compensate, at least in part, for loss of *Atgl*. The relative expression of *Hsl* was determined in KSAKO mouse kidneys by qRT-PCR. The relative expression of *Hsl* mRNA in KSAKO mice kidneys was found to be induced by 74% ($P<0.05$) (Figure 25).

Body Weights

Animal body weights were measured weekly for 20 wks (Figure 26), and no significant difference in body weight was detected at any single time point (Figure 27). However, analysis of the incremental change in body weights by analysis of areas under the curve demonstrated that KSAKO animals gained weight faster than WT mice ($P<0.05$) (Figure 28).

Tissue Weights

Tissues were excised and weighed from 20 wk-old mice that had been fasted for 16 h overnight. KSAKO kidney and liver weights were both increased by ~12% compared to WT mice (P<0.05). The heart, spleen, and lungs of KSAKO mice were not significantly different in weight between WT and KSAKO mice (P>0.05) (Figure 29).

Adipose tissue depots were excised and weighed. We found the following significant (P<0.05) decreases in KSAKO adipose tissue masses compared to WT tissues: BAT (17%), subcutaneous (45%), peri-renal (86%), and retro-peritoneal (81%). The gonadal and visceral adipose depots did not significantly differ in weight between WT and KSAKO mice (Figure 30).

Inflammatory marker mRNA expression in KSAKO mouse kidney

Impaired TAG hydrolysis is expected to cause TAG accumulation with lipotoxic consequences including cell and tissue damage that may stimulate an immune response. The relative mRNA expression of inflammatory markers, including *Il-6*, *Il-1b*, and *TNF-alpha* was determined by qRT-PCR. The relative expression of *Il-6* was induced by 312% in KSAKO kidney compared to WT mice (P<0.01). The relative expression of *Il-1b* and *TNF-alpha* were unchanged in KSAKO kidney compared to WT mice. Fibrosis is also commonly induced in kidney in response to cellular or tissue injury, and typically accompanies or follows immunocyte infiltration. The relative expression of *fibronectin* in KSAKO kidney was induced by 38% compared to WT mice (P<0.05) (Figure 31).

TAG levels in kidney tissue

TAG levels in KSAKO kidney tissue not found to be significantly different from WT mice at 20 wks as measured by lipid extraction and gas chromatography (Figure 32). TAG levels in renal tubules, specifically, were not analyzed.

Serum TAG concentration

Serum TAG concentration was measured in WT and KSAKO mice at 20 wks using a colorimetric protocol. Serum TAG concentration were increased by 25% however this was not found to be significantly different in KSAKO mice compared to WT mice (Figure 33).

Glucose Tolerance and Insulin Sensitivity

Glucose tolerance testing was performed on mice after a 16 h overnight fast. At 9 weeks of age, after intraperitoneal glucose injection, KSAKO mice had a significantly lower plasma glucose response compared to WT mice as assessed by area under the curve ($P<0.05$). KSAKO mice had significantly lower plasma glucose concentrations at 30 and 45 minutes after glucose injection ($P<0.05$) (Figure 34). At 16 weeks of age, after intraperitoneal glucose injection, KSAKO mice had a significantly elevated plasma glucose response compared to WT mice as assessed by area under the curve ($P<0.05$). KSAKO mice had significantly elevated plasma glucose concentrations at 15, 30 and 45 minutes after glucose injection ($P<0.05$) (Figure 36).

Insulin tolerance testing was performed on mice after a 5 h fast. At 9 weeks of age, after *i.p.* insulin injection, KSAKO mice had a significantly lower plasma glucose level compared to WT mice as assessed by area under the curve ($P<0.05$). Specifically, KSAKO mice had significantly lower plasma glucose concentrations at 30, 45, 90 and 120 minutes after insulin injection

(*P*<0.05) (Figure 35). At 16 weeks of age, after *i.p.* insulin injection, KSAKO mice had a significantly higher plasma glucose level compared to WT mice as assessed by area under the curve (*P*<0.05). KSAKO mice had significantly elevated plasma glucose concentrations at 30 and 45 minutes after insulin injection (*P*<0.05) (Figure 37).

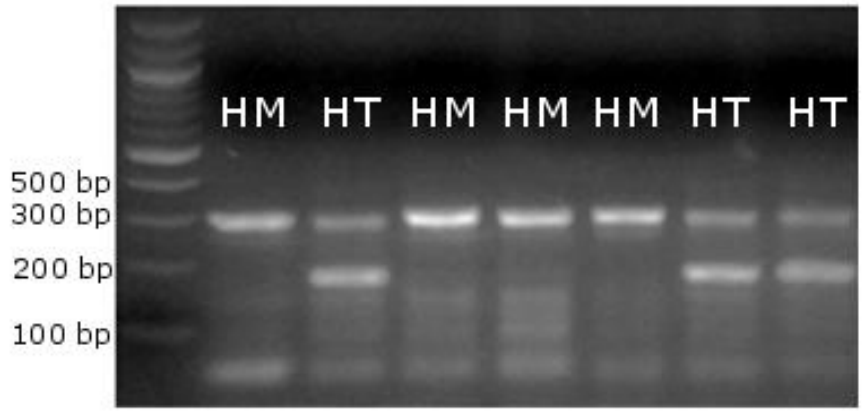

Figure 17: ATGL genotyping for presence of the floxed allele.
Genotyping for the *Atgl* floxed allele to distinguish heterozygotes from homozygotes was performed by PCR and gel electrophoresis. Mice homozygous for the *Atgl* floxed allele amplified a single band at 315 bp. Mice heterozygous for the *Atgl* floxed allele gave two bands at 315 bp and 180 bp. HM=homozygous for *Atgl* floxed allele, HT= heterozygous for *Atgl* floxed allele.

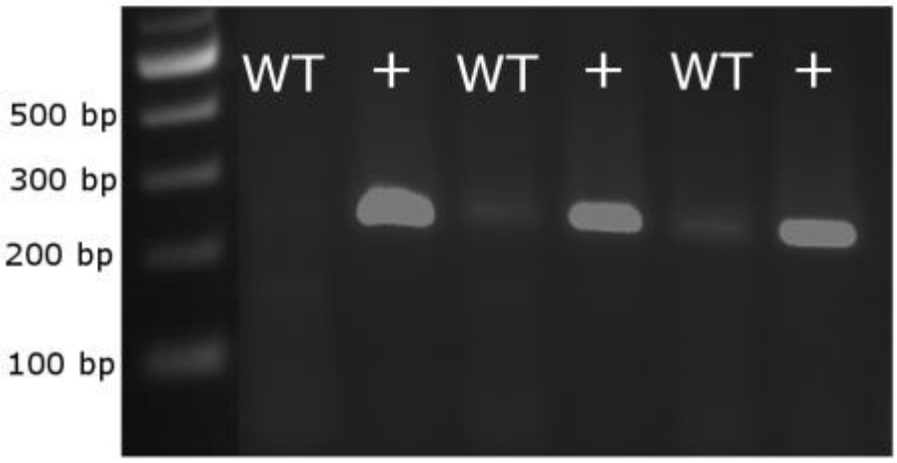

Figure 18: Cre genotyping.
Genotyping for the *Cre recombinase* gene to further distinguish KSAKO or Htz mice from WT mice was determined by PCR and gel electrophoresis. Mice transgenic for *Cre* show a bright band at 270 bp whereas mice that lack *Cre* show no band. WT= no *Cre* transgene, += *Cre* transgene is present.

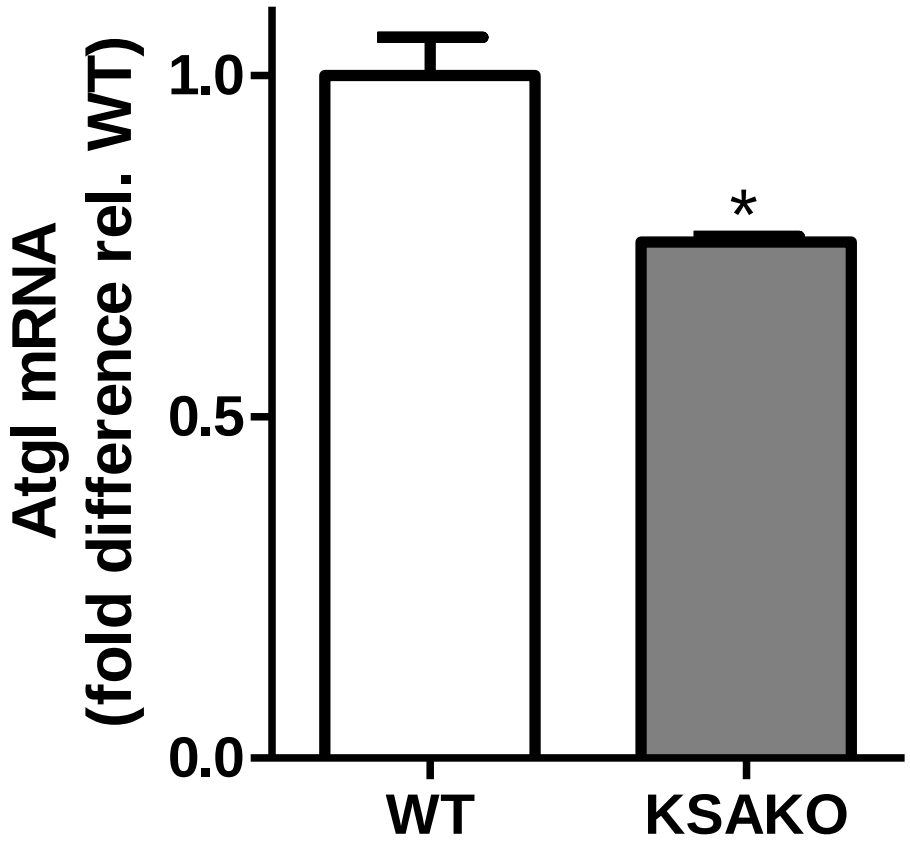

Figure 19: ATGL mRNA expression in kidney.
Atgl mRNA expression in kidney of male WT and KSAKO mice (age 20 weeks). (n=4-6); *P<0.05

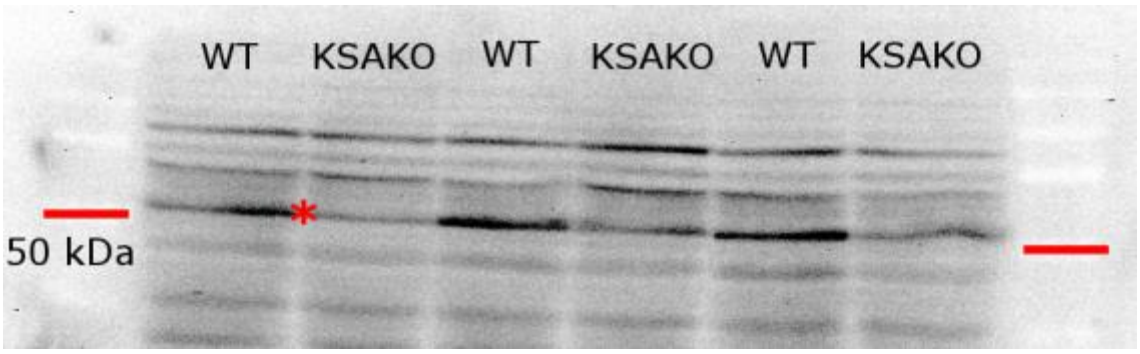

Figure 20: Kidney ATGL protein level in WT and KSAKO mice.
Immunoblot of ATGL (~54 kDa) protein in 20 wk old WT and KSAKO mouse kidneys. Red bars indicate 50 kDa molecular weight marker. * indicates ATGL protein band.

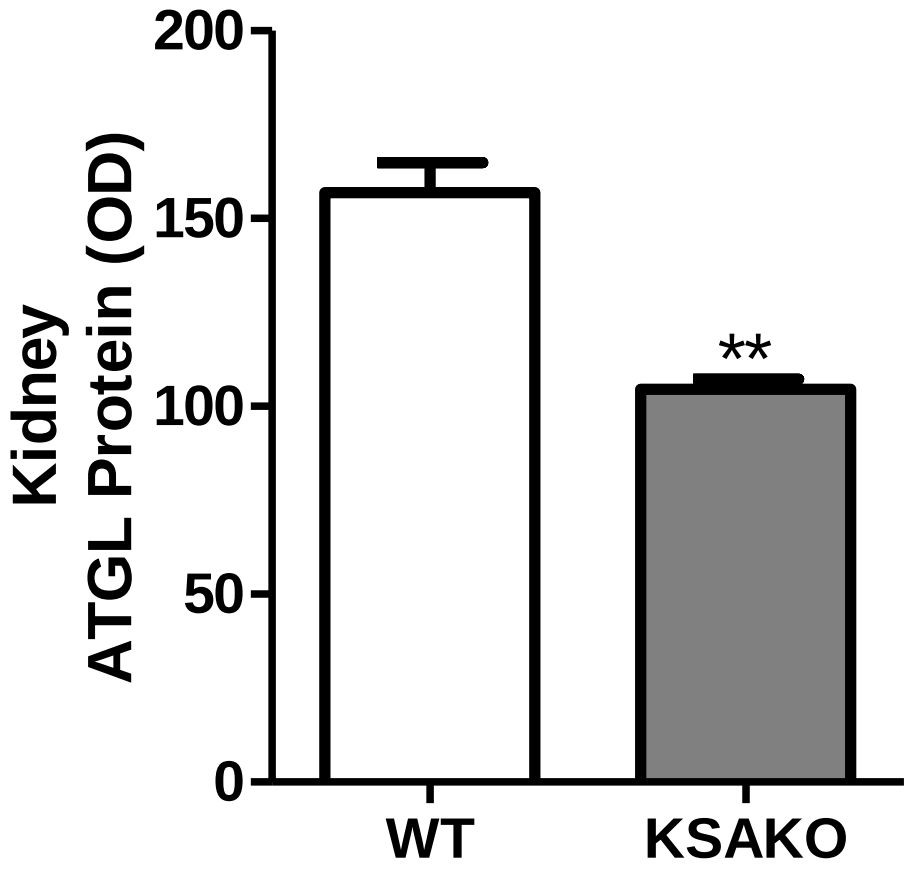

Figure 21: Quantification of ATGL protein in kidney.
Immunoblot quantification of ATGL protein level in kidneys of male mice (20 wks). ATGL protein level in kidney tissue of KSAKO mice is significantly decreased compared to WT mice (n=4-6); ***P*<0.01.

Figure 22: Heart ATGL protein level in KSAKO mice.
Immunoblot of ATGL (~54 kDa) protein in heart tissue of WT, Htz, and KSAKO mice at 20 wks of age. Red bar indicates 50 kDa molecular weight marker.

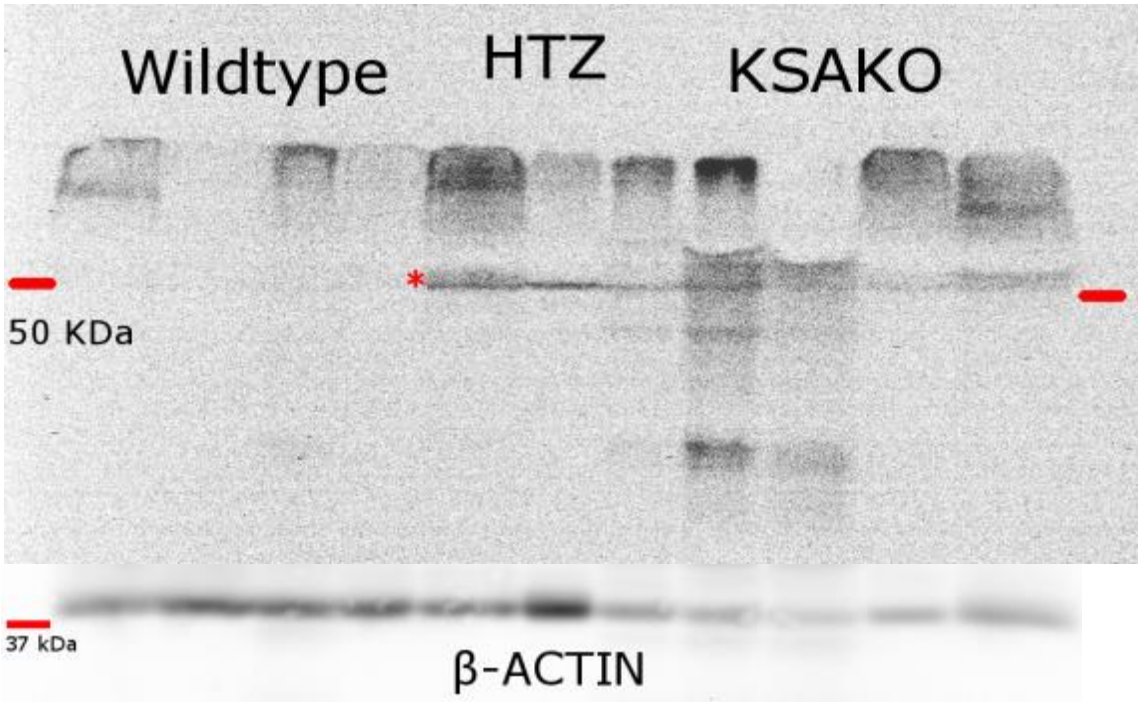

Figure 23: ATGL protein level in peri-renal white adipose tissue.
Immunoblot of ATGL (~54 kDa) protein in peri-renal adipose tissue of WT, Htz, and KSAKO mice at 20 wks of age. β-Actin (42 kDa) is shown as a loading control to indicate that the greater expression of ATGL in Htz and KSAKO mice is not due to unequal loading.

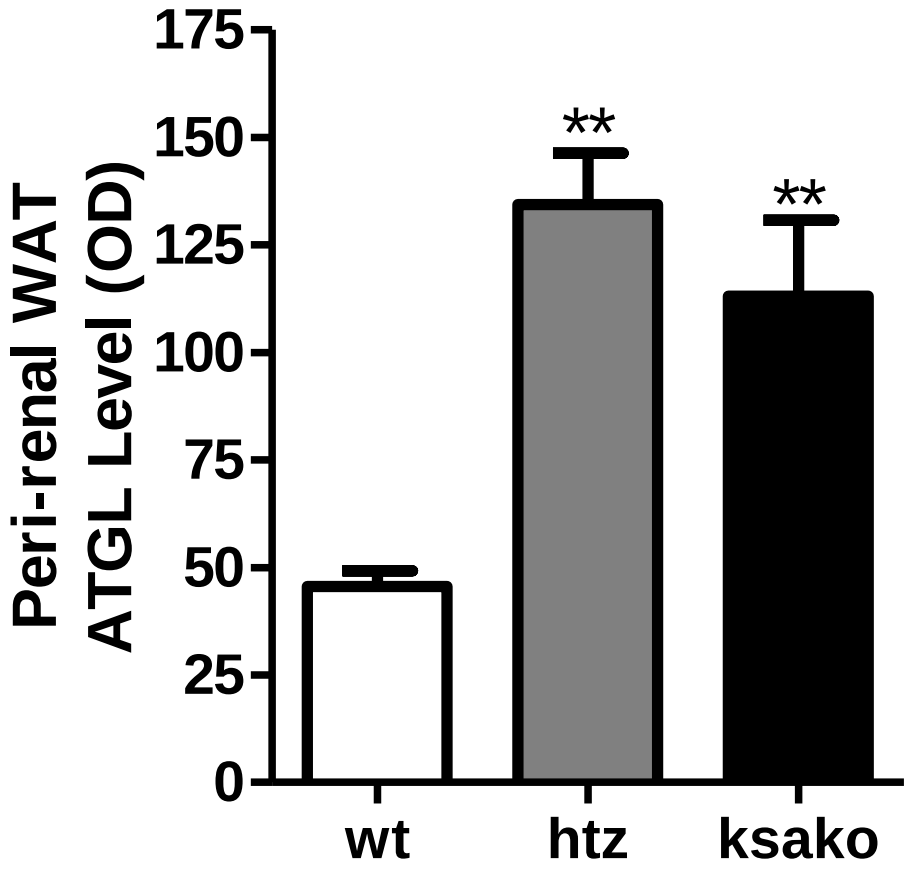

Figure 24: Quantification of peri-renal adipose tissue ATGL protein level.
Quantification of peri-renal adipose tissue ATGL protein level in WT and KSAKO male mice (20 wks). ATGL protein level is increased in peri-renal adipose tissue of KSAKO mice compared to WT mice. (n=4-6); ***P*<0.01.

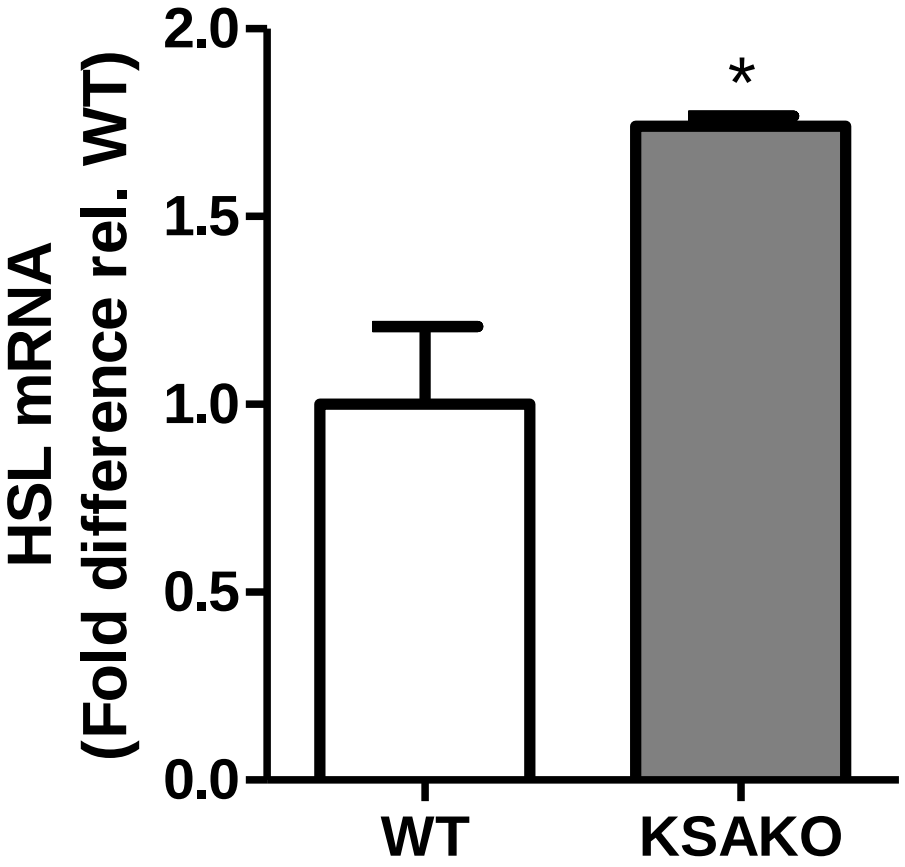

Figure 25: Expression of *Hsl* mRNA in kidney.
Gene expression of *Hsl* mRNA in kidney tissue of KSAKO mice compared to WT mice (20 wks) as determined by qPCR. (n=4-6); *P<0.05.

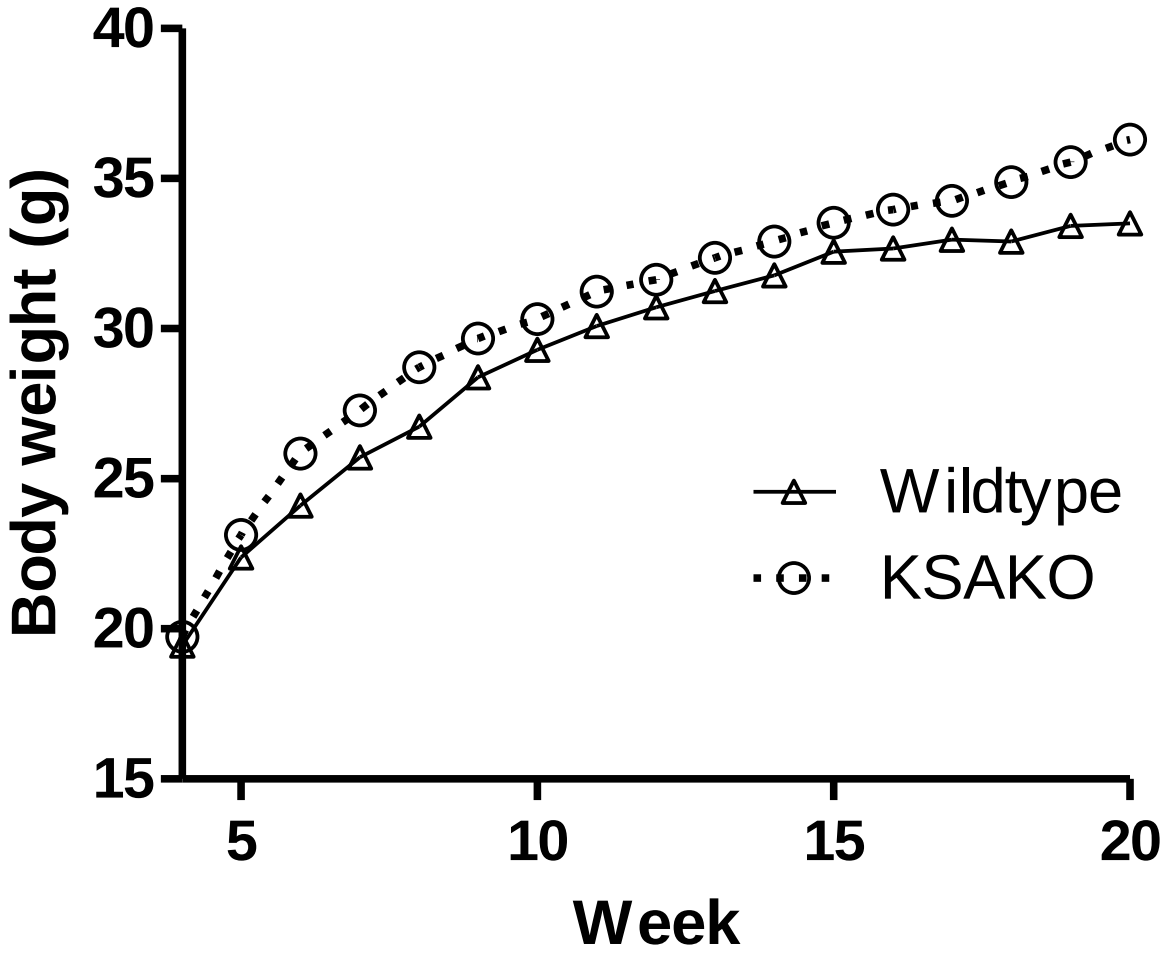

Figure 26: Body weight of KSAKO mice.
Body weights of male KSAKO mice compared to WT mice as measured weekly from age 4-20 wks. (n=9-22).

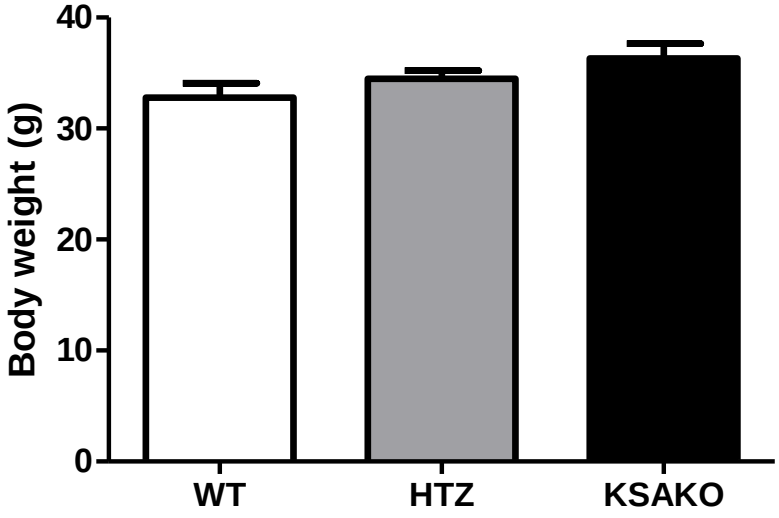

Figure 27: Body weight of KSAKO mice at 20wks.
Body weights of WT, Htz, and KSAKO male mice at 20 wks of age. There were no significant differences in body weight between the three groups. (n=5-22); *P*>0.05

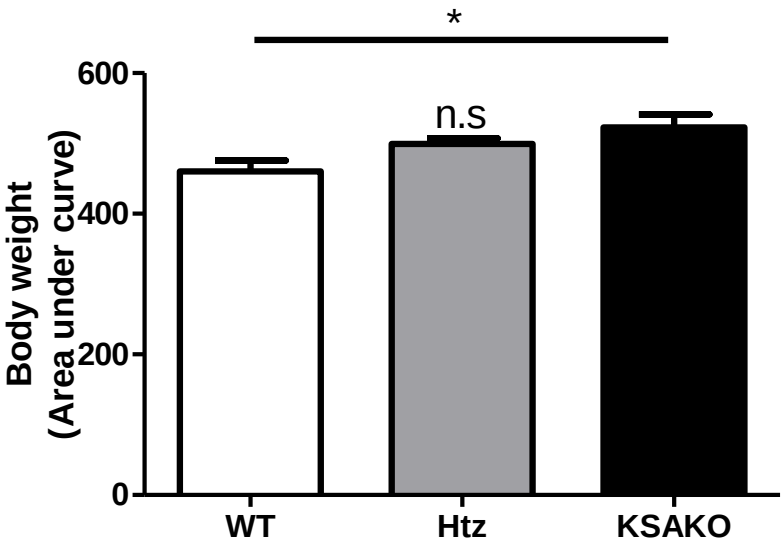

Figure 28: Area under curve analysis of body weights for KSAKO mice.
Area under the curve analysis of KSAKO male mice body weights over the first 4-20 weeks of life. KSAKO mice had a significantly larger area under the curve compared to WT mice (*P*<0.05). Htz mice had an intermediate phenotype that did not differ significantly from either WT or KSAKO mice. (n=5-22); **P*<0.05

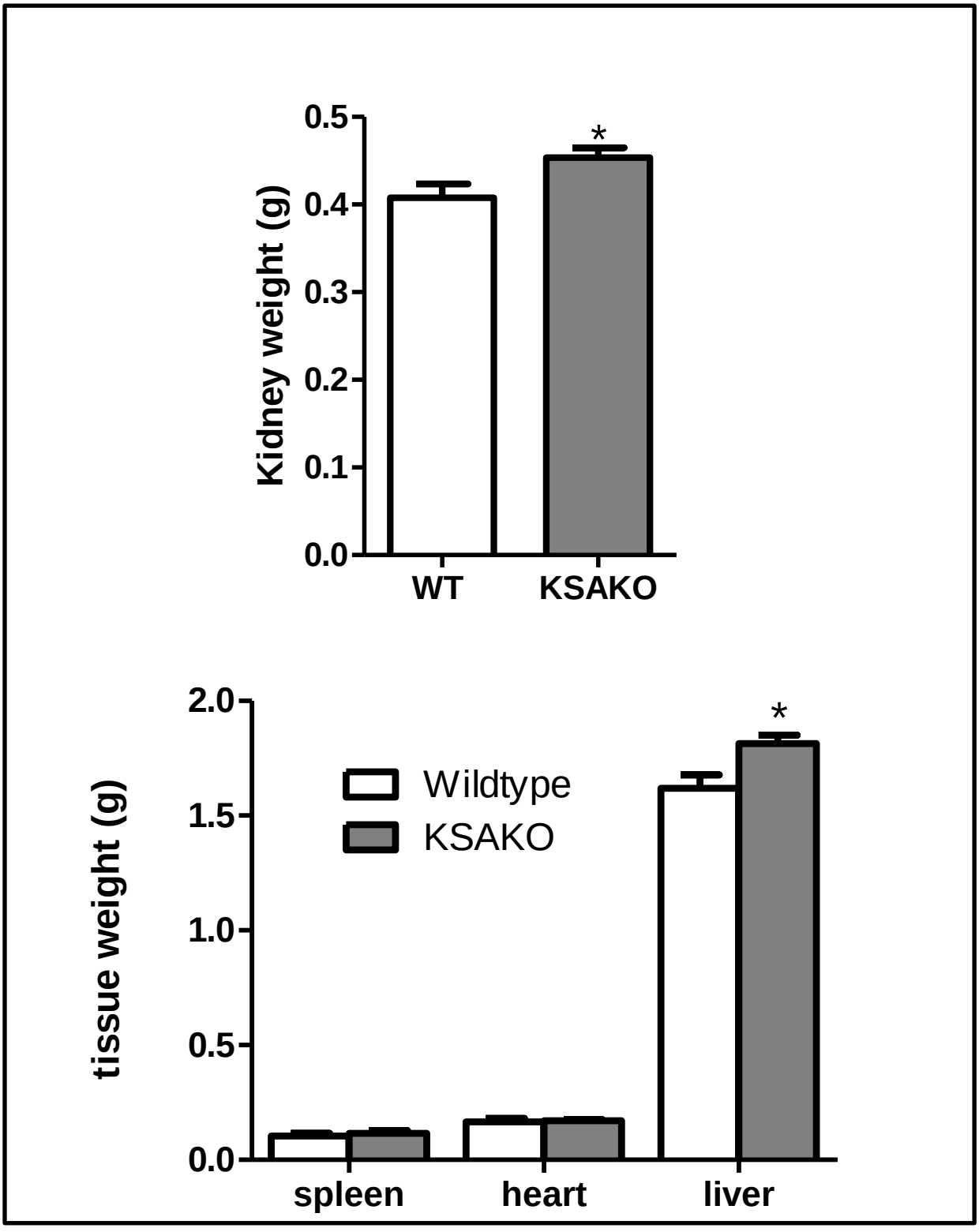

Figure 29: Tissue weights in KSAKO mice.
Tissue weights of male WT and KSAKO mice at 20 wks of age. The kidney and liver weights were significantly greater in KSAKO than WT mice. There were no significant differences between spleen and heart weights of KSAKO and WT mice. (n=4-6); *P<0.05

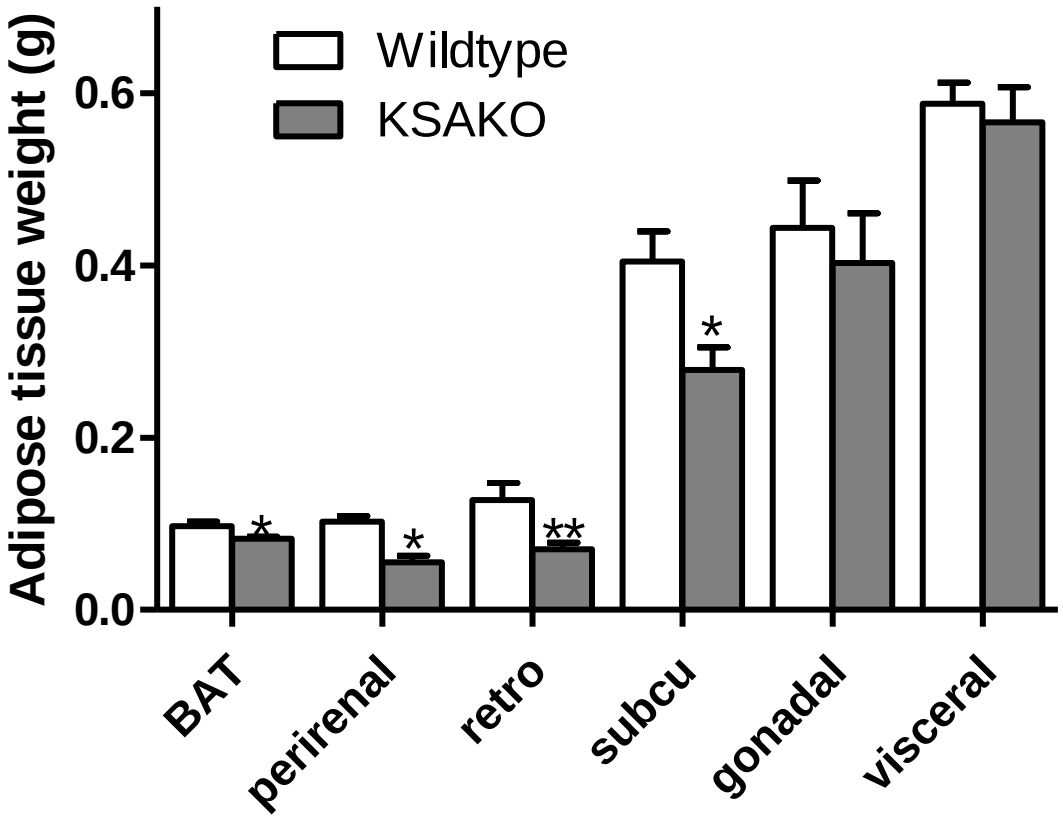

Figure 30: Adipose tissue depot masses in KSAKO mice.
Adipose tissue depots weights of male WT and KSAKO mice, age 20 wks. KSAKO mice had significantly lower brown adipose tissue (BAT), perirenal and retroperitoneal (retro), and subcutaneous (subcu) tissue weights compared to WT mice. There were no significant differences in gonadal and visceral adipose tissue weights between WT and KSAKO mice. BAT = brown adipose tissue; retro = retroperitoneal; subcu = subcutaneous. (n=4-6); *P<0.05; **P<0.01

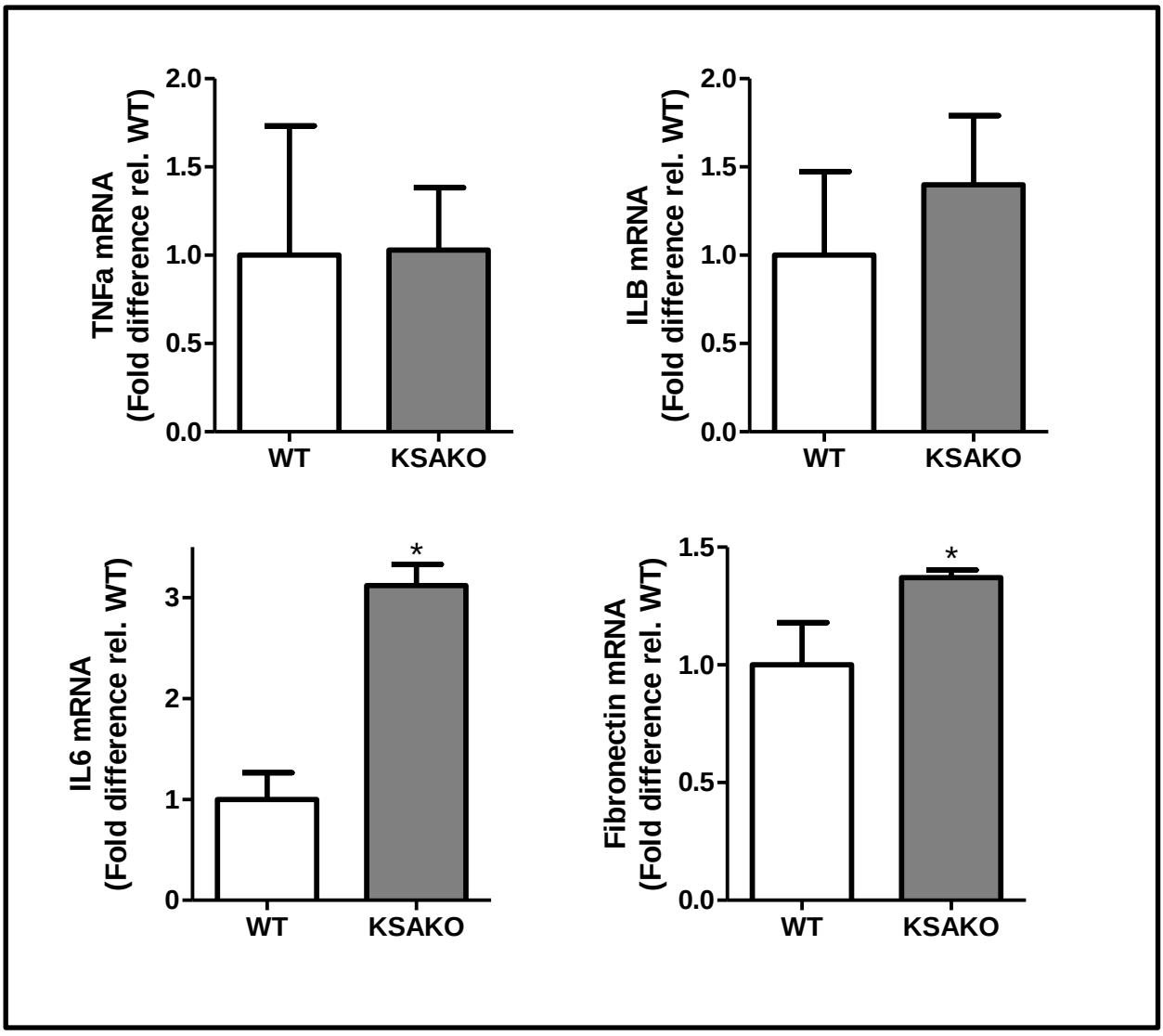

Figure 31: Gene expression of markers of inflammation and fibrosis.
mRNA expression was assessed by qPCR in 20 wk old WT and KSAKO male mice and normalized to *18s*. (n=4-6); **P*<0.05.

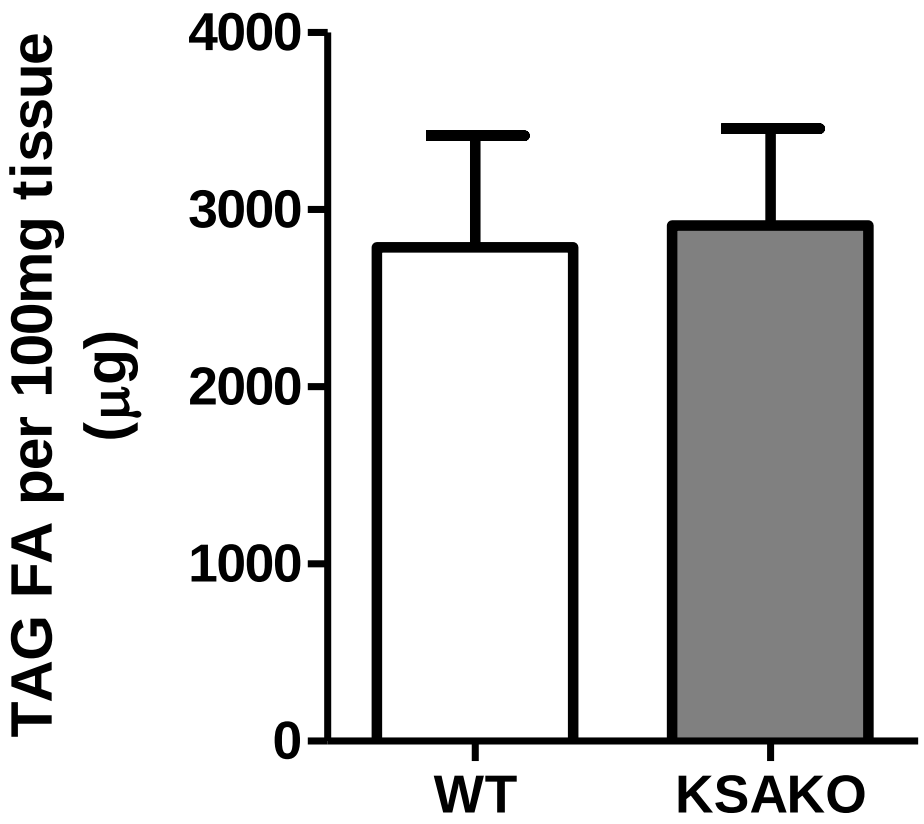

Figure 32: Kidney TAG content.
Kidney TAG was determined by measuring the total free fatty acid content in this lipid species by gas chromatography. No significant differences were detected in the TAG content of kidneys from KSAKO and WT mice at 20 weeks of age when measured following a 16 h fast. (n=5).

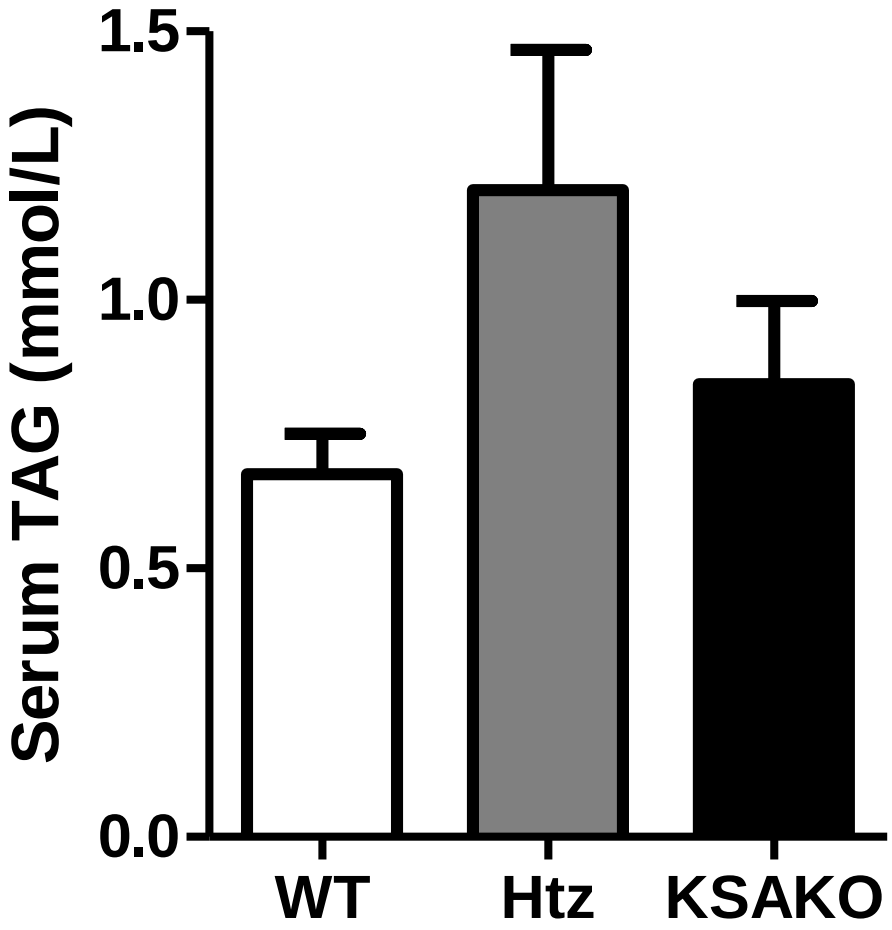

Figure 33: Serum TAG concentrations in 20 wk-old WT, Htz and KSAKO mice.
There was an ~25% increase in serum TAG concentration in KSAKO mice compared to wildtype mice that did not reach significance with the number of animals tested. (n=4-6).

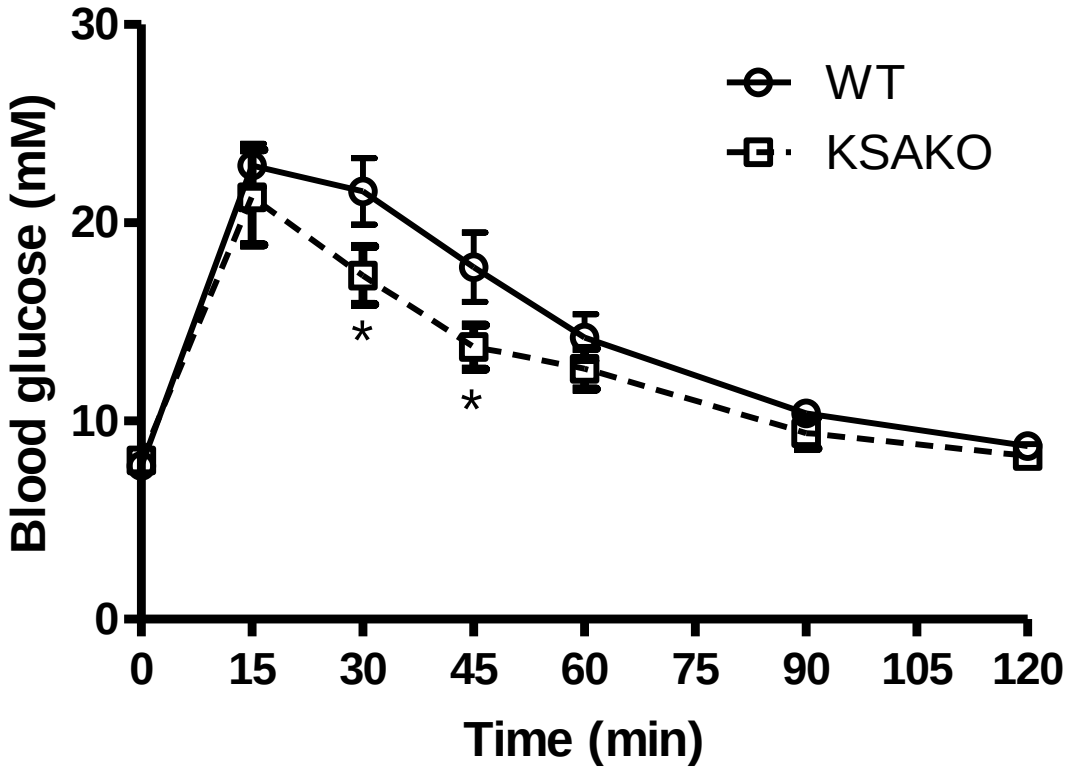

Figure 34: Glucose tolerance testing in 9 wk old mice.
Blood glucose response to *i.p.* injection of glucose in 9 wk old male WT and KSAKO mice. (n=10-12); *P<0.05.

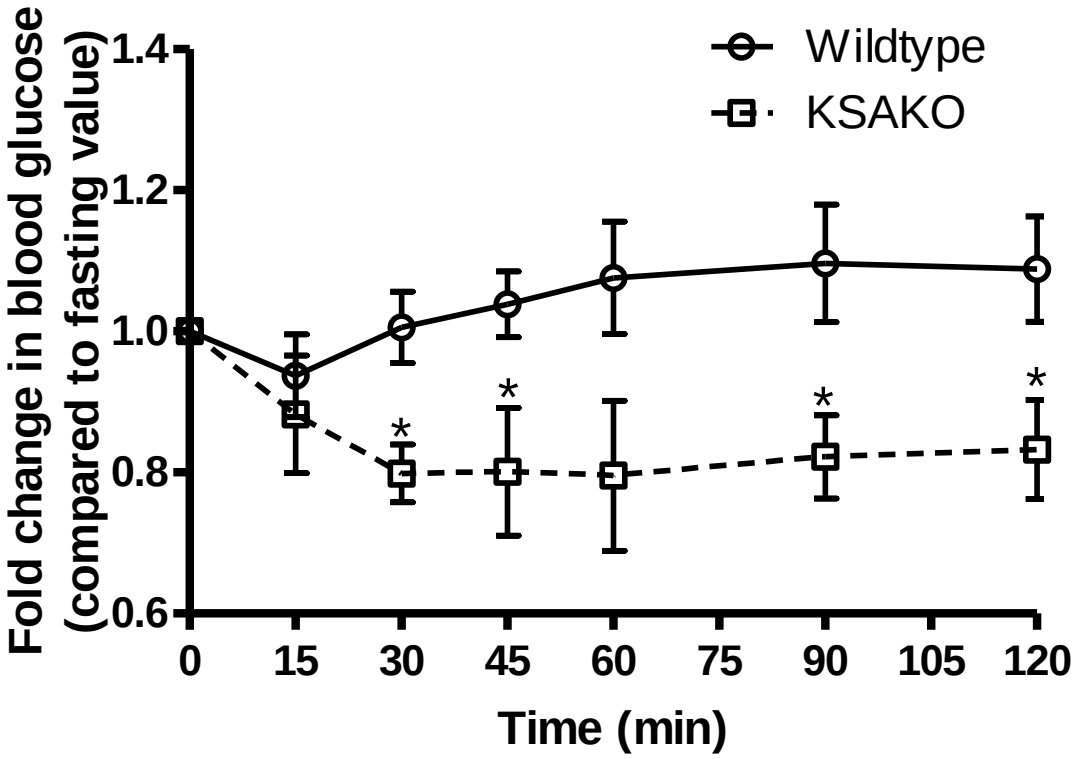

Figure 35: Insulin tolerance in 9 wk old mice.
Blood glucose response to *i.p.* injection of insulin in wildtype and KSAKO male mice. (n=10-12), **P*<0.05.

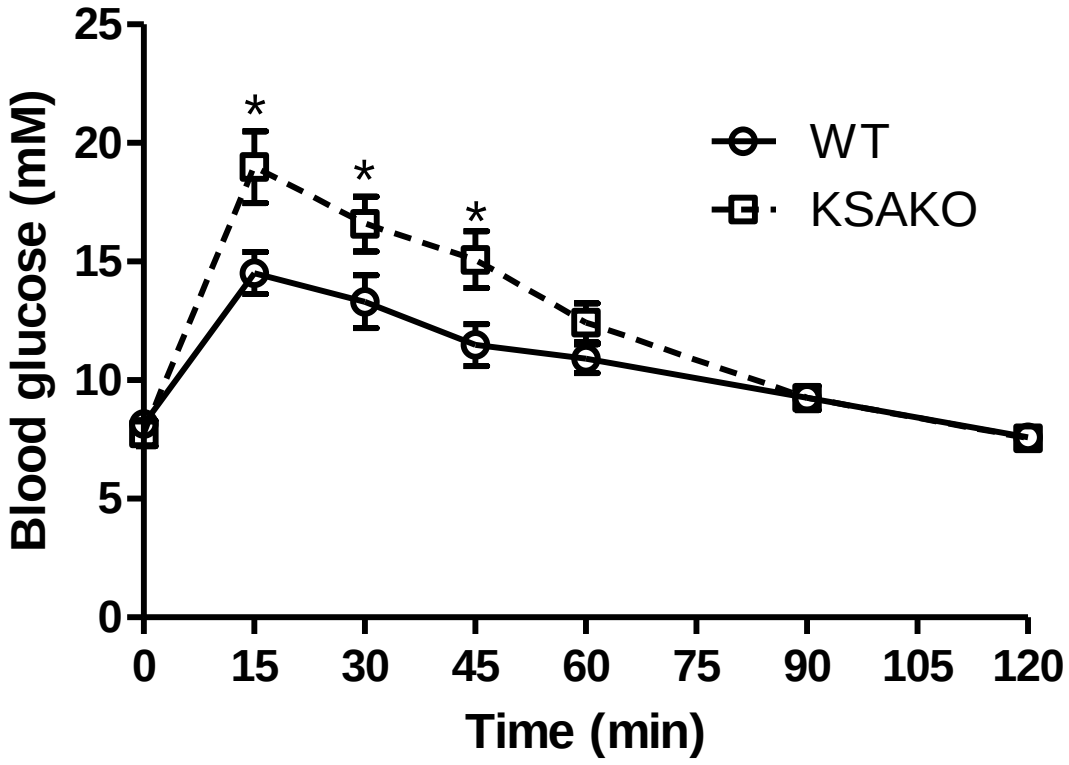

Figure 36: Glucose tolerance in 16 wk old mice.
Blood glucose response to i.p. injection of glucose in WT and KSAKO male mice at 16 wks of age. (n=10-12); *P<0.05.

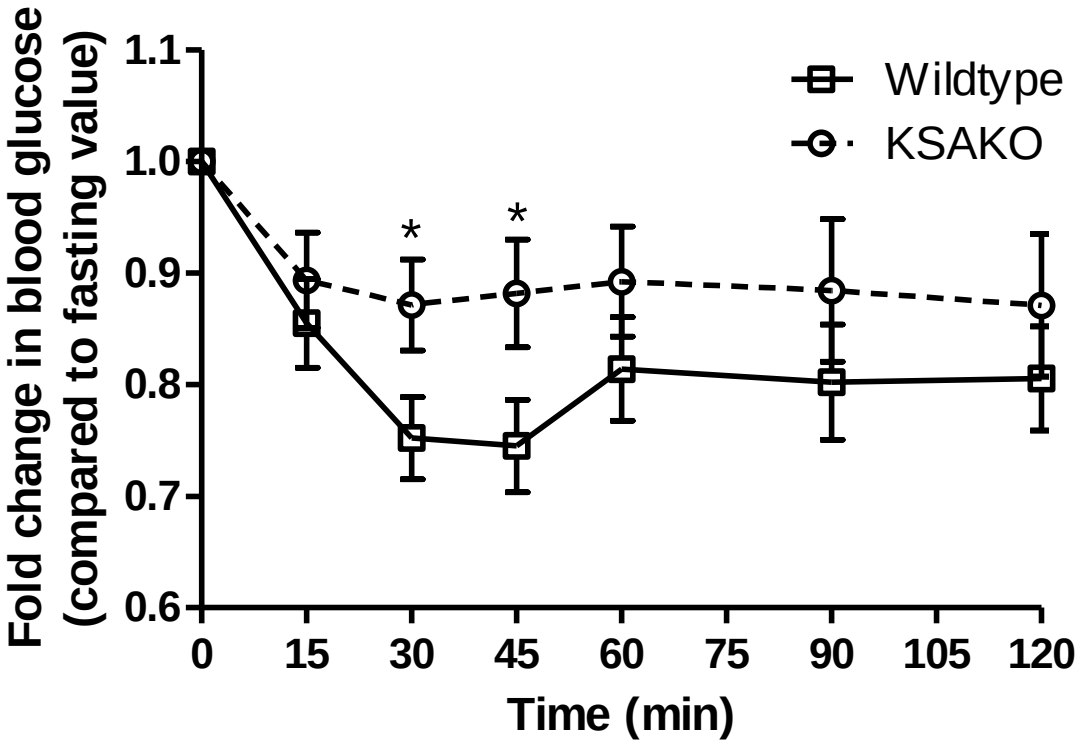

Figure 37: Insulin tolerance in 16 wk old mice.
Blood glucose response to *i.p.* injection of insulin in WT and KSAKO mice at 16 wks of age. (n=10-12); **P*<0.05.

Discussion

The reported link between early renal dysfunction and lipid accumulation, as well as the association between obesity, ectopic renal lipid accumulation and CKD, has led us to hypothesize a role for lipid accumulation and lipotoxicity as an initiating defect in renal disease. To study the effects of lipid droplet accumulation and renal lipotoxicity in the absence of confounding factors we require a renal tubule-specific model, and therefore a renal tubule-specific target to elicit lipid accumulation. Previous studies have identified the ablation of intracellular lipases such as ATGL and HSL as models for lipid accumulation (25,89). The global disruption of ATGL results in TAG accumulation in most tissues, and animals prematurely die of cardiac failure due to lipid accumulation in the heart, where the most severe steatosis occurs (25). The second largest effect of TAG accumulation in this model occurred in the kidney. However, it was unclear whether this effect was due to a specific renal ATGL deficit or to the global dysfunction in lipid metabolism that was evident in that model. After characterizing lipolysis in the kidney we discovered evidence suggesting that renal *Atgl* would likely be a suitable genetic target for ablation in order to create a model of lipid accumulation in the kidney.

We utilized the Cre-Lox-P system to excise the first exon of *Atgl* in the kidney using *Cre recombinase* under control of the renal tubule-specific Cdh16 promoter (85,86). This created a model of murine ATGL knockout primarily in proximal tubules and glomerular cells that we termed kidney renal tubule-specific ATGL Knockout (KSAKO). We confirmed that this led to a reduction in *Atgl* in kidney by analysis of mRNA expression and protein levels. A 25% reduction of *Atgl* mRNA and a 33% reduction in ATGL protein level in whole kidneys were evident. The

partial reduction was expected, rather than complete ablation, because Cre-recombinase expression was targeted primarily to proximal tubule cells rather than all renal cell types. We confirmed that our model is renal tubule-specific by immunoblotting for ATGL in other tissues as well (i.e. heart and adipose) and found no decrease in expression across WT, Htz, and KSAKO mice.

Targeted ATGL ablation resulted in a non-significant change in body weight in the KSAKO mice by 20 weeks of age. However, area under the curve analysis suggests that KSAKO mice gained weight faster, perhaps due to lipid accumulation. To further investigate the change in body weight we assessed tissue weight gain under fasted conditions. We observed an increase in KSAKO kidney and liver weights with no change in heart or spleen. The increase in kidney weights suggested lipid accumulation, which we were expecting to find. However, when the kidneys were subjected to lipid extraction and analysis it was found that TAG levels were not different between WT and KSAKO mice. The expected increase in TAG may not have been evident in the entire kidney because ATGL loss from the kidney was relatively mild and specific only to renal proximal tubule and glomerular cells, resulting in a diluting effect by the many other cell types with normal *Atgl* expression. Lipid accumulation in the kidney has previously been reported to increase in the fasted stated (67), which may also have lowered the sensitivity of detecting differences in lipid levels between WT and KSAKO mice. Accordingly, this analysis should be reproduced with kidneys from fed mice, where the difference between TAG in KSAKO and WT mice may be greater. More sensitive measures should also be employed, such as histochemistry, in order to identify specific cells types with elevated TAG storage. Additionally, other time points should be considered for analysis of renal TAG. This measure was taken at a

single time point (20 weeks) at which time we also found a compensatory increase in *Hsl* expression that may have reduced the severity of lipid accumulation, although this effect was not sufficient to rescue the complex phenotype that these mice developed.

Any change in body weight suggests a possible alteration to lipid storage by adipose tissue. To determine differences in adipose tissue mass we excised specific depots and found decreases in various subcutaneous and visceral white adipose tissue depots, and BAT. This finding does not explain the relative increase in body mass that was evident in KSAKO mice, but it is in agreement with findings of reduced adiposity in CKD, which in some reports occurs in association with increased lipolysis (90). To investigate a potential role for increased lipolysis in mediating effects in the current study, we assessed the level of ATGL and found that it was significantly induced in KSAKO peri-renal WAT. The induction of ATGL in WAT therefore likely contributed to an elevation of lipolysis, and a reduction in the weight of WAT depots. The reduction of mass of peri-renal and other visceral fat depots in our KSAKO model parallels that of visceral tissue loss in patients with CKD (91) and animal models of CKD (92). The loss of visceral adipose tissue mass in models of CKD has also been associated with a downregulation of WAT lipoprotein lipase (LPL) (93), and an increase in circulating inhibitors of this enzyme (94) (95), (93). Whether this effect contributes to the decrease in mass of WAT depots from our KSAKO mice remains to be tested.

KSAKO mice exhibited reduced WAT mass with preliminary evidence of elevated and dysregulated lipolysis. Two possible mechanisms include the leakage of uremic toxins from the urinary filtrate back into the blood (93,94,96,97), and the release of microRNAs (miRNAs) resulting from kidney dysfunction (98). Uremia is a condition where excess urea, creatinine, and

other nitrogenous compounds that would normally be found in the urine accumulate in the blood, and it is a common pathology of CKD that is also associated with the development of insulin resistance. Uremic proteins may be responsible for direct interruption of AKT signalling in cells, promoting insulin resistance (99). However, uremic proteins have also been shown to induce lipolysis in cultured adipocytes (96), which may promote WAT lipid depletion. If this lipid becomes redistributed to skeletal muscle and liver, it may also contribute to development of the insulin resistance that is evident in our model. Further studies will be required to determine if this is the case.

Micro RNAs (miRNAs) are recently identified players in metabolic signalling. MiRNAs are small non-coding RNA post-transcriptional regulators that can be released from tissues like the kidney into the blood, where they are then able to vastly act at distal organ sites to vastly affect gene regulation, since more than half of human protein-coding genes contain miRNA target sites in their 3' untranslated region. In this regard, miRNAs are potentially able to modulate the pathology of many conditions in health and disease (100). Changes to adipose tissue mass that are evident in KSAKO mice may be the result of changing concentrations of circulating miRNAs originating from the kidney. In our model, we saw a similar change in adipose tissue mass, accompanied by development of insulin resistance, to that observed in HIV, cancer cachexia and aging (92,101-103). MiRNAs that have been implicated in mediating metabolic events in these conditions include miRNA133, 143, 145, 21 (104-106). Both 143 and 145 play a role in modulating adipocyte activity. MiRNA143 has been shown to induce adipocyte differentiation (107), and a decreased circulating concentration may have a negative impact on the ability to store lipid. MiR145 decreases lipolysis in adipocytes (108). Lower concentrations in the plasma

may therefore contribute to reduced inhibition, and thus an inappropriate increase in lipolysis as is seen in these conditions. Other candidate miRNAs may play a role in metabolic and pathological changes originating in kidneys of KSAKO mice. For example, MiR21 has been shown to decrease PPAR ligand-activation by inhibiting lipid metabolism, and the silencing of MiR21 has been found to limit renal fibrosis (105). MiR486 is decreased in CKD and it is able to inactivate the transcription factor FOXO (109), which has been shown to activate lipolysis in adipocytes (110). The modulation of lipid metabolism genes by miRNAs altered in CKD suggests a renal-adipose axis, and whether MiR486 or other miRNAs originating from the kidney play a role in dysregulated WAT lipolysis in KSAKO mice should be investigated.

Dysregulated WAT metabolism may cause other metabolic problems, including elevated circulating TAG that is a common pathological change in kidney disease. The same factors that contribute to decreased adipose tissue mass are mechanistically implicated in increasing circulating TAG. Impaired WAT LPL-mediated clearance of circulating TAG (93) can result in a prolonged post-prandial rise in fat-rich lipoproteins, while elevated lipolysis increases circulating NEFA that drive hepatic VLDL synthesis. Because a loss of WAT was evident in our model, we assessed plasma TAG, and found evidence of increased concentrations in both KSAKO mice and Htz that we believe will reach significance with a larger samples size. Although we did not yet measure serum NEFA, our finding of increased lipase expression and reduced WAT depot size suggests that this blood lipid is also altered in KSAKO mice, and should be directly analyzed. Elevated serum NEFA, as well as elevated circulating TAG, are implicated in the generation of lipotoxic environments and the development of insulin resistance (21,22). Importantly, patients with ESRD, but no prior history of diabetes, are at increased risk of

developing the disease (10,11), strongly suggesting a link with events in the kidney, although these are currently poorly defined.

We assessed glycemic control in our KSAKO model by measuring glucose tolerance and insulin sensitivity at 9 weeks and 16 weeks of age. At 9 weeks, KSAKO mice cleared injected glucose faster than WT mice. This may indicate a renal-tubule-specific, and insulin-independent effect demonstrating improved utilization of glucose by the kidneys, where ATGL loss would limit the provision of competing fatty acid substrates for beta-oxidation. However, KSAKO mice also exhibited better insulin-dependent glucose disposal, demonstrating a larger and more rapid blood glucose decrease in response to *i.p.* insulin injection than wildtype mice. It is therefore likely that tissues other than the kidney are also involved in mediating this effect, since the only cells in the kidney that are responsive to the action of insulin for the regulation of glucose transport are podocytes (111), and these do not make up a large enough mass to explain changes observed. More likely, impairing the mobilization of fatty acids in renal tubule cells led to increased fatty acid storage and therefore decreased circulating NEFA, which could help to enhance both glucose utilization and insulin sensitivity in a variety of tissues such as adipose, skeletal muscle, and liver. Improved glycemia resulting from the impairment of fatty acid mobilization is also seen in global ATGL knockout mice, where complete loss of ATGL in all tissues severely impacts the use of fatty acids, and causes tissues to rely on glucose for energy metabolism. As predicted, however, the metabolic benefit of ATGL gene ablation in kidney did not last.

By 16 weeks of age, we found KSAKO mice to be significantly more insulin resistant than WT mice. Fasted KSAKO mice had a much larger spike in blood glucose concentration when glucose

was injected *i.p.*, which took longer to return to baseline, and they had a severely blunted hypoglycemic response to insulin injection. Thus, by 16 weeks, any benefit gained from an increase in glucose use is outweighed by the negative impact of ATGL loss in the kidney. Insulin resistance and CKD are often found together (7,11,97,112-115). However, our model clearly demonstrates that insulin resistance follows impairment in the ability to mobilize fatty acids in the kidney. The temporal nature of this finding is important for establishing a causal role for defective kidney lipid metabolism in systemic metabolic disease. Indeed, the demonstration that kidney dysfunction causes insulin resistance strongly supports a "two-way street" relationship between obesity and renal disease. Understanding the nature of the mechanisms that underlie this relationship will take considerable additional effort, although I have begun to investigate some of these.

A prominent feature of CKD is the elevation of the inflammatory marker interleukin (IL)-6 (116). I measured mRNA expression of the inflammatory markers *Il-6*, *Il-1b* and *TNF-alpha* in whole kidneys from 16-week old mice and found only *Il-6* mRNA to be elevated by ATGL ablation. IL-6 is known to be involved in the recruitment, activation and proliferation of immunocytes, progressing the inflammatory response in kidney. IL-6 also exacerbates CKD-associated co-morbidities by inhibiting the synthesis of adiponectin, an anti-atherogenic adipokine, in WAT (117). Atherogenesis is a serious complication of CKD and patients with CKD often die of CVD before succumbing to ESRD (118,119), per se. IL-6 is involved in the atherosclerotic process during the fibrous plaque development stage (120). We therefore also assessed whether fibrosis had been initiated in the kidney by measuring the expression of

fibrinogen in whole kidneys, and found it to be induced. Serum fibrinogen levels are a predictor of mortality in patients with CKD (121) in part due to the risk of cardiovascular events.

The detrimental impact of altered lipid metabolism in the kidney as a result of *Atgl* ablation suggests that increasing renal lipolysis may be a mechanism to dissipate excess TAG stores and offer renoprotective effects, and hope for the treatment of kidney disease. The ablation of renal ATGL caused significant defects to whole body metabolism and, thus, the induction of renal lipolysis may prove beneficial in remedying these defects. Activation of PPARα by fenofibrate increases lipolysis and the oxidation of fatty acids (122). Fenofibrate treatment of rats has been shown to offer partial or full protection from renal lipotoxicity in diet-induced obesity models (123,124). Likewise, activation of AMPK, an activator of ATGL-mediated lipolysis (34), has been shown to reduce the severity of renal pathology associated with exposure to a high-fat diet (125). Dissipation of TAG in non-adipose tissues by treatment of rats with thiazolidinediones (TZDs) also ameliorates renal steatosis and lipotoxicity, and this effect was found to be dependent on the reduction in lipid loading, rather than treatment with TZDs per se (126). Similar effects may be achieved through tissue-specific increases in TAG hydrolysis. The continued study of renal lipolysis and potential activators of lipid enzymes involved in this process may prove to yield novel therapeutic options for the treatment of kidney disease and other metabolic conditions where WAT redistribution is of consequence.

Timeline Analysis

Defects in the ability to clear cellular lipids can result in lipid accumulation, promoting a lipotoxic environment. Cellular overstorage of lipids is a hallmark of the dysregulated obese state (15). A major complication of obesity is renal disease, which is associated with renal steatosis (21,22). The mechanisms mediating the declining kidney function associated with obesity are poorly understood, and recent literature suggests that kidney dysfunction alone can initiate or worsen metabolic syndrome, and increase the risk of cardiovascular disease (10-12). In association with obesity, kidney injury may result from lipid accumulation, diabetes, hypertension or a combination of several co-morbidities. To investigate the role of lipid accumulation alone in kidney pathology associated with obesity we created a model of renal lipid accumulation.

The clearance of cellular lipid stores is mediated by lipolysis. The disruption of lipolysis by ablation of ATGL has been demonstrated to result in cellular lipid accumulation in most tissues (25,34). The renal tubule specific ablation of ATGL created in this thesis allows for the study of targeted disruption of lipolysis in the kidney.

The KSAKO model created was a conditional knockout model under the control of *Cre* recombinase expression. Although this model was conditional under the expression of *Cre*, loss of *Atgl* was designed to begin at conception. KSAKO mice were essentially equal in terms of ratios of genotypes birthed, suggesting Mendelian genetics was not altered with *Atgl* ablation nor that this model was embryonic lethal.

The resulting disruption to lipolysis in the kidney from *Atgl* loss is hypothesized to increase glucose utilization in the kidney in response to the inability to mobilize fatty acids for

beta-oxidation. As well, recent literature points to a possible role for the kidney in whole body glycemic control (10,11). Investigation of glycemic control was carried out by determining glucose and insulin tolerance testing in KSAKO and WT mice. The measurement of glycemic control at two time points allowed for the establishment of a timeline of pathology. As hypothesized, glucose sensitivity was increased in KSAKO mice compared to wildtype mice at the 9-week time point. The disruption in lipolysis likely increased utilization of glucose by the kidney, which increased blood glucose clearance. The essentially equal body weights observed in control and KSAKO mice at 9 weeks also suggested that excess lipids were not present at this time. However, we did not directly assess adipose tissue mass or organ weights at this time, and we may have seen opposing changes without a change in whole body mass. We further assessed glycemic control at 16 weeks of age to determine the effect of chronic *Atgl* ablation on glucose tolerance. The targeted loss of *Atgl* for 16 weeks was associated with insulin resistance and glucose intolerance. The apparent reversal of glucose tolerance to intolerance from the 9 week to the 16 week time point indicates a functional disruption occurring secondary to altered renal lipolysis. Glucose intolerance was hypothesized to be a result of renal steatosis, however neither this nor a change in body weight was detected at the 16 week time point. However, the induction of *Hsl* at 16 weeks implies that lipid accumulation likely occurred at an earlier time point and that lipotoxicity may have played a role in the development of insulin resistance prior to the 16 week time point. This is supported by the lack of evidence detected for the involvement of inflammation in the progression of glucose intolerance. Markers of inflammation were measured at 20 weeks of age and results suggested that inflammation was

only beginning to occur. Thus, it is unlikely that inflammation played a major role in the development of insulin resistance that was detected 4 weeks prior, at 16 weeks of age.

At 20 weeks, it was also demonstrated that adipose tissue weights were decreased, and there was evidence of elevated adipocyte lipolysis. This indicates further evidence of dysregulated lipid handling in the body which may have played a role in altering glycemic control. Dysregulated WAT can result in elevated serum TAG, which we found evidence for, and likely contributed to the insulin resistance found at the 16 week time point. The dysregulation of WAT may have resulted from pathological kidney signalling to WAT at an earlier time point – for example, through changes in serum urinary proteins or miRNAs. It is not clear when the disruption to WAT occurred, and whether this occurred prior to measurement of insulin resistance at 16 weeks. Further investigation will be required to evaluate whether WAT dysregulation played a role in the development of insulin resistance in this model or whether pathological kidney changes alone were enough to interfere with whole body glucose disposal.

A time line of events has been established to study the involvement of renal lipid metabolism in the pathogenesis of insulin resistance. Further investigation is required to elucidate the mechanism(s) involved in mediating insulin resistance in this model. The time line will be useful in identifying initiating factors that contribute to kidney pathology. The association of the KSAKO model with that of CKD may provide novel targets for the prevention and treatment of CKD.

Future Directions

ATGL has been shown to be an important mediator of lipid metabolism in WAT, liver and heart, with genetic ablation resulting in lipid accumulation. We demonstrate that renal tubule-specific ATGL ablation results in a dysregulation to glucose metabolism, mediated through an as-of-yet undetermined mechanism. Our studies demonstrate the importance of renal ATGL in kidney homeostasis, and a possible role for renal lipolysis in initiating kidney damage. To provide definitive proof that lipid accumulation is a mediator of renal injury, it will be important to perform further studies in this KSAKO model.

First, further work is needed to identify predicted effects of *Atgl* deficiency on lipid accumulation in specific cell types of the kidney. This renal tubule-specific model should show a reduction in ATGL levels in less than half of kidney cells, resulting in lipid accumulation only in these specific kidney ultra-structures. Identification and characterization of compensatory changes, such as an induction of HSL will also be important, as will characterization of timelines for the appearance of inflammatory markers and fibrosis. Examination of kidneys of older (>25 week old) mice will also be of interest.

Second, it will be important to investigate the timeline of extra-renal pathological changes in this KSAKO model, including what changes are associated with the early increase in insulin sensitivity that was seen at 9 weeks of age, and why this effect is reversed by 16 weeks of age. This work is comprised of many questions. When do adipose tissue depots begin to be dissipated? What factors link renal tubule-specific changes to dysregulated systemic metabolism? Are the changes progressive, and do they lead to greater severity of insulin resistance and eventual CVD with age? Evaluating renal pathology and systemic factors such as

blood lipids, glycemic control, and adipose tissue measures at 4, 8, 20, and 30 week time points will help to elucidate the progression of renal pathology with ATGL loss and its effect on global metabolism.

Third, it will be interesting to characterize sex differences in the KSAKO model. I have performed preliminary studies on female KSAKO mice, suggesting that they have a radically different phenotype from male KSAKO mice, including improved insulin sensitivity and glycemic control at 16 weeks of age that is associated with a lower body weight gain from age 4 to 20 weeks and possible increases in adipose tissue weights (Appendix). Whether differences in kidney and liver weights are also evident remains to be evaluated.

The KSAKO model demonstrates the importance of renal lipolysis in regulating extra-renal effects such as WAT mass and systemic effects such as blood TAG concentration and glycemic control. The regulation of such wide-ranging effects likely requires the action of circulating endocrine factors. Possible mechanisms behind WAT dysregulation following disruption to renal lipolysis may involve toxic uremic proteins (93,94,96,97) and miRNA's (98). Uremia is a common pathological consequence of CKD and is associated with the development of insulin resistance. Uremic toxins may be responsible for direct interruption of AKT signalling, promoting insulin resistance (99). Uremic toxins have also been shown to induce lipolysis in cultured adipocytes (96), which may promote lipid redistribution, as seen in our model. Direct measurement of serum creatinine and urea will be required to determine whether KSAKO mice develop uremia. Circulating miRNAs derived from the kidney may also mediate changes that were evident in KSAKO mice, including changes to adipose tissue depot masses, serum TAG concentrations, and development of impaired glycemic control. Dysregulated miRNAs have been found in to

mediate similar pathological changes to that which we saw in our model, including the redistribution of adipose tissue (92,101-103). Profiling of blood miRNAs in WT and KSAKO mice by next-generation sequencing will be important for identification of predicted and novel miRNAs that may mediate changes. The continued study of renal lipolysis and potential activators of lipid enzymes involved in this process may yield novel therapeutic options for the treatment of kidney disease and associated metabolic conditions.

CONCLUSION

The topics in this thesis evaluated the suitability of renal ATGL ablation for the creation of a model of lipid accumulation in the kidney to study its role in the development in kidney dysfunction and associated co-morbidities including CVD and diabetes. I characterized ATGL and HSL expression and evaluated the nutritional regulation of lipolysis in murine whole kidneys. This first study allowed me to identify ATGL as an important modulator of lipid storage in the kidney, and was chosen as a suitable target for renal tubule specific genetic ablation. The renal tubule specific ablation of ATGL resulted in numerous metabolic changes including insulin resistance and adipose tissue redistribution. The work completed was meant to identify lipid accumulation in the kidney as an initial defect in kidney function leading to the progressive disruption of global metabolism. Further work must be done on this model to elucidate the extent of cell specific lipid accumulation and kidney dysfunction. The characterization of KSAKO mice as a model for CKD would promote the factor of lipid accumulation as an early modulator in kidney disease and would positively benefit this field of research. Future projects should include the identification of signalling molecules involved in the renal-adipose axis to understand the cause and detriments of adipose redistribution, and characterization of the effect of renal lipid accumulation on cardiovascular measures, since this is an important co-morbidity in patients with CKD. The completion of this work would allow for a more thorough understanding of the early defects responsible for the development and progression of kidney disease, and should identify novel therapeutic options for the treatment of CKD.

REFERENCES

1. Marvyn, P. M., Bradley, R. M., Button, E. B., Mardian, E. B., and Duncan, R. E. (2015) Fasting upregulates adipose triglyceride lipase and hormone-sensitive lipase levels and phosphorylation in mouse kidney. *Biochemistry and Cell Biology*

2. CIHI. (2012) Treatment of end-stage organ failure in Canada. in *Healthcare quarterly (Toronto, Ont.)*

3. NIDDK, N. (2012) Kidney Disease Statistics for the United States. National Kidney and Urologic Diseases Information Clearinghouse

4. Bailie, G. R., Uhlig, K., and Levey, A. S. (2005) Clinical practice guidelines in nephrology: evaluation, classification, and stratification of chronic kidney disease. *Pharmacotherapy* **25**, 491-502

5. Honeycutt, A. A., Segel, J. E., Zhuo, X., Hoerger, T. J., Imai, K., and Williams, D. (2013) Medical costs of CKD in the Medicare population. *J Am Soc Nephrol* **24**, 1478-1483

6. Fryar, C., Carroll, M., Ogden, C.,. (2014) Prevalence of Overweight, Obesity, and Extreme Obesity Among Adults: United States, 1960–1962 Through 2011–2012.

7. Kincaid-Smith, P. (2004) Hypothesis: obesity and the insulin resistance syndrome play a major role in end-stage renal failure attributed to hypertension and labelled 'hypertensive nephrosclerosis'. *Journal of hypertension* **22**, 1051-1055

8. Obrador, G. T., and Pereira, B. J. (2002) Anaemia of chronic kidney disease: an under-recognized and under-treated problem. *Nephrology, dialysis, transplantation : official publication of the European Dialysis and Transplant Association - European Renal Association* **17**, 44-46

9. Hsu, C. Y., McCulloch, C. E., Iribarren, C., Darbinian, J., and Go, A. S. (2006) Body mass index and risk for end-stage renal disease. *Annals of internal medicine* **144**, 21-28

10. Carbone, F., Montecucco, F., Mach, F., Pontremoli, R., and Viazzi, F. (2013) The liver and the kidney: two critical organs influencing the atherothrombotic risk in metabolic syndrome. *Thrombosis and haemostasis* **110**, 940-958

11. Chou, C. Y., Liang, C. C., Kuo, H. L., Chang, C. T., Liu, J. H., Lin, H. H., Wang, I. K., Yang, Y. F., and Huang, C. C. (2014) Comparing risk of new onset diabetes mellitus in chronic

kidney disease patients receiving peritoneal dialysis and hemodialysis using propensity score matching. *PloS one* **9**, e87891

12. Chawla, L. S., Herzog, C. A., Costanzo, M. R., Tumlin, J., Kellum, J. A., McCullough, P. A., and Ronco, C. (2014) Proposal for a functional classification system of heart failure in patients with end-stage renal disease: proceedings of the acute dialysis quality initiative (ADQI) XI workgroup. *Journal of the American College of Cardiology* **63**, 1246-1252

13. Ronco, C., House, A. A., and Haapio, M. (2008) Cardiorenal syndrome: refining the definition of a complex symbiosis gone wrong. *Intensive care medicine* **34**, 957-962

14. Singla, P., Bardoloi, A., and Parkash, A. A. (2010) Metabolic effects of obesity: A review. *World journal of diabetes* **1**, 76-88

15. van Herpen, N. A., and Schrauwen-Hinderling, V. B. (2008) Lipid accumulation in non-adipose tissue and lipotoxicity. *Physiology & behavior* **94**, 231-241

16. Duncan, R. E., Ahmadian, M., Jaworski, K., Sarkadi-Nagy, E., and Sul, H. S. (2007) Regulation of lipolysis in adipocytes. *Annu Rev Nutr* **27**, 79-101

17. Baines, R. J., Chana, R. S., Hall, M., Febbraio, M., Kennedy, D., and Brunskill, N. J. (2012) CD36 mediates proximal tubular binding and uptake of albumin and is upregulated in proteinuric nephropathies. *American journal of physiology. Renal physiology* **303**, F1006-1014

18. Bobulescu, I. A., Lotan, Y., Zhang, J., Rosenthal, T. R., Rogers, J. T., Adams-Huet, B., Sakhaee, K., and Moe, O. W. (2014) Triglycerides in the human kidney cortex: relationship with body size. *PloS one* **9**, e101285

19. Moorhead, J. F., Chan, M. K., El-Nahas, M., and Varghese, Z. (1982) Lipid nephrotoxicity in chronic progressive glomerular and tubulo-interstitial disease. *Lancet* **2**, 1309-1311

20. Herman-Edelstein, M., Scherzer, P., Tobar, A., Levi, M., and Gafter, U. (2014) Altered renal lipid metabolism and renal lipid accumulation in human diabetic nephropathy. *J Lipid Res* **55**, 561-572

21. Wang, Z., Jiang, T., Li, J., Proctor, G., McManaman, J. L., Lucia, S., Chua, S., and Levi, M. (2005) Regulation of renal lipid metabolism, lipid accumulation, and glomerulosclerosis in FVBdb/db mice with type 2 diabetes. *Diabetes* **54**, 2328-2335

22. Hao, J., Liu, S. X., Zhao, S., Liu, Q. J., Liu, W., and Duan, H. J. (2012) High-fat diet causes increased serum insulin and glucose which synergistically lead to renal tubular lipid deposition and extracellular matrix accumulation. *The British journal of nutrition* **107**, 74-85

23. Sun, L., Halaihel, N., Zhang, W., Rogers, T., and Levi, M. (2002) Role of sterol regulatory element-binding protein 1 in regulation of renal lipid metabolism and glomerulosclerosis in diabetes mellitus. *J Biol Chem* **277**, 18919-18927

24. Lobo, J. c., Stockler-Pinto, M., Farage, N. E., Faulin, T. d. E. S., Abdalla, D. S. P., Torres, J. P. M., Velarde, L. G. C., and Mafra, D. (2013) Reduced Plasma Zinc Levels, Lipid Peroxidation, and Inflammation Biomarkers Levels in Hemodialysis Patients: Implications to Cardiovascular Mortality. *Ren Fail* **35**, 680-685

25. Haemmerle, G., Lass, A., Zimmermann, R., Gorkiewicz, G., Meyer, C., Rozman, J., Heldmaier, G., Maier, R., Theussl, C., Eder, S., Kratky, D., Wagner, E. F., Klingenspor, M., Hoefler, G., and Zechner, R. (2006) Defective Lipolysis and Altered Energy Metabolism in Mice Lacking Adipose Triglyceride Lipase. *Science* **312**, 734-737

26. Rui, L. (2014) Energy metabolism in the liver. *Comprehensive Physiology* **4**, 177-197

27. Friedman, J. E., Neufer, P. D., and Dohm, G. L. (1991) Regulation of glycogen resynthesis following exercise. Dietary considerations. *Sports medicine (Auckland, N.Z.)* **11**, 232-243

28. Huynh, F. K., Green, M. F., Koves, T. R., and Hirschey, M. D. (2014) Measurement of fatty acid oxidation rates in animal tissues and cell lines. *Methods in enzymology* **542**, 391-405

29. Gibbons, G. F., and Wiggins, D. (1995) Intracellular triacylglycerol lipase: its role in the assembly of hepatic very-low-density lipoprotein (VLDL). *Advances in Enzyme Regulation* **35**, 179-198

30. Kanaley, J. A., Shadid, S., Sheehan, M. T., Guo, Z., and Jensen, M. D. (2009) Relationship between plasma free fatty acid, intramyocellular triglycerides and long-chain acylcarnitines in resting humans. *The Journal of physiology* **587**, 5939-5950

31. Villena, J. A., Roy, S., Sarkadi-Nagy, E., Kim, K. H., and Sul, H. S. (2004) Desnutrin, an adipocyte gene encoding a novel patatin domain-containing protein, is induced by fasting and glucocorticoids: ectopic expression of desnutrin increases triglyceride hydrolysis. *J Biol Chem* **279**, 47066-47075

32. Zimmermann, R., Strauss, J. G., Haemmerle, G., Schoiswohl, G., Birner-Gruenberger, R., Riederer, M., Lass, A., Neuberger, G., Eisenhaber, F., Hermetter, A., and Zechner, R. (2004) Fat mobilization in adipose tissue is promoted by adipose triglyceride lipase. *Science* **306**, 1383-1386

33. Jenkins, C. M., Mancuso, D. J., Yan, W., Sims, H. F., Gibson, B., and Gross, R. W. (2004) Identification, cloning, expression, and purification of three novel human calcium-independent phospholipase A2 family members possessing triacylglycerol lipase and acylglycerol transacylase activities. *J Biol Chem* **279**, 48968-48975

34. Ahmadian, M., Abbott, M. J., Tang, T., Hudak, C. S., Kim, Y., Bruss, M., Hellerstein, M. K., Lee, H. Y., Samuel, V. T., Shulman, G. I., Wang, Y., Duncan, R. E., Kang, C., and Sul, H. S. (2011) Desnutrin/ATGL is regulated by AMPK and is required for a brown adipose phenotype. *Cell Metab* **13**, 739-748

35. Eichmann, T. O., Kumari, M., Haas, J. T., Farese, R. V., Jr., Zimmermann, R., Lass, A., and Zechner, R. (2012) Studies on the substrate and stereo/regioselectivity of adipose triglyceride lipase, hormone-sensitive lipase, and diacylglycerol-O-acyltransferases. *The Journal of biological chemistry* **287**, 41446-41457

36. Gruber, A., Cornaciu, I., Lass, A., Schweiger, M., Poeschl, M., Eder, C., Kumari, M., Schoiswohl, G., Wolinski, H., Kohlwein, S. D., Zechner, R., Zimmermann, R., and Oberer, M. (2010) The N-terminal region of comparative gene identification-58 (CGI-58) is important for lipid droplet binding and activation of adipose triglyceride lipase. *J Biol Chem* **285**, 12289-12298

37. MacPherson, R. E., Ramos, S. V., Vandenboom, R., Roy, B. D., and Peters, S. J. (2013) Skeletal muscle PLIN proteins, ATGL and CGI-58, interactions at rest and following stimulated contraction. *American journal of physiology.Regulatory, integrative and comparative physiology* **304**, R644-650

38. Mason, R. R., Meex, R. C., Lee-Young, R., Canny, B. J., and Watt, M. J. (2012) Phosphorylation of adipose triglyceride lipase Ser(404) is not related to 5'-AMPK activation during moderate-intensity exercise in humans. *American journal of physiology. Endocrinology and metabolism* **303**, E534-541

39. Hardie, D. G., Ross, F. A., and Hawley, S. A. (2012) AMPK: a nutrient and energy sensor that maintains energy homeostasis. *Nature reviews. Molecular cell biology* **13**, 251-262

40. Hollenberg, C. H., Raben, M. S., and Astwood, E. B. (1961) The lipolytic response to corticotropin. *Endocrinology* **68**, 589-598

41. Rizack, M. (1961) An epinephrine-sensitive lipolytic activity in adipose tissue. *J Biol Chem* **236**, 657-662

42. Osterlund, T., Contreras, J. A., and Holm, C. (1997) Identification of essential aspartic acid and histidine residues of hormone-sensitive lipase: apparent residues of the catalytic triad. *FEBS Lett* **403**, 259-262

43. Holm, C., Davis, R. C., Osterlund, T., Schotz, M. C., and Fredrikson, G. (1994) Identification of the active site serine of hormone-sensitive lipase by site-directed mutagenesis. *FEBS Lett* **344**, 234-238

44. Butcher, R. W., Ho, R. J., Meng, H. C., and Sutherland, E. W. (1965) Adenosine 3',5'-monophosphate in biological materials. II. The measurement of adenosine 3',5'-monophosphate in tissues and the role of the cyclic nucleotide in the lipolytic response of fat to epinephrine. *The Journal of biological chemistry* **240**, 4515-4523

45. Garton, A. J., Campbell, D. G., Cohen, P., and Yeaman, S. J. (1988) Primary structure of the site on bovine hormone-sensitive lipase phosphorylated by cyclic AMP-dependent protein kinase. *FEBS letters* **229**, 68-72

46. Anthonsen, M. W., Ronnstrand, L., Wernstedt, C., Degerman, E., and Holm, C. (1998) Identification of novel phosphorylation sites in hormone-sensitive lipase that are phosphorylated in response to isoproterenol and govern activation properties in vitro. *J Biol Chem* **273**, 215-221

47. Miyoshi, H., Souza, S. C., Zhang, H. H., Strissel, K. J., Christoffolete, M. A., Kovsan, J., Rudich, A., Kraemer, F. B., Bianco, A. C., Obin, M. S., and Greenberg, A. S. (2006) Perilipin promotes hormone-sensitive lipase-mediated adipocyte lipolysis via phosphorylation-dependent and -independent mechanisms. *The Journal of biological chemistry* **281**, 15837-15844

48. Ragolia, L., and Begum, N. (1998) Protein phosphatase-1 and insulin action. *Molecular and cellular biochemistry* **182**, 49-58

49. Garton, A. J., Campbell, D. G., Carling, D., Hardie, D. G., Colbran, R. J., and Yeaman, S. J. (1989) Phosphorylation of bovine hormone-sensitive lipase by the AMP-activated protein kinase. A possible antilipolytic mechanism. *European journal of biochemistry / FEBS* **179**, 249-254

50. Yeaman, S. J. (1990) Hormone-sensitive lipase--a multipurpose enzyme in lipid metabolism. *Biochim Biophys Acta* **1052**, 128-132

51. Donsmark, M., Langfort, J., Holm, C., Ploug, T., and Galbo, H. (2004) Contractions induce phosphorylation of the AMPK site Ser565 in hormone-sensitive lipase in muscle. *Biochemical and biophysical research communications* **316**, 867-871

52. Tornqvist, H., and Belfrage, P. (1976) Purification and some properties of a monoacylglycerol-hydrolyzing enzyme of rat adipose tissue. *J Biol Chem* **251**, 813-819

53. Karlsson, M., Contreras, J. A., Hellman, U., Tornqvist, H., and Holm, C. (1997) cDNA cloning, tissue distribution, and identification of the catalytic triad of monoglyceride lipase. Evolutionary relationship to esterases, lysophospholipases, and haloperoxidases. *J Biol Chem* **272**, 27218-27223

54. Chau, L. Y., and Tai, H. H. (1988) Monoglyceride and diglyceride lipases from human platelet microsomes. *Biochim Biophys Acta* **963**, 436-444

55. Kamijo, A., Kimura, K., Sugaya, T., Yamanouchi, M., Hase, H., Kaneko, T., Hirata, Y., Goto, A., Fujita, T., and Omata, M. (2002) Urinary free fatty acids bound to albumin aggravate tubulointerstitial damage. *Kidney international* **62**, 1628-1637

56. Thomas, M. E., and Schreiner, G. F. (1993) Contribution of proteinuria to progressive renal injury: consequences of tubular uptake of fatty acid bearing albumin. *American journal of nephrology* **13**, 385-398

57. Hohenegger, M., and Schuh, H. (1980) Uptake and fatty acid synthesis by the rat kidney. *Int J Biochem* **12**, 169-172

58. Barac-Nieto, M., and Cohen, J. J. (1971) The metabolic fates of palmitate in the dog kidney in vivo. Evidence for incomplete oxidation. *Nephron* **8**, 488-499

59. Moestrup, S. K., and Nielsen, L. B. (2005) The role of the kidney in lipid metabolism. *Current opinion in lipidology* **16**, 301-306

60. Graversen, J. H., Castro, G., Kandoussi, A., Nielsen, H., Christensen, E. I., Norden, A., and Moestrup, S. K. (2008) A pivotal role of the human kidney in catabolism of HDL protein components apolipoprotein A-I and A-IV but not of A-II. *Lipids* **43**, 467-470

61. Takemura, T., Yoshioka, K., Aya, N., Murakami, K., Matumoto, A., Itakura, H., Kodama, T., Suzuki, H., and Maki, S. (1993) Apolipoproteins and lipoprotein receptors in glomeruli in human kidney diseases. *Kidney international* **43**, 918-927

62. Grone, H. J., Walli, A. K., Grone, E., Kramer, A., Clemens, M. R., and Seidel, D. (1990) Receptor mediated uptake of apo B and apo E rich lipoproteins by human glomerular epithelial cells. *Kidney international* **37**, 1449-1459

63. Kennedy, D. J., Chen, Y., Huang, W., Viterna, J., Liu, J., Westfall, K., Tian, J., Bartlett, D. J., Tang, W. H., Xie, Z., Shapiro, J. I., and Silverstein, R. L. (2013) CD36 and Na/K-ATPase-alpha1 form a proinflammatory signaling loop in kidney. *Hypertension* **61**, 216-224

64. Gold, M., and Spitzer, J. J. (1964) Metabolism of Free Fatty Acids by Myocardium and Kidney. *The American Journal of Physiology* **206**, 153-158

65. Hollenberg, C. H., and Horowitz, I. (1962) The lipolytic activity of rat kidney cortex and medulla. *Journal of lipid research* **3**, 445-447

66. Nieth, H., and Schollmeyer, P. (1966) Substrate-utilization of the human kidney. *Nature* **209**, 1244-1245

67. Krzystanek, M., Pedersen, T. X., Bartels, E. D., Kjaehr, J., Straarup, E. M., and Nielsen, L. B. (2010) Expression of apolipoprotein B in the kidney attenuates renal lipid accumulation. *J Biol Chem* **285**, 10583-10590

68. Jani, R., Molina, M., Matsuda, M., Balas, B., Chavez, A., DeFronzo, R. A., and Abdul-Ghani, M. (2008) Decreased non-insulin-dependent glucose clearance contributes to the rise in fasting plasma glucose in the nondiabetic range. *Diabetes care* **31**, 311-315

69. Katz, L. D., Glickman, M. G., Rapoport, S., Ferrannini, E., and DeFronzo, R. A. (1983) Splanchnic and peripheral disposal of oral glucose in man. *Diabetes* **32**, 675-679

70. Ayala, J. E., Samuel, V. T., Morton, G. J., Obici, S., Croniger, C. M., Shulman, G. I., Wasserman, D. H., and McGuinness, O. P. (2010) Standard operating procedures for describing and performing metabolic tests of glucose homeostasis in mice. *Disease models & mechanisms* **3**, 525-534

71. Jacobson, L., Ansari, T., and McGuinness, O. P. (2006) Counterregulatory deficits occur within 24 h of a single hypoglycemic episode in conscious, unrestrained, chronically cannulated mice. *American journal of physiology. Endocrinology and metabolism* **290**, E678-684

72. Liu, C. Y., Liang, L. C., and Chang, L. C. (1995) Differential responses of hormone-sensitive lipase gene to nutritional transition in adipose tissue, liver, and skeletal muscle of pigs. *Biochem Mol Biol Int* **36**, 689-694

73. Holm, C., Belfrage, P., and Fredrikson, G. (1987) Immunological evidence for the presence of hormone-sensitive lipase in rat tissues other than adipose tissue. *Biochemical and biophysical research communications* **148**, 99-105

74. Duncan, R. E., Sarkadi-Nagy, E., Jaworski, K., Ahmadian, M., and Sul, H. S. (2008) Identification and functional characterization of adipose-specific phospholipase A2 (AdPLA). *J Biol Chem* **283**, 25428-25436

75. Bligh, E. G., and Dyer, W. J. (1959) A rapid method of total lipid extraction and purification. *Can J Biochem Phys* **37**, 911-917

76. Carmen, G. Y., and Victor, S. M. (2006) Signalling mechanisms regulating lipolysis. *Cell Signal* **18**, 401-408

77. Davies, S. P., Sim, A. T., and Hardie, D. G. (1990) Location and function of three sites phosphorylated on rat acetyl-CoA carboxylase by the AMP-activated protein kinase. *European journal of biochemistry / FEBS* **187**, 183-190

78. Guder, W. G., Wagner, S., and Wirthensohn, G. (1986) Metabolic fuels along the nephron: pathways and intracellular mechanisms of interaction. *Kidney international* **29**, 41-45

79. Wang, Z., Ying, Z., Bosy-Westphal, A., Zhang, J., Heller, M., Later, W., Heymsfield, S. B., and Muller, M. J. (2012) Evaluation of specific metabolic rates of major organs and tissues: comparison between nonobese and obese women. *Obesity* **20**, 95-100

80. Wang, Y. X. (2010) PPARs: diverse regulators in energy metabolism and metabolic diseases. *Cell research* **20**, 124-137

81. Le Hir, M., and Dubach, U. C. (1982) Peroxisomal and mitochondrial beta-oxidation in the rat kidney: distribution of fatty acyl-coenzyme A oxidase and 3-hydroxyacyl-coenzyme A dehydrogenase activities along the nephron. *The journal of histochemistry and cytochemistry : official journal of the Histochemistry Society* **30**, 441-444

82. Tang, T., Abbott, M. J., Ahmadian, M., Lopes, A. B., Wang, Y., and Sul, H. S. (2013) Desnutrin/ATGL activates PPARdelta to promote mitochondrial function for insulin secretion in islet beta cells. *Cell Metab* **18**, 883-895

83. Ong, K. T., Mashek, M. T., Davidson, N. O., and Mashek, D. G. (2014) Hepatic ATGL mediates PPAR-alpha signaling and fatty acid channeling through an L-FABP independent mechanism. *J Lipid Res* **55**, 808-815

84. Haemmerle, G., Moustafa, T., Woelkart, G., Buttner, S., Schmidt, A., van de Weijer, T., Hesselink, M., Jaeger, D., Kienesberger, P. C., Zierler, K., Schreiber, R., Eichmann, T., Kolb, D., Kotzbeck, P., Schweiger, M., Kumari, M., Eder, S., Schoiswohl, G., Wongsiriroj, N., Pollak, N. M., Radner, F. P., Preiss-Landl, K., Kolbe, T., Rulicke, T., Pieske, B., Trauner, M., Lass, A., Zimmermann, R., Hoefler, G., Cinti, S., Kershaw, E. E., Schrauwen, P., Madeo, F., Mayer, B., and Zechner, R. (2011) ATGL-mediated fat catabolism regulates cardiac mitochondrial function via PPAR-alpha and PGC-1. *Nature medicine* **17**, 1076-1085

85. Breiderhoff, T., Himmerkus, N., Stuiver, M., Mutig, K., Will, C., Meij, I. C., Bachmann, S., Bleich, M., Willnow, T. E., and Muller, D. (2012) Deletion of claudin-10 (Cldn10) in the thick ascending limb impairs paracellular sodium permeability and leads to hypermagnesemia and nephrocalcinosis. *Proc Natl Acad Sci U S A* **109**, 14241-14246

86. Chen, J., Futami, K., Petillo, D., Peng, J., Wang, P., Knol, J., Li, Y., Khoo, S. K., Huang, D., Qian, C. N., Zhao, P., Dykema, K., Zhang, R., Cao, B., Yang, X. J., Furge, K., Williams, B. O., and Teh, B. T. (2008) Deficiency of FLCN in mouse kidney led to development of polycystic kidneys and renal neoplasia. *PloS one* **3**, e3581

87. Laboratory, T. J. (2014) DNA Isolation protocols.

88. Folch, J., Lees, M., and Sloane Stanley, G. H. (1957) A simple method for the isolation and purification of total lipides from animal tissues. *J Biol Chem* **226**, 497-509

89. Haemmerle, G., Zimmermann, R., Hayn, M., Theussl, C., Waeg, G., Wagner, E., Sattler, W., Magin, T. M., Wagner, E. F., and Zechner, R. (2002) Hormone-sensitive lipase deficiency in mice causes diglyceride accumulation in adipose tissue, muscle, and testis. *The Journal of biological chemistry* **277**, 4806-4815

90. Zhu, Y., Chen, Y. L., Li, C., Ding, X. Y., Xu, G. Y., Hu, L. L., Hou, F. F., and Zhou, Q. G. (2014) The effect of inhibition of endoplasmic reticulum stress on lipolysis in white adipose tissue in a rat model of chronic kidney disease. *Acta pharmacologica Sinica* **35**, 356-362

91. Kalantar-Zadeh, K., Kuwae, N., Wu, D. Y., Shantouf, R. S., Fouque, D., Anker, S. D., Block, G., and Kopple, J. D. (2006) Associations of body fat and its changes over time with

quality of life and prospective mortality in hemodialysis patients. *Am J Clin Nutr* **83**, 202-210

92. Zhao, H. L., Sui, Y., Guan, J., He, L., Zhu, X., Fan, R. R., Xu, G., Kong, A. P., Ho, C. S., Lai, F. M., Rowlands, D. K., Chan, J. C., and Tong, P. C. (2008) Fat redistribution and adipocyte transformation in uninephrectomized rats. *Kidney international* **74**, 467-477

93. Vaziri, N. D., and Liang, K. (1996) Down-regulation of tissue lipoprotein lipase expression in experimental chronic renal failure. *Kidney international* **50**, 1928-1935

94. Cheung, A. K., Parker, C. J., Ren, K., and Iverius, P. H. (1996) Increased lipase inhibition in uremia: identification of pre-beta-HDL as a major inhibitor in normal and uremic plasma. *Kidney international* **49**, 1360-1371

95. Chan, D. T., Dogra, G. K., Irish, A. B., Ooi, E. M., Barrett, P. H., Chan, D. C., and Watts, G. F. (2009) Chronic kidney disease delays VLDL-apoB-100 particle catabolism: potential role of apolipoprotein C-III. *J Lipid Res* **50**, 2524-2531

96. Axelsson, J., Astrom, G., Sjolin, E., Qureshi, A. R., Lorente-Cebrian, S., Stenvinkel, P., and Ryden, M. (2011) Uraemic sera stimulate lipolysis in human adipocytes: role of perilipin. *Nephrology, dialysis, transplantation : official publication of the European Dialysis and Transplant Association - European Renal Association* **26**, 2485-2491

97. DeFronzo, R. A., Alvestrand, A., Smith, D., Hendler, R., Hendler, E., and Wahren, J. (1981) Insulin resistance in uremia. *J Clin Invest* **67**, 563-568

98. Lorenzen, J. M., Haller, H., and Thum, T. (2011) MicroRNAs as mediators and therapeutic targets in chronic kidney disease. *Nature reviews. Nephrology* **7**, 286-294

99. Noh, H., Yu, M. R., Kim, H. J., Jang, E. J., Hwang, E. S., Jeon, J. S., Kwon, S. H., and Han, D. C. (2014) Uremic toxin p-cresol induces Akt-pathway-selective insulin resistance in bone marrow-derived mesenchymal stem cells. *Stem cells (Dayton, Ohio)* **32**, 2443-2453

100. Sayed, D., and Abdellatif, M. (2011) MicroRNAs in development and disease. *Physiological reviews* **91**, 827-887

101. Fliers, E., Sauerwein, H. P., Romijn, J. A., Reiss, P., van der Valk, M., Kalsbeek, A., Kreier, F., and Buijs, R. M. (2003) HIV-associated adipose redistribution syndrome as a selective autonomic neuropathy. *Lancet* **362**, 1758-1760

102. Beaufrere, B., and Morio, B. (2000) Fat and protein redistribution with aging: metabolic considerations. *European journal of clinical nutrition* **54 Suppl 3**, S48-53

103. Tsoli, M., Schweiger, M., Vanniasinghe, A. S., Painter, A., Zechner, R., Clarke, S., and Robertson, G. (2014) Depletion of white adipose tissue in cancer cachexia syndrome is associated with inflammatory signaling and disrupted circadian regulation. *PloS one* **9**, e92966

104. Ben-Dov, I. Z., Tan, Y. C., Morozov, P., Wilson, P. D., Rennert, H., Blumenfeld, J. D., and Tuschl, T. (2014) Urine microRNA as potential biomarkers of autosomal dominant polycystic kidney disease progression: description of miRNA profiles at baseline. *PloS one* **9**, e86856

105. Chau, B. N., Xin, C., Hartner, J., Ren, S., Castano, A. P., Linn, G., Li, J., Tran, P. T., Kaimal, V., Huang, X., Chang, A. N., Li, S., Kalra, A., Grafals, M., Portilla, D., MacKenna, D. A., Orkin, S. H., and Duffield, J. S. (2012) MicroRNA-21 promotes fibrosis of the kidney by silencing metabolic pathways. *Science translational medicine* **4**, 121ra118

106. Chen, N. X., Kiattisunthorn, K., O'Neill, K. D., Chen, X., Moorthi, R. N., Gattone, V. H., 2nd, Allen, M. R., and Moe, S. M. (2013) Decreased microRNA is involved in the vascular remodeling abnormalities in chronic kidney disease (CKD). *PloS one* **8**, e64558

107. Esau, C., Kang, X., Peralta, E., Hanson, E., Marcusson, E. G., Ravichandran, L. V., Sun, Y., Koo, S., Perera, R. J., Jain, R., Dean, N. M., Freier, S. M., Bennett, C. F., Lollo, B., and Griffey, R. (2004) MicroRNA-143 regulates adipocyte differentiation. *J Biol Chem* **279**, 52361-52365

108. Lin, Y. Y., Chou, C. F., Giovarelli, M., Briata, P., Gherzi, R., and Chen, C. Y. (2014) KSRP and MicroRNA 145 are negative regulators of lipolysis in white adipose tissue. *Mol Cell Biol* **34**, 2339-2349

109. Xu, J., Li, R., Workeneh, B., Dong, Y., Wang, X., and Hu, Z. (2012) Transcription factor FoxO1, the dominant mediator of muscle wasting in chronic kidney disease, is inhibited by microRNA-486. *Kidney international* **82**, 401-411

110. Chakrabarti, P., and Kandror, K. V. (2009) FoxO1 controls insulin-dependent adipose triglyceride lipase (ATGL) expression and lipolysis in adipocytes. *The Journal of biological chemistry* **284**, 13296-13300

111. Coward, R. J., Welsh, G. I., Yang, J., Tasman, C., Lennon, R., Koziell, A., Satchell, S., Holman, G. D., Kerjaschki, D., Tavare, J. M., Mathieson, P. W., and Saleem, M. A. (2005)

The human glomerular podocyte is a novel target for insulin action. *Diabetes* **54**, 3095-3102

112. de Vinuesa, S. G., Goicoechea, M., Kanter, J., Puerta, M., Cachofeiro, V., Lahera, V., Gomez-Campdera, F., and Luno, J. (2006) Insulin resistance, inflammatory biomarkers, and adipokines in patients with chronic kidney disease: effects of angiotensin II blockade. *J Am Soc Nephrol* **17**, S206-212

113. Sit, D., Kadiroglu, A. K., Kayabasi, H., and Yilmaz, M. E. (2006) The prevalence of insulin resistance in nondiabetic nonobese patients with chronic kidney disease. *Advances in therapy* **23**, 988-998

114. Go, A. S., Chertow, G. M., Fan, D., McCulloch, C. E., and Hsu, C. Y. (2004) Chronic kidney disease and the risks of death, cardiovascular events, and hospitalization. *The New England journal of medicine* **351**, 1296-1305

115. Liao, M. T., Sung, C. C., Hung, K. C., Wu, C. C., Lo, L., and Lu, K. C. (2012) Insulin resistance in patients with chronic kidney disease. *Journal of biomedicine & biotechnology* **2012**, 691369

116. Stenvinkel, P., Ketteler, M., Johnson, R. J., Lindholm, B., Pecoits-Filho, R., Riella, M., Heimburger, O., Cederholm, T., and Girndt, M. (2005) IL-10, IL-6, and TNF-alpha: central factors in the altered cytokine network of uremia--the good, the bad, and the ugly. *Kidney international* **67**, 1216-1233

117. Bruun, J. M., Lihn, A. S., Verdich, C., Pedersen, S. B., Toubro, S., Astrup, A., and Richelsen, B. (2003) Regulation of adiponectin by adipose tissue-derived cytokines: in vivo and in vitro investigations in humans. *American journal of physiology. Endocrinology and metabolism* **285**, E527-533

118. Foley, R. N., Parfrey, P. S., and Sarnak, M. J. (1998) Clinical epidemiology of cardiovascular disease in chronic renal disease. *American journal of kidney diseases : the official journal of the National Kidney Foundation* **32**, S112-119

119. Di Angelantonio, E., Chowdhury, R., Sarwar, N., Aspelund, T., Danesh, J., and Gudnason, V. (2010) Chronic kidney disease and risk of major cardiovascular disease and non-vascular mortality: prospective population based cohort study. *BMJ (Clinical research ed.)* **341**, c4986

120. Elhage, R., Clamens, S., Besnard, S., Mallat, Z., Tedgui, A., Arnal, J., Maret, A., and Bayard, F. (2001) Involvement of interleukin-6 in atherosclerosis but not in the

prevention of fatty streak formation by 17beta-estradiol in apolipoprotein E-deficient mice. *Atherosclerosis* **156**, 315-320

121. Goicoechea, M., de Vinuesa, S. G., Gomez-Campdera, F., Aragoncillo, I., Verdalles, U., Mosse, A., and Luno, J. (2008) Serum fibrinogen levels are an independent predictor of mortality in patients with chronic kidney disease (CKD) stages 3 and 4. *Kidney international. Supplement*, S67-70

122. Kersten, S., Seydoux, J., Peters, J. M., Gonzalez, F. J., Desvergne, B., and Wahli, W. (1999) Peroxisome proliferator-activated receptor alpha mediates the adaptive response to fasting. *The Journal of clinical investigation* **103**, 1489-1498

123. Chen, L. L., Zhang, J. Y., and Wang, B. P. (2006) Renoprotective effects of fenofibrate in diabetic rats are achieved by suppressing kidney plasminogen activator inhibitor-1. *Vascular pharmacology* **44**, 309-315

124. Chung, H. W., Lim, J. H., Kim, M. Y., Shin, S. J., Chung, S., Choi, B. S., Kim, H. W., Kim, Y. S., Park, C. W., and Chang, Y. S. (2012) High-fat diet-induced renal cell apoptosis and oxidative stress in spontaneously hypertensive rat are ameliorated by fenofibrate through the PPARalpha-FoxO3a-PGC-1alpha pathway. *Nephrology, dialysis, transplantation : official publication of the European Dialysis and Transplant Association - European Renal Association* **27**, 2213-2225

125. Decleves, A. E., Mathew, A. V., Cunard, R., and Sharma, K. (2011) AMPK mediates the initiation of kidney disease induced by a high-fat diet. *J Am Soc Nephrol* **22**, 1846-1855

126. Bobulescu, I. A., Dubree, M., Zhang, J., McLeroy, P., and Moe, O. W. (2009) Reduction of renal triglyceride accumulation: effects on proximal tubule Na+/H+ exchange and urinary acidification. *American journal of physiology. Renal physiology* **297**, F1419-1426

Figures S1-S3 represent immunohistochemical detections in mouse kidney. (n=1)

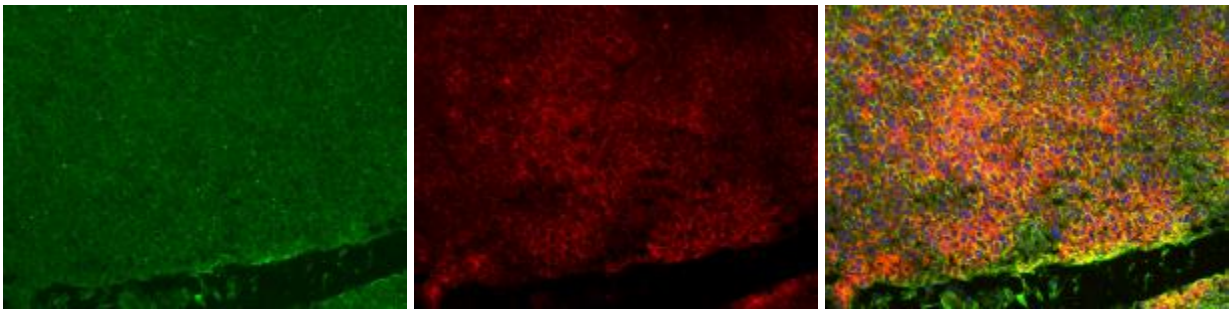

Figure S1: Kidney ATGL (green), Ppar-gamma (red), merge.

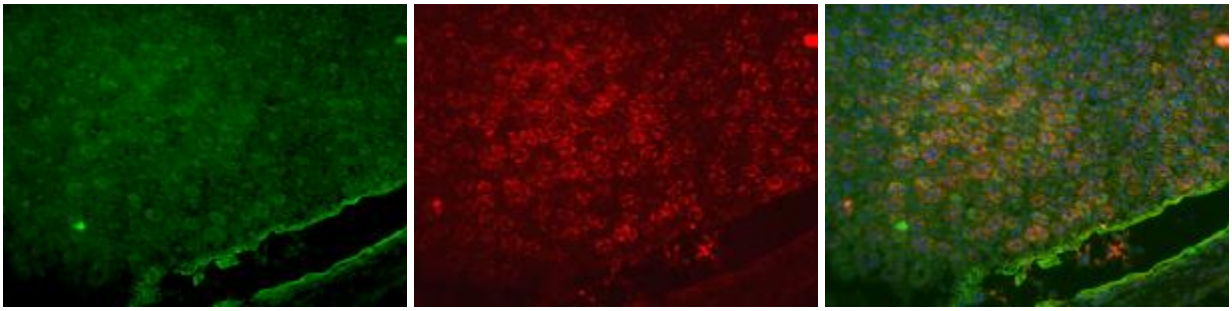

Figure S2: Kindey ATGL (green), Leptin (red), merge.

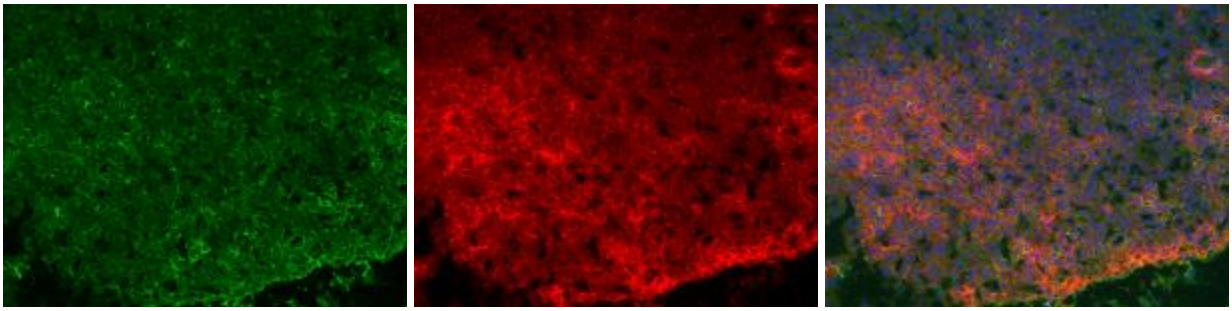

Figure S3: Kidney ATGL (green), IRS1 (red), merge.

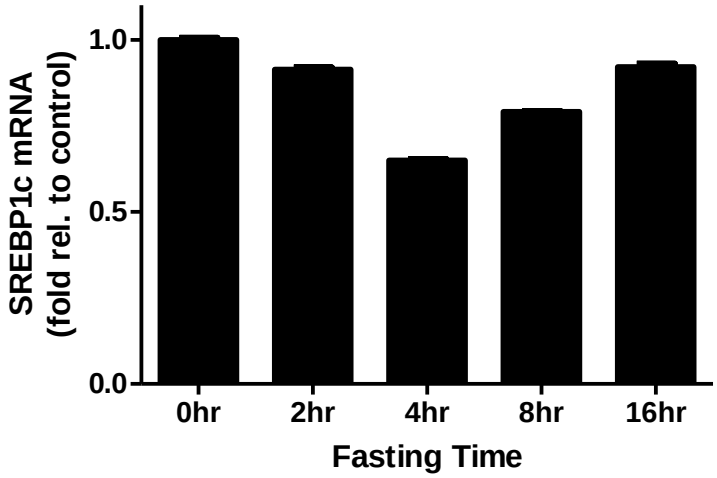

Figure S4: Kidney SREBP1c mRNA expression in female fasted mice at 20wks of age. (n=4-6)

Figures S5-S11 represents the initial work completed on KSAKO female mice.

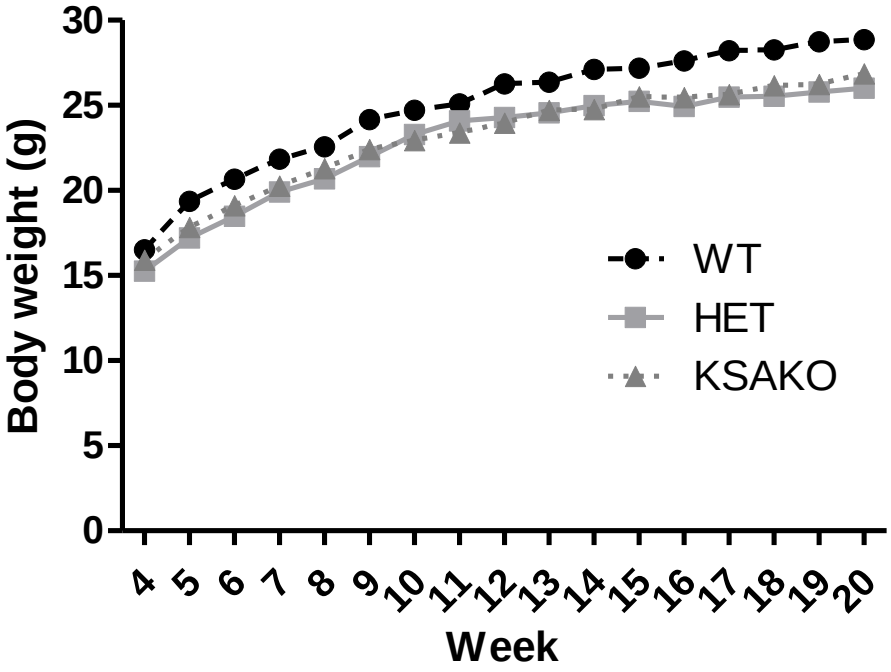

Figure S5: Body weights of female KSAKO mice over 20wks compared to WT and HET. Female mice demonstrate opposite effect from males. Body weights tend to derease in KSAKO mice.

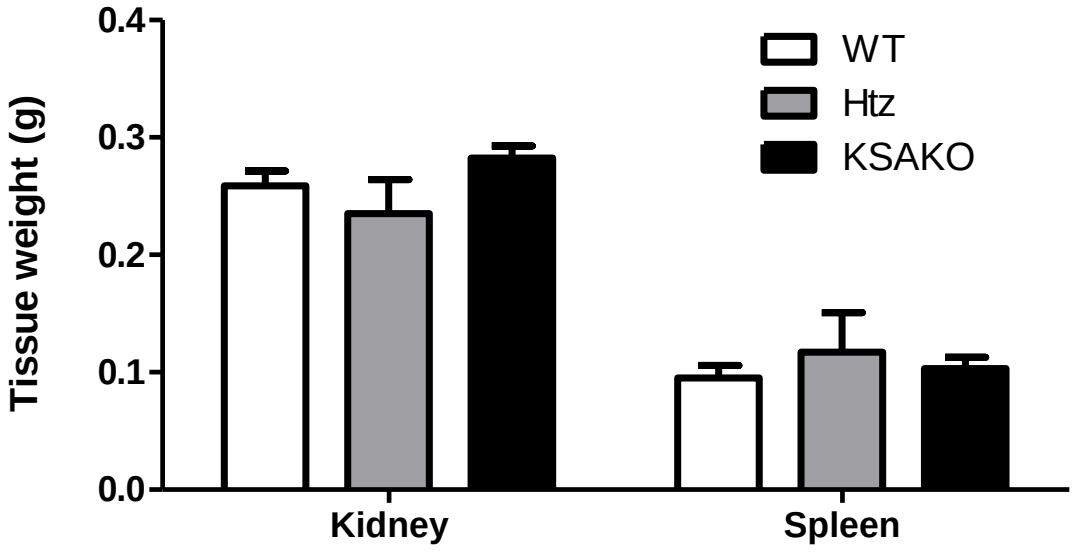

Figure S6: Tissue weights in female KSAKO mice at 20 wks of age.

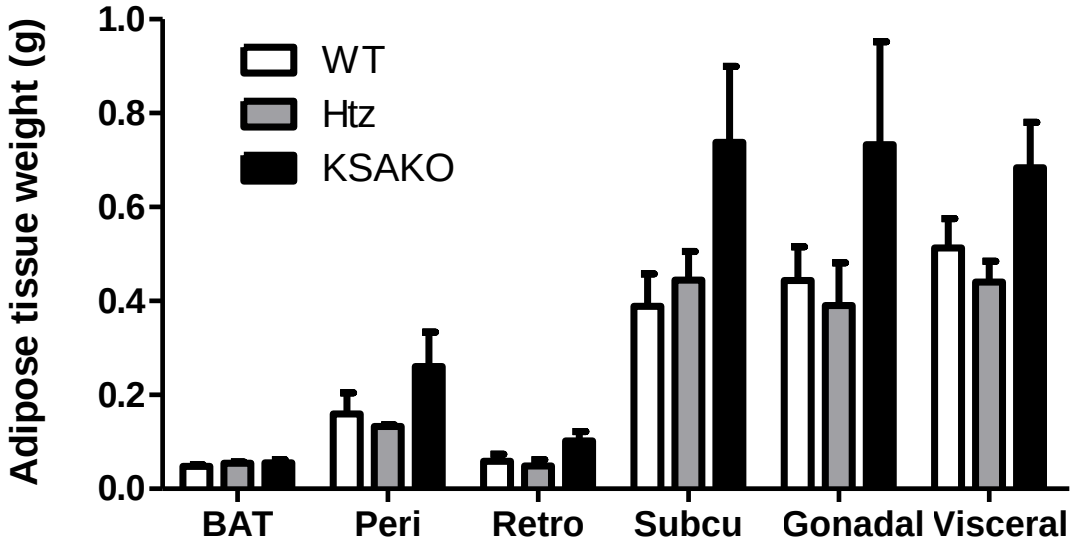

Figure S7: Adipose tissue depot weights of female KSAKO mice at 20 wks of age.
Female KSAKO mice demonstrate an opposite effect from KSAKO males. Adipose depots tend to increase in KSAKO mice.

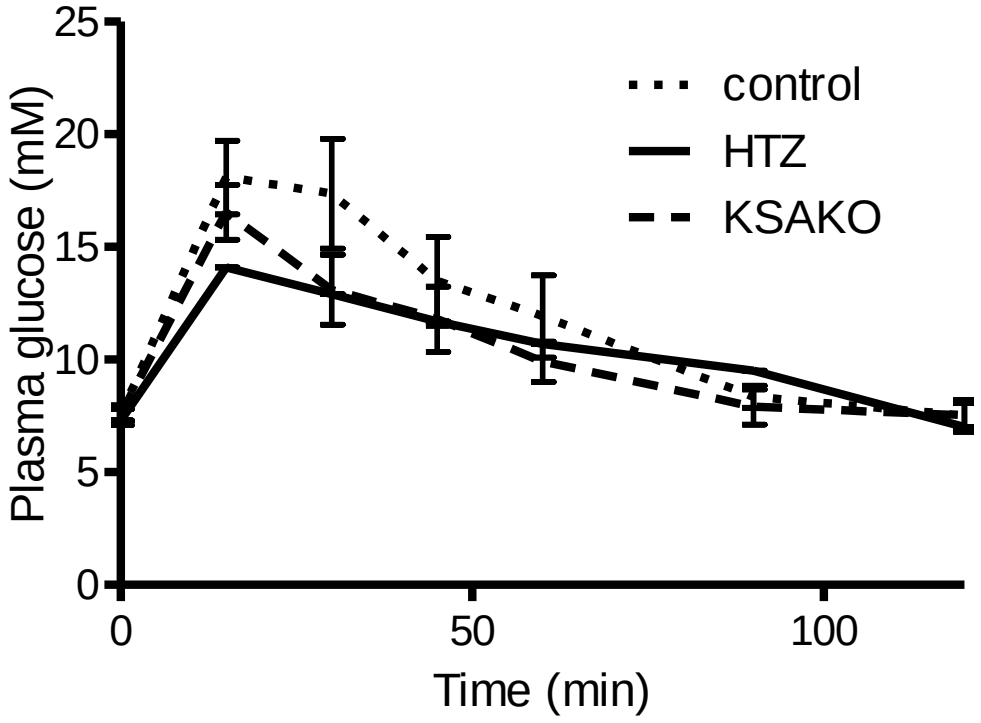

Figure S8: Glucose tolerance test in female KSAKO mice at 9 wks of age.

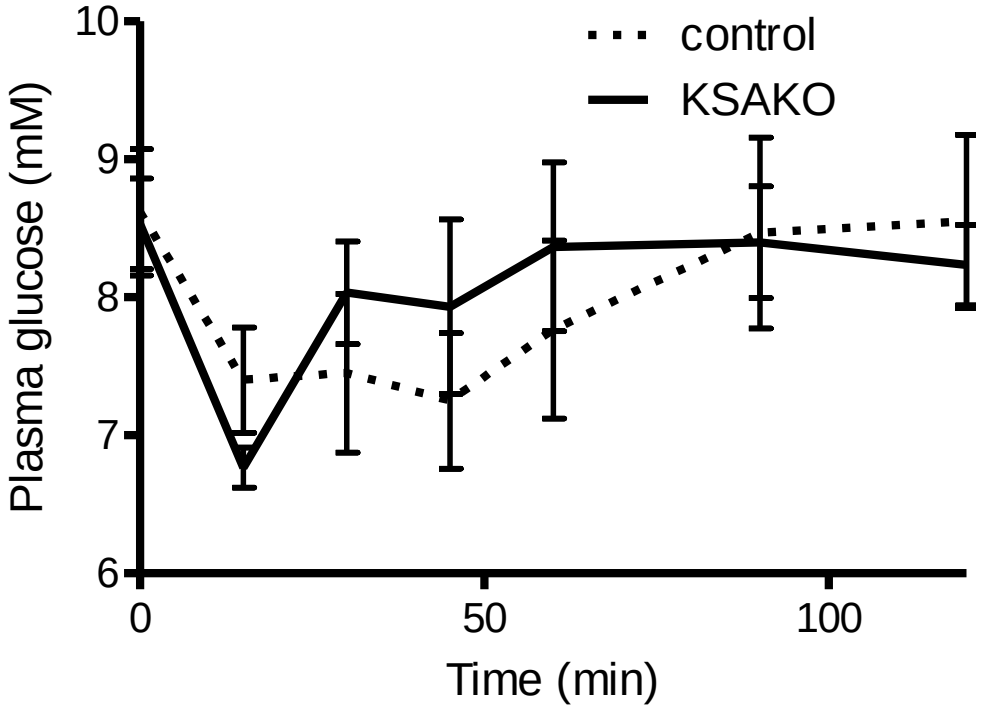

Figure S9: Insulin tolerance test in female KSAKO mice at 9 wks of age.

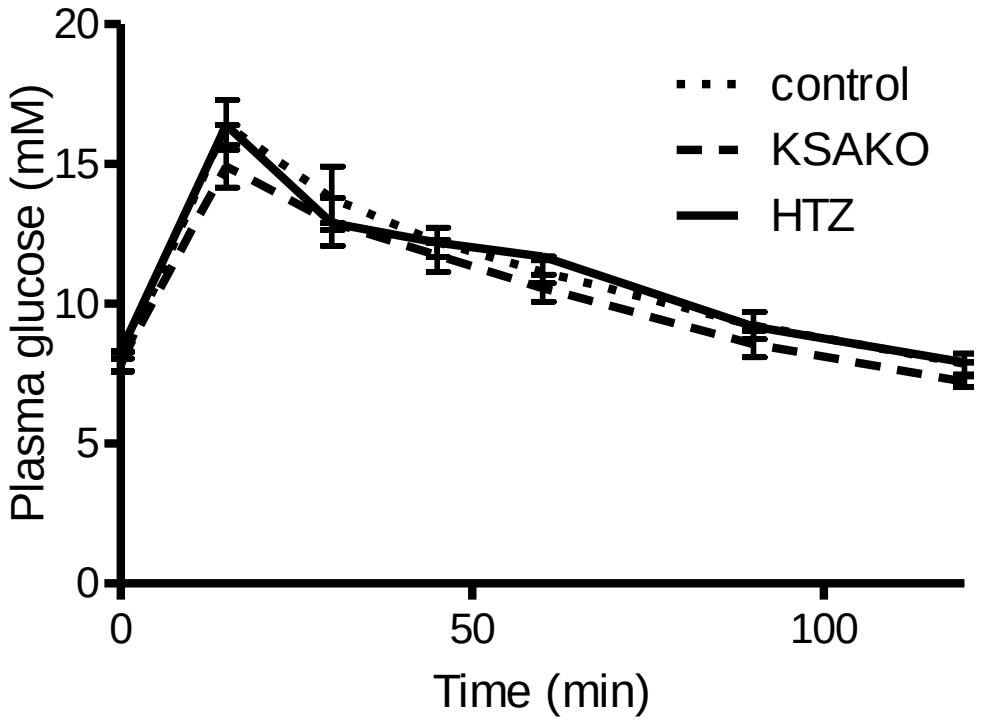

Figure S10: Glucose tolerance test in female KSAKO mice at 16 wks of age.

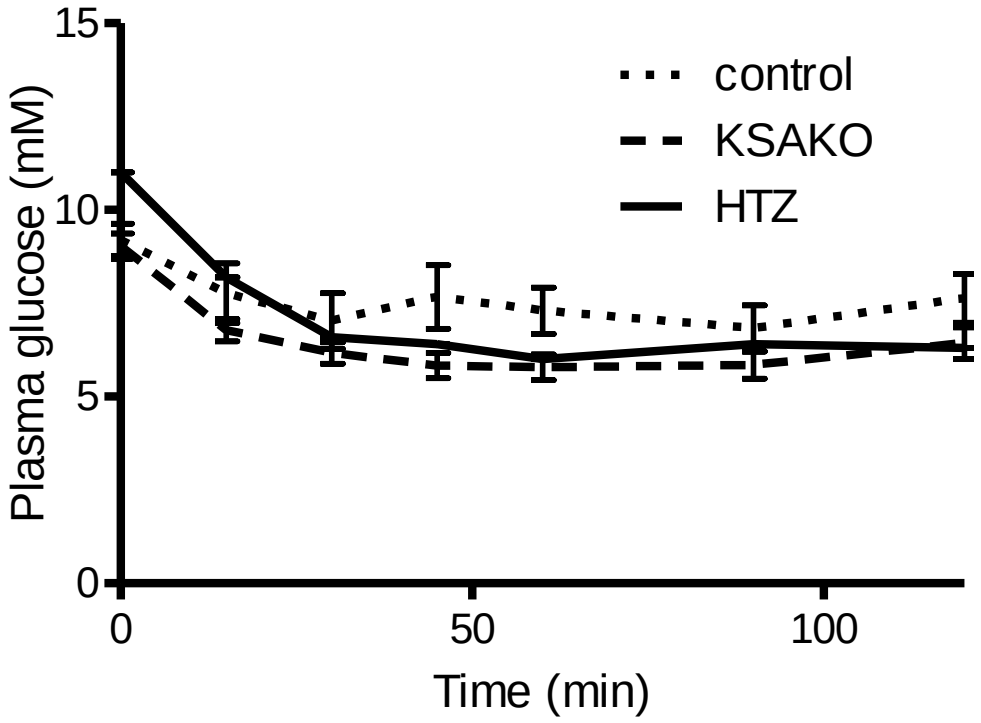

Figure S11: Insulin tolerance test in female KSAKO mice at 16 wks of age.

Figures S12-S21 represent work completed on a 3day high fat diet study.

The study consisted of female mice aged 16-20 wks divided into 4 study conditions. Either chow diet or high fat diet fed for 3 days and then either sacrificed or fasted for 16hr prior to sacrifice.

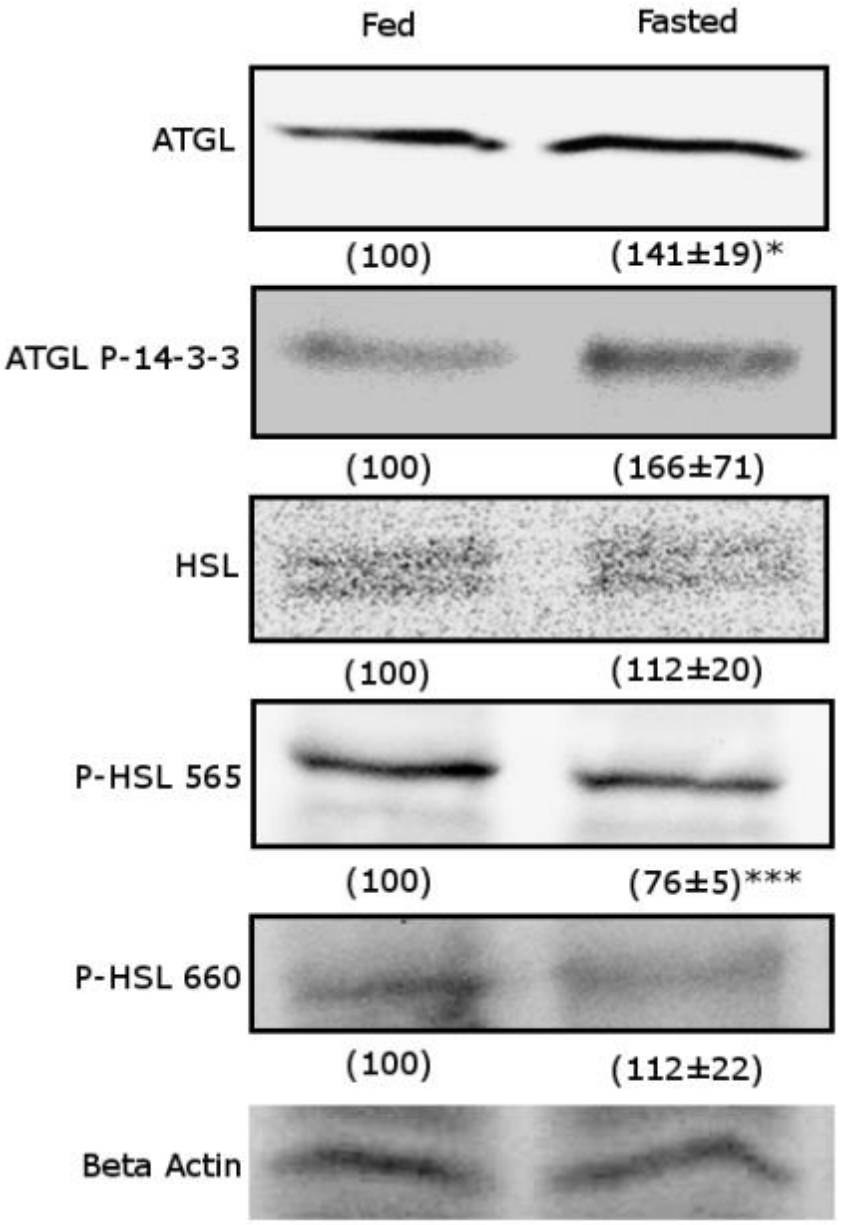

Figure S12: Representative immunoblots of liver protein levels following a 16 hr fast in 16 wk old female mice.

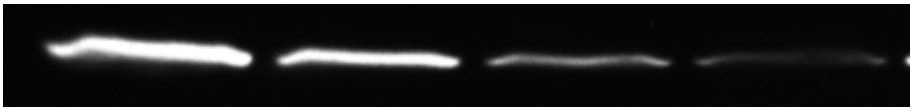

Figure S13: Immunoblot of liver ATGL protein in female mice at 16 wks of age.
Left to right: Chow diet fed, Chow diet fasted, High fat diet fed, High fat diet fasted.

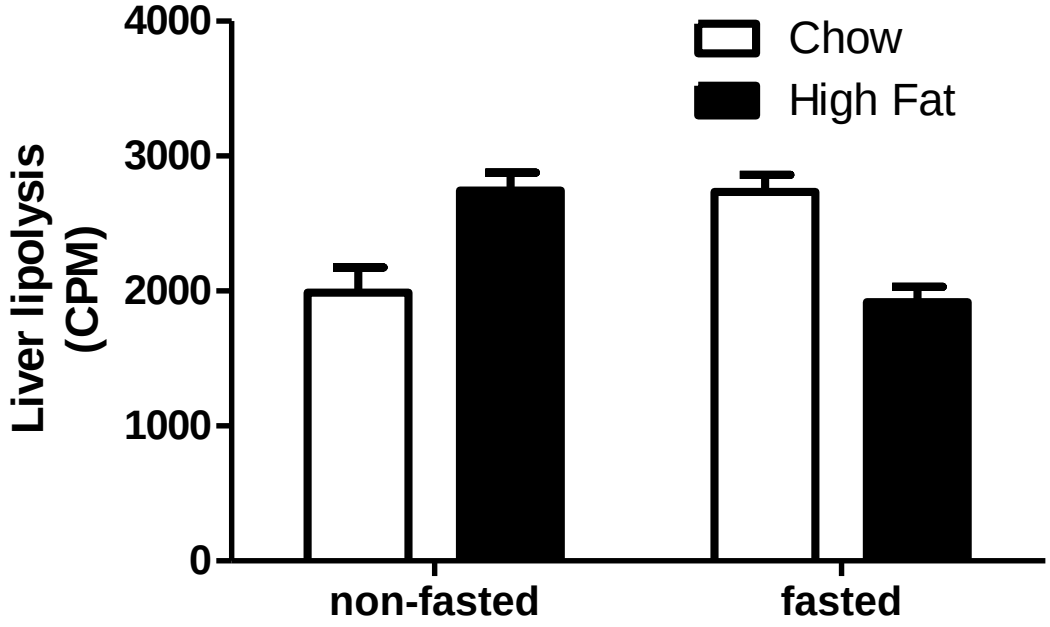

Figure S14: TAG hydrolysis activity in liver tissue of female mice.

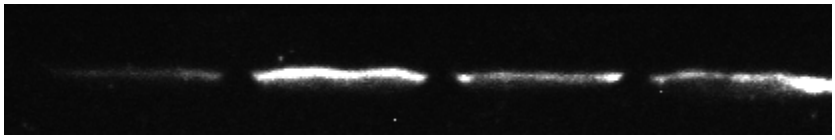

Figure S15: Immunoblot of kidney ATGL protein.
Left to right: Chow diet fed, Chow diet fasted, Highfat diet fed, High fat diet fasted.

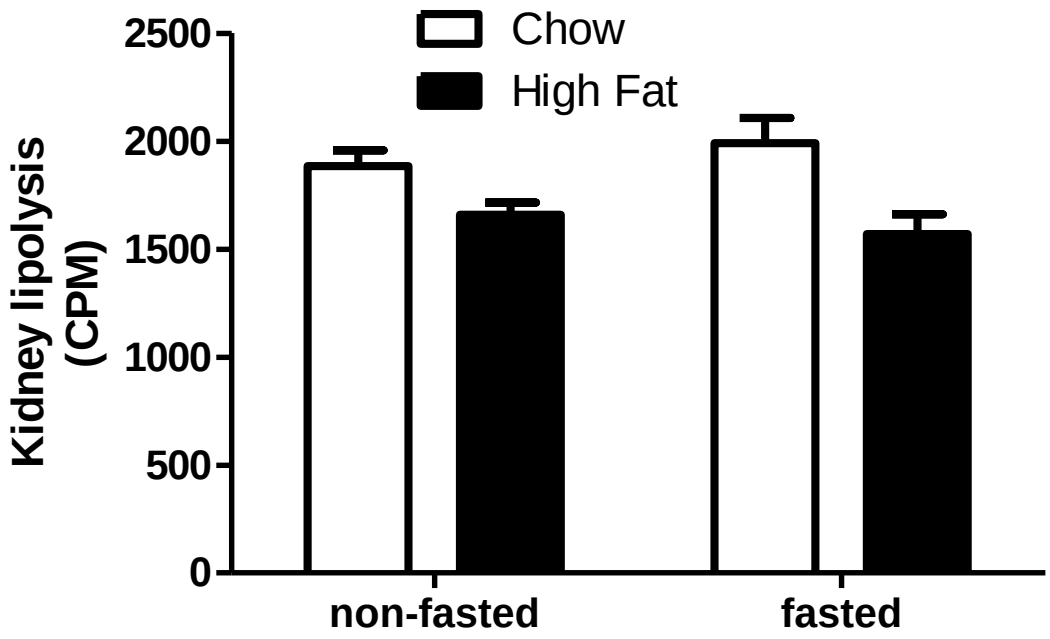

Figure S16: TAG hydrolysis activity in kidney tissue of female mice.

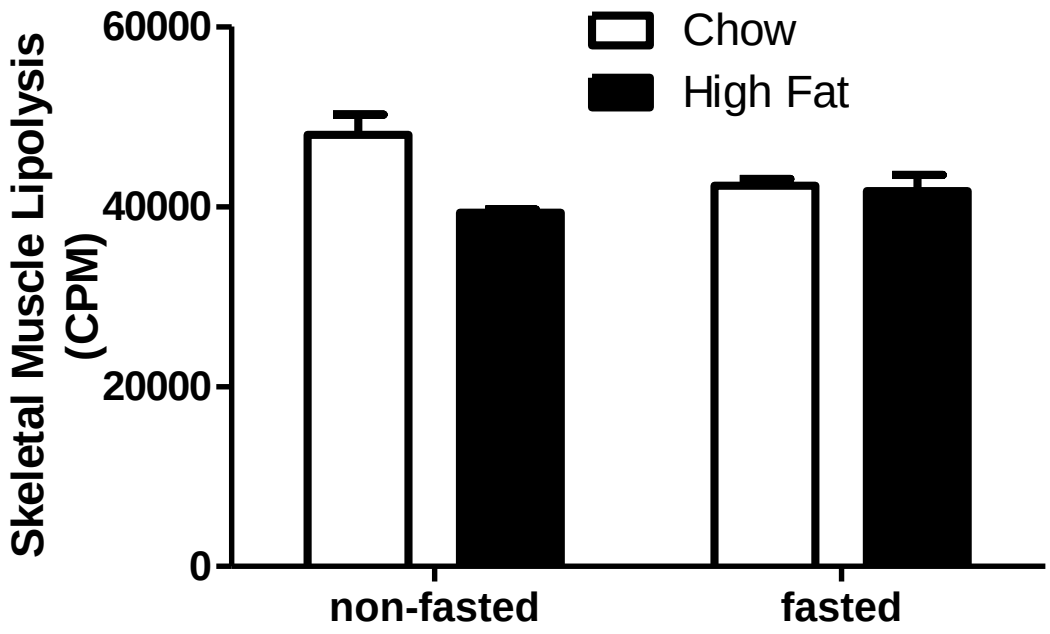

Figure S17: TAG hydrolysis activity in skeletal muscle tissue of female mice.

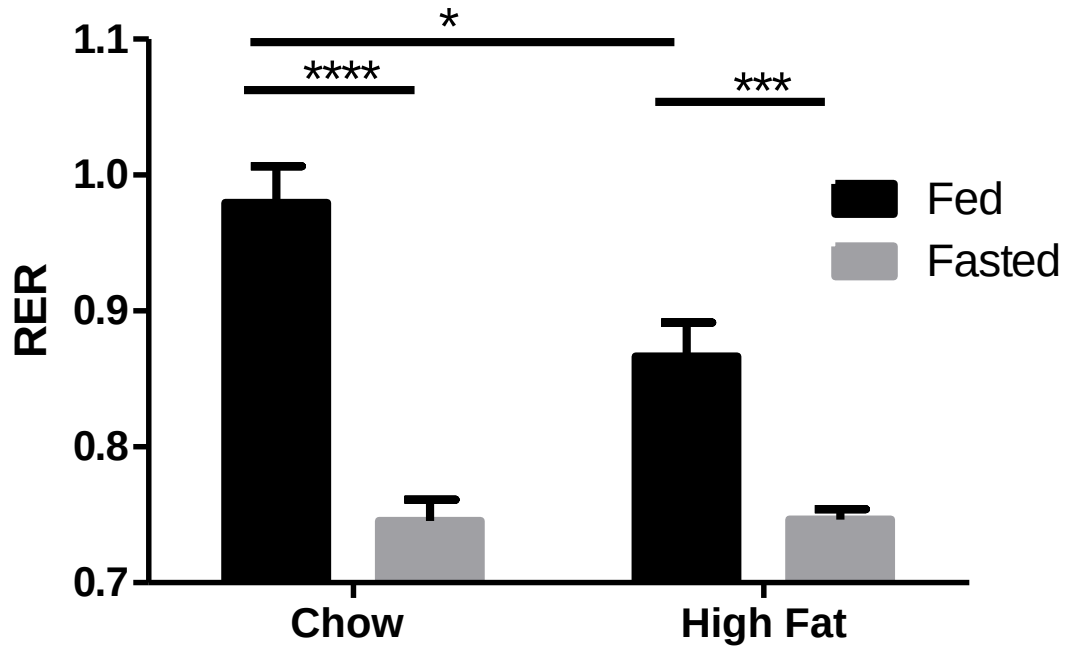

Figure S18: Respiratory exchange ratio in female mice after a 3 day high fat diet.

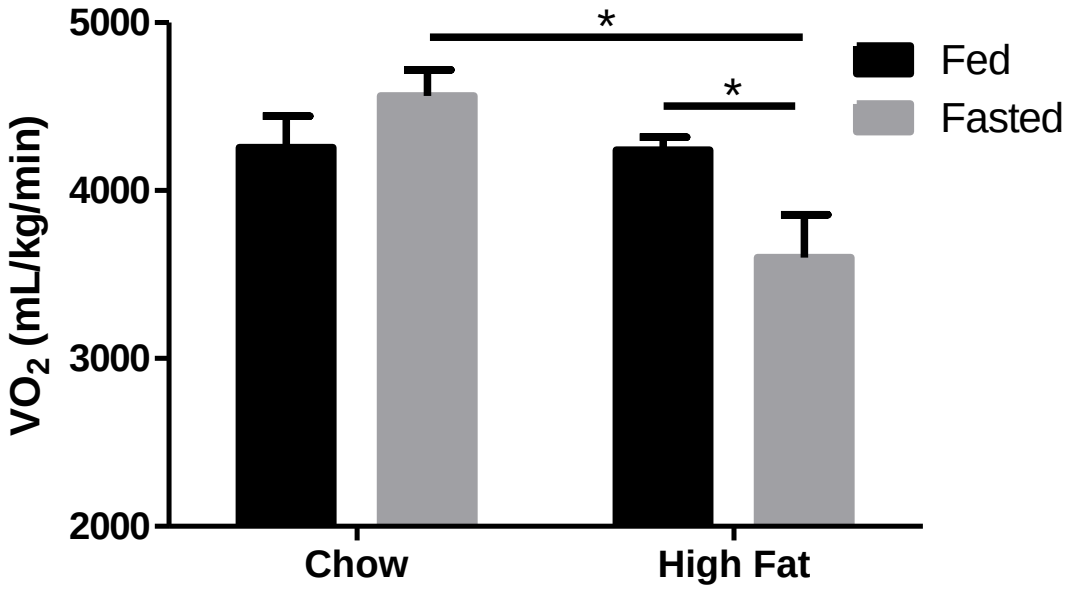

Figure S19: Oxygen consumption in female mice after a 3 day high fat diet.

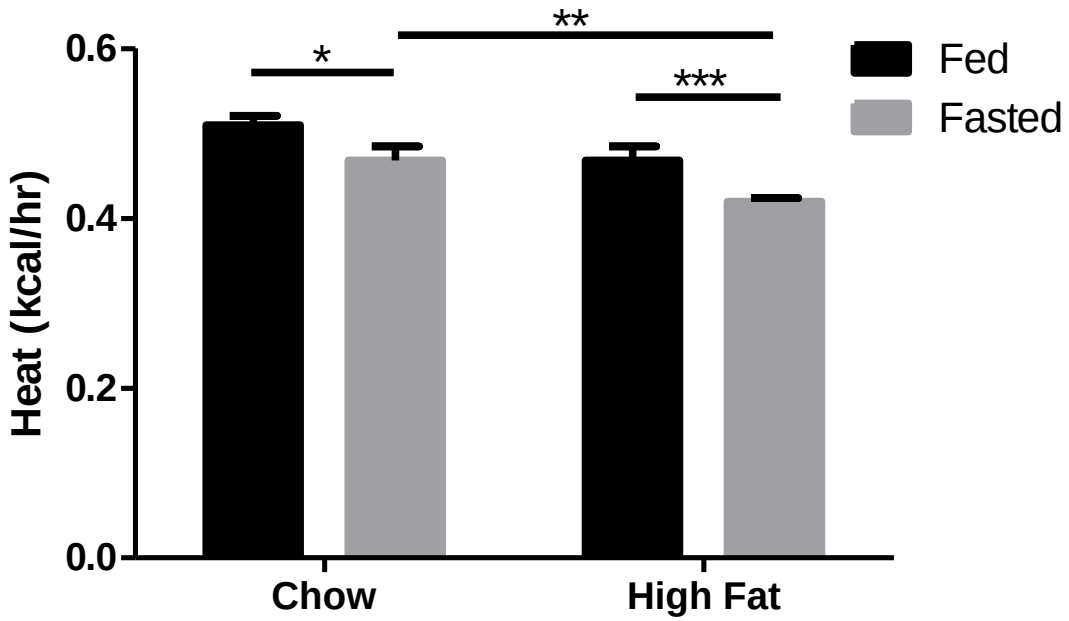

Figure S20: Energy expenditure in female mice after a 3 day high fat diet.

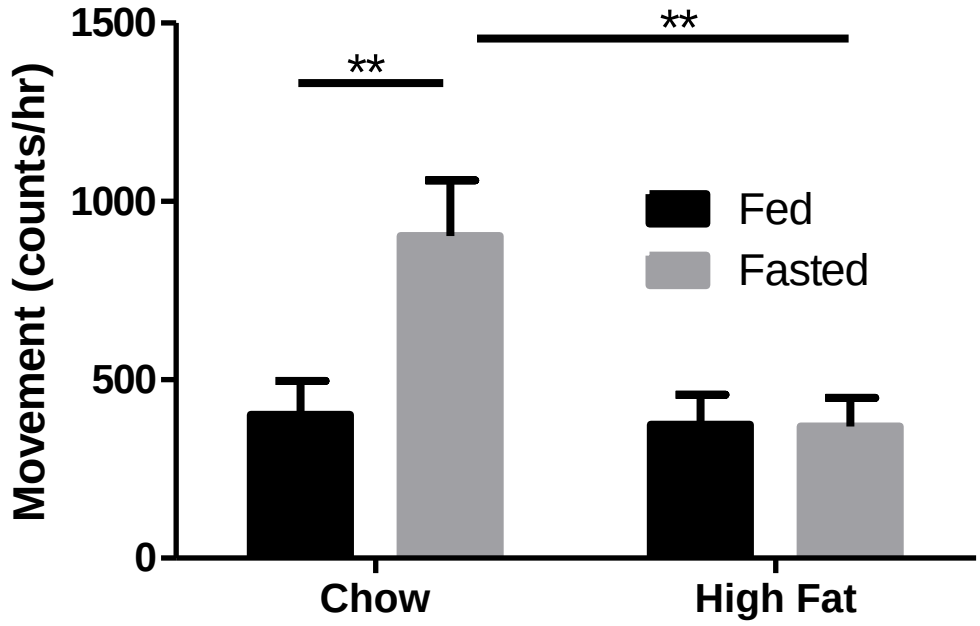

Figure S21: Physical activity in female mice after a 3 day high fat diet.

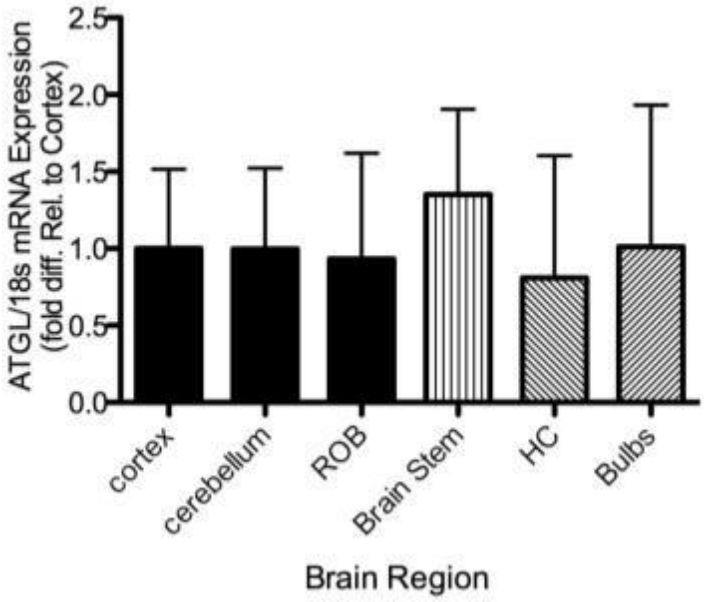

Figure S22: *Atgl* mRNA expression in different brain regions. (ROB-rest of brain; HC-hippocampus)

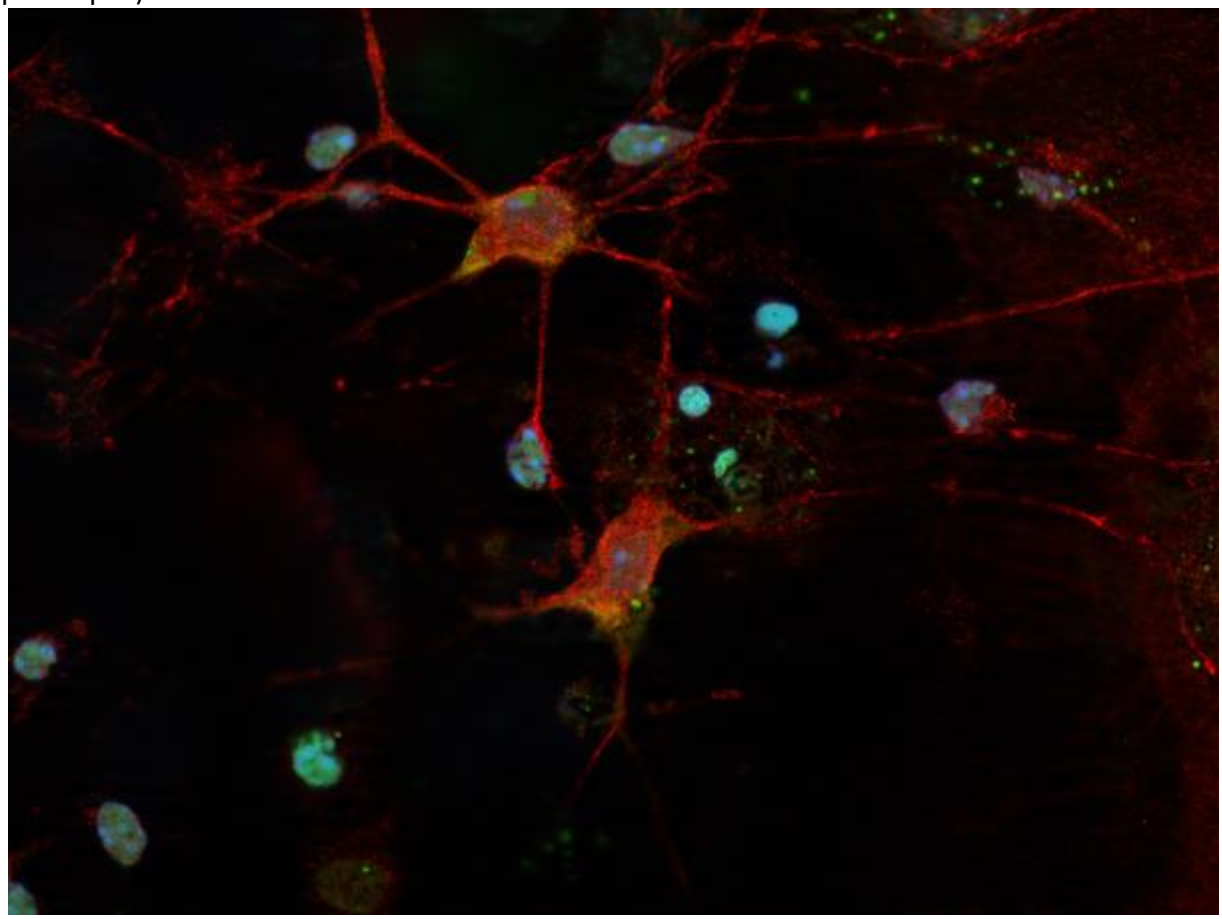

Figure S23: Immunohistochemical detection of ATGL protein in SHSY-5Y cell line along neural dendrites. ATGL (red), NeuroTrace Stain (Life Technologies)(green), DAPI (blue)